

AD-A193 043

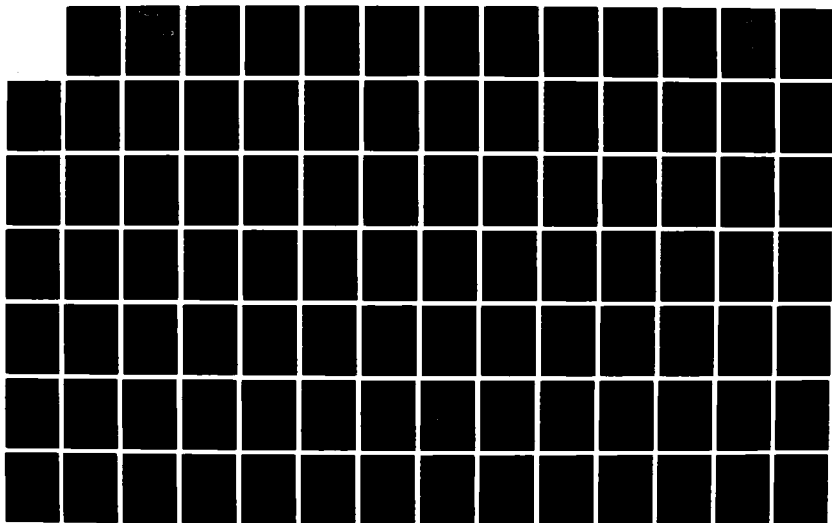
EXPERIMENTAL VERIFICATION OF AUV (AUTONOMOUS UNDERWATER  
VEHICLE) PERFORMANCE(U) NAVAL POSTGRADUATE SCHOOL  
MONTEREY CA G M BRUNNER MAR 88

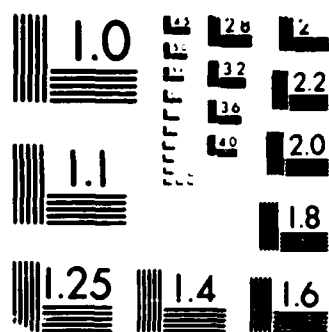
1/2

UNCLASSIFIED

F/G 13/10

NL





MICROCOPY RESOLUTION TEST CHART  
 U.S. GOVERNMENT PRINTING OFFICE

2

AD-A193 843

# NAVAL POSTGRADUATE SCHOOL

Monterey, California

ENC FILE COPY



## THESIS

DTIC  
ELECTE  
JUN 14 1988  
S H D

### EXPERIMENTAL VERIFICATION OF AUV PERFORMANCE

by

Glenn M. Brunner

March 1988

Thesis Advisor:

A. J. Healey

Approved for public release; distribution is unlimited.

## REPORT DOCUMENTATION PAGE

1a. REPORT SECURITY CLASSIFICATION UNCLASSIFIED			1b. RESTRICTIVE MARKINGS		
2a. SECURITY CLASSIFICATION AUTHORITY			3. DISTRIBUTION/AVAILABILITY OF REPORT Approved for public release; distribution is UNLIMITED		
2b. DECLASSIFICATION/DOWNGRADING SCHEDULE					
4. PERFORMING ORGANIZATION REPORT NUMBER(S)			5. MONITORING ORGANIZATION REPORT NUMBER(S)		
6a. NAME OF PERFORMING ORGANIZATION NAVAL POSTGRADUATE SCHOOL		6b. OFFICE SYMBOL (If applicable)		7a. NAME OF MONITORING ORGANIZATION NAVAL POSTGRADUATE SCHOOL	
6c. ADDRESS (City, State, and ZIP Code) MONTEREY, CA 93943-5000				7b. ADDRESS (City, State, and ZIP Code) MONTEREY, CA 93943-5000	
8a. NAME OF FUNDING/SPONSORING ORGANIZATION		8b. OFFICE SYMBOL (If applicable)		9. PROCUREMENT INSTRUMENT IDENTIFICATION NUMBER	
ADDRESS (City, State, and ZIP Code)		10. SOURCE OF FUNDING NUMBERS			
		PROGRAM ELEMENT NO		PROJECT NO	TASK NO
				WORK UNIT ACCESSION NO	
11. TITLE (Include Security Classification) EXPERIMENTAL VERIFICATION OF AUV PERFORMANCE					
12. PERSONAL AUTHOR(S) BRUNNER, GLENN M.					
13a. TYPE OF REPORT THESIS MECHANICAL ENGINEER		13b. TIME COVERED FROM TO		14. DATE OF REPORT (Year, Month, Day) 1988 MARCH	
15. PAGE COUNT 152					
16. SUPPLEMENTARY NOTATION "The views expressed in this thesis are those of the author and do not reflect the official policy or position of the Department of Defense or the U.S. Government."					
17. COSATI CODES			18. SUBJECT TERMS (Continue on reverse if necessary and identify by block number)		
FIELD	GROUP	SUB-GROUP	AUTONOMOUS UNDERWATER VEHICLE, AUV, EXPERIMENTAL MODEL		
			PERFORMANCE TEST, CLASSICAL CONTROLLER DESIGN.		
19. ABSTRACT (Continue on reverse if necessary and identify by block number) System identification for an Autonomous Underwater Vehicle model design is performed using Recursive Least Squares to provide a best fit discretized transfer function between dive plane command signals and vehicle response data. The data was provided by constructing a radio controlled vehicle model and performing vertical plane maneuvers in a water tank. The analog input and output signals were digitized and recorded. The vehicle design, sensor calibration, and resulting responses are discussed. Vertical plane equations of motion were derived and theoretical plant models formulated. Also, analog controller designs were performed based on the theoretical plant models. This study will lead to adaptive model controllers for the future.					
20. DISTRIBUTION/AVAILABILITY OF ABSTRACT <input checked="" type="checkbox"/> UNCLASSIFIED/UNLIMITED <input type="checkbox"/> SAME AS RPT <input type="checkbox"/> DTIC USERS			21. ABSTRACT SECURITY CLASSIFICATION UNCLASSIFIED		
22a. NAME OF RESPONSIBLE INDIVIDUAL HEALEY			22b. TELEPHONE (Include Area Code) (408) 646-2586		22c. OFFICE SYMBOL 69Hy

Approved for public release; distribution is unlimited.

Experimental Verification of AUV Performance

by

Glenn M. Brunner  
Lieutenant, United States Navy  
B.S.M.E., Purdue University, 1980

Submitted in partial fulfillment of the  
requirements for the degree of

MASTER OF SCIENCE IN MECHANICAL ENGINEERING  
AND MECHANICAL ENGINEER

from the

NAVAL POSTGRADUATE SCHOOL  
March, 1988

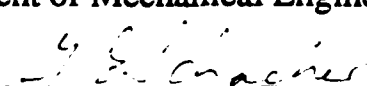
Author:

  
Glenn M. Brunner

Approved by:

  
A. J. Healey, Thesis Advisor

  
A. J. Healey, Chairman,  
Department of Mechanical Engineering

  
Gordon E. Schacher, Dean of Science and Engineering

## ABSTRACT

System identification for an Autonomous Underwater Vehicle model design is performed using Recursive Least Squares to provide a best fit discretized transfer function between dive plane command signals and vehicle response data. The data was provided by constructing a radio controlled vehicle model and performing vertical plane maneuvers in a water tank. The analog input and output signals were digitized and recorded. The vehicle design, sensor calibration, and resulting responses are discussed. Vertical plane equations of motion were derived and theoretical plant models formulated. Also, analog controller designs were performed based on the theoretical plant models. This study will lead to adaptive model controllers for the future.

Accession For	
NTIS GRA&I	<input checked="checked" type="checkbox"/>
DTIC TAB	<input type="checkbox"/>
Unannounced	<input type="checkbox"/>
Justification	
By	
Distribution/	
Availability Codes	
Dist	Avail and/or Special
A-1	

## TABLE OF CONTENTS

I. INTRODUCTION.....	1
A.SPECIFIC OBJECTIVES .....	4
B.DESIGN APPROACH.....	4
II. CLASSICAL CONTROLLER DESIGN.....	6
A.INTRODUCTION.....	6
B.DEPTH CONTROL .....	7
C.ROLL CONTROL .....	20
D.COURSE CONTROL SYSTEM.....	32
E.SPEED CONTROL.....	34
F.EQUATIONS OF MOTION.....	34
G.SIMPLIFIED CONTROLLER SIMULATION.....	47
III. DESIGN OF TEST MODEL AND FACILITY.....	49
A.INTRODUCTION .....	49
B.MODEL SIZE .....	49
C.HULL FABRICATION .....	49
D.CALCULATION OF DISPLACEMENT AND FIRST-ORDER SYSTEM COEFFICIENTS.....	52
E.MOTOR REQUIREMENTS.....	57
F.GYRO SELECTION .....	63
G.PRESSURE INSTRUMENTS.....	64
H.ELECTRONICS AND POWER.....	66
I.TEST TANK CONTROL STATION.....	68
IV. CALIBRATION AND TEST PROCEDURES .....	69
A.INTRODUCTION .....	69
B.GYRO CALIBRATION.....	70
C.PRESSURE CELL CALIBRATION.....	75
D.BALASTING.....	79
E.MEASUREMENT OF $J_x$ AND $J_z$ .....	80
F.PRELIMINARY TESTING FOR STABILITY .....	84
G.DIVE PLANE AND ROLL PLANE COMMAND SIGNAL.....	85
H.DATA ACQUISITION.....	88

V. RESULTS.....	92
A.INTRODUCTION .....	92
B.PREDICTED TRANSFER FUNCTIONS.....	93
C.COMPUTER SOLUTION APPROACH.....	94
D.RESPONSE OF PITCHRATE TO DIVE PLANE ANGLE .....	95
E.TRANSFER FUNCTION IDENTIFICATION .....	97
F.DISCUSSION .....	99
VI. CONCLUSIONS AND RECOMMENDATIONS .....	114
A.CONCLUSIONS.....	114
B.RECOMMENDATIONS.....	115
LIST OF REFERENCES.....	117
APPENDIX A.....	118
APPENDIX B.....	122
APPENDIX C.....	132



## LIST OF FIGURES

Figure No.	Title	Page
1	Test Model	3
2	Depth Controller Block Diagram	7
3	First Order Plant Model	10
4	Closed Loop System Block Diagram	11
5	RLP[Kpz=1,U=0.5]	13
6	RLP[Kpz=1,U=1]	14
7	RLP[Kpz=0.5,U=0.5]	15
8	RLP[Kpz=0.5,U=1]	16
9	RLP[Kpz=0.25,U=1]	17
10	RLP[Kpz=0.25,Kdz=0.5]	18
11	TR[Kpz=0.25,Kdz=5]	21
12	TR[Kpz=0.25,Kdz=0.5]	22
13	RLP[Kpz=0.25,Kdz=0]	23
14	RLP[Kpz=0.25,B=0.72]	24
15	TR[Kpz=0.25,U=1]	25
16	TR[Kpz=0.25,U=3]	26
17	RLP[Kdz=0.0,B=0.72]	27
18	Depth Controller	28
19	Roll/Yaw Controller	29
20	RLP Roll	31
21	RLP Yaw	33
22	Speed Controller	35
23	Principle Dimensions	37
24	Damping About 'Y' Axis	55
25	Damping About 'X' Axis	56
26	Damping About 'Z' Axis	56
27	Electronic Circuit	67
28	Station Layout	68
29	Pitch-rate Gyro	71
30	Yaw-rate Gyro	71
31	Roll-rate Gyro	72
32	Pitch-rate Gyro at Low Ref. Voltage	72
33	Yaw-rate Gyro at Low Ref. Voltage	73
34	Roll-rate Gyro at Low Ref. Voltage	73

35	Velocity Cell Calibration Curve	76
36	Depth Cell Calibration Curve (Bench)	77
37	Speed Calibration Curve	77
38	Depth Cell Calibration Curve	78
39	Inertia Test	82
40	Uncompensated Roll Control Signal	86
41	Compensated Roll Control Signal	86
42	Uncompensated Dive Plane Control Signal	87
43	Compensated Dive Plane Control Signal	87
44	Signal Flow	91
45	Run 7/3A	102
46	Run 7/3B	103
47	Run 7/5A	104
48	Run 7/5B	105
49	Run 8/1A	106
50	Run 8/1B	107
51	Run 8/1C	108
52	Run 9/1A	109
53	Run 9/1B	110
54	Run 9/1C	111
55	Run 9/2A	112
56	Run 9/2B	113

## I. INTRODUCTION

The main goal of this thesis was to investigate a technique for determining the discrete transfer function relation between the command signals to an underwater vehicle and the response of the vehicle to those command signals. With this transfer function some insight into the actual values of the hydrodynamic coefficients of the governing equations of motion may be gained. A strong interest exists in the Navy concerning the use of an Autonomous Underwater Vehicle (AUV) in various operations, such as ASW, reconnaissance, decoy and surveillance. It was the purpose of this work to build and test a model of a vehicle which might be used as an AUV. The model was self propelled and remotely controlled by radio transmission. This allowed realistic output data for known inputs to control surfaces. The model size was kept small, only 30 inches in length, because of test facility limitations. Tests were conducted in the vertical plane since depth is easily monitored by pressure cells and dive maneuvers could be relatively well executed and monitored.

Establishing this type of test program provides a means of developing the knowledge base for construction of test vehicles and the corresponding test procedures for evaluating a particular shape. Using available software to analyze data and provide the correlations between input and output signals provides the means to check the quality of the system model simulation. Ultimately, on-line refinement of the system model, based on real-time vehicle performance data, allows for real-time model parameter

identification and adaptive control. This is perceived to be necessary in future AUV control design.

It has been established that robust controllers can be designed for underwater vehicles for dive plane trajectory tracking. This requires the generation of dynamic models of vehicle performance. These models are difficult to derive analytically, and usually need the evaluation of hydrodynamic coefficients. An alternative approach uses system identification techniques to develop vehicle transfer functions from experimental maneuvering tests. Any AUV control system will ultimately incorporate adaptive parameter identification, so this research project was initiated to develop suitable techniques and algorithms that may be used for that purpose.

A vehicle shape, not necessarily representative of any specific vehicle, was selected as the basis for the design and development of a test model. Refer to Figure 1. The model was equipped with radio control, rate gyro sensors, a pressure cell depth sensor and a pressure cell speed sensor. Two DC motors provided propulsion power and a digital data acquisition system was configured and operated in performing a series of experimental dive plane dynamic response tests. The specific objectives of this work are given below.

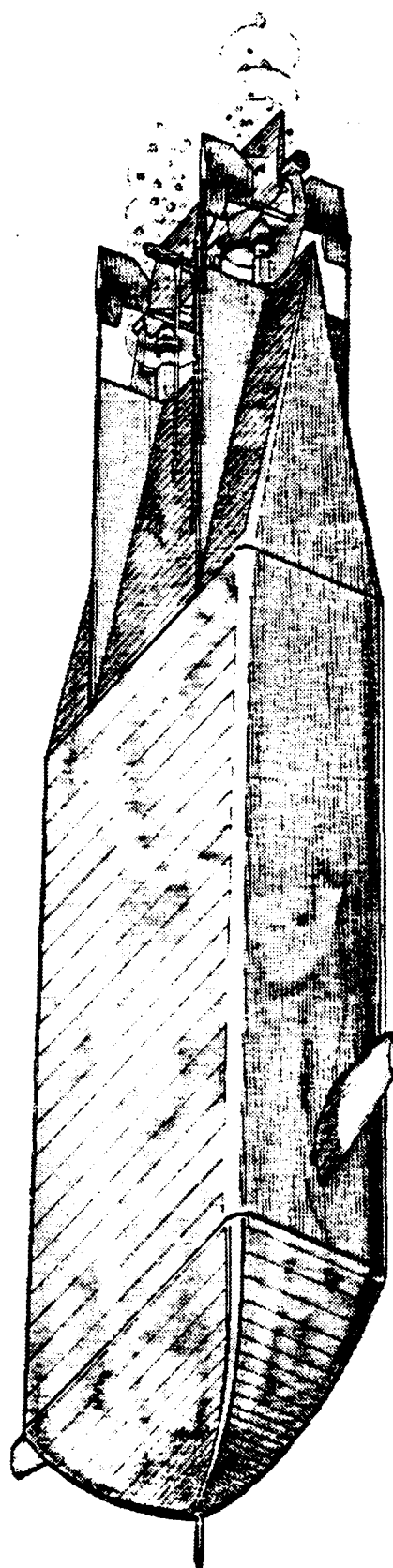


Figure 1 Test Model

## A. SPECIFIC OBJECTIVES

The specific objectives were:

- 1) Select a reasonable vehicle design which has potential for use as an AUV and that also has available operational characteristics, such as the hydrodynamic coefficients of the governing equations of motion.
- 2) Design and build a test model based on the full size vehicle's shape.
- 3) As part of the overall design process, investigate the available sensory devices. Equipment such as gyros, inertial sensors and pressure cells would be selected based upon size, cost, sensitivity and range.
- 4) Establish a testing technique to provide the needed response data and digitize this data for input to files for analysis.
- 5) Design control systems which can be implemented easily for vehicle control during testing operations.
- 6) Establish a system model and perform simulation studies.
- 7) Utilize available software to perform an analysis of the data and provide the system transfer function for comparison to the model simulation.

## B. DESIGN APPROACH

The first step was to select the vehicle shape. The design drawings for the vehicle were made and construction commenced. Component selection was also performed at the outset since it impacts the model design. While the test model was being built, the preliminary plant simulation studies were performed and simple controller designs established which could, if needed, be readily implemented. These controllers were designed for operation on analog computers since a digital computer control system was not expected to

be ready in time. As it turned out, insufficient time was available to implement the analog controllers as well. When vehicle construction was complete, calibration of components, such as gyros, control surfaces and pressure cells was performed. Preliminary test run output data as well as input command signal data was recorded on stripcharts. Implementation of an analog-to-digital board and digital computer system for the remaining bulk of the test runs provided the necessary data banks for transfer function analysis. The 's' domain simulation model was determined. Two models were used. A simple third order model derived from the pitch equation of motion and a more complicated 4th order model derived when considering both the pitch and heave vertical plane equations of motion. These transfer functions were then multiplied by the applicable calibration constants and the equation coefficients determined. Equation coefficients consisted of linear combinations of hydrodynamic coefficients and vehicle speed. A zero order hold was used for transformation from the 's' domain to the 'z' domain. The sampling period was 0.05 seconds. Data analysis software, MATRIXX, was utilized to perform transfer function analysis.

## **II. CLASSICAL CONTROLLER DESIGN**

### **A. INTRODUCTION**

This chapter describes classical control techniques for operation of a vehicle, as well as providing the necessary model for data analysis. Classical control techniques should provide adequate control of the model; however, it is noted that this form of controller may not provide the best choice for actual AUV control. A model based controller or some form of adaptive control technique may be more beneficial from the viewpoint of maximizing performance at most or all possible vehicle speeds and environmental conditions. While the control system discussed here was not actually implemented on the test model vehicle, the discussion following is useful as it provides a framework for the implementation of a classical controller at a later date, and illustrates the necessary design trade-offs.

The controller design was based on the following guidelines.

- (1) Keep the system simple to facilitate its construction.
- (2) Based upon a selected reference speed of 1.0 ft/sec, optimize the controller to prevent overshoot of the vehicle beyond command depth.
- (3) Maintain control over commanded pitch angle. This should prevent loss of vehicle control when a large input command signal for depth is provided.

While dynamic tests were performed using direct control of the model control surfaces and motor speeds, it will ultimately be desired to test the vehicle by providing an input to an automatic control circuit. The control circuit would then generate a radio control signal to maneuver the vehicle.



This takes the man out of the loop and allows for evaluation of vehicle maneuvering characteristics without human control input. Although four independent control systems were designed; speed, depth, course and roll, the lack of time and availability of facilities limited this research primarily to pitch and depth response.

## B. DEPTH CONTROL

The basic concept drawing is shown in Figure 2 below.

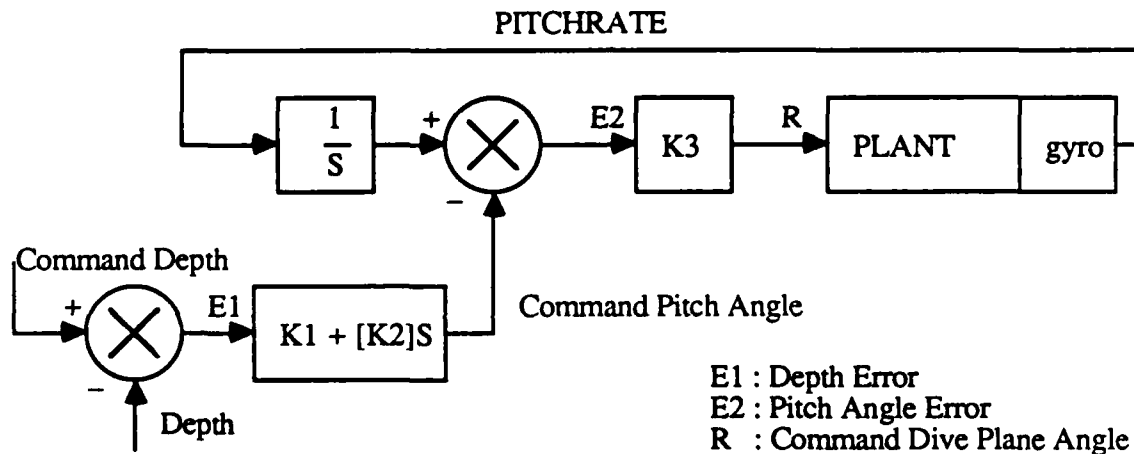


Figure 2 Depth Controller Block Diagram

In this system rate gyro output signal was integrated to provide the pitch angle. This angle was then compared to a command pitch angle. The command pitch angle was generated by comparing desired depth to actual depth as measured by the pressure cell. This depth error was then multiplied by a proportional gain and derivative gain. The derivative gain would provide the needed anticipatory response to minimize overshoot. The command pitch angle was designed to put the vehicle in an optimum dive

angle for a particular depth change requirement or error signal. The maximum dive angle was selected as 45 degrees. Command pitch angle and actual pitch angle are compared to generate a pitch angle error. This error was multiplied by a proportional gain to give a dive plane angle order. The maximum dive plane angle is 30 degrees. The forward and aft dive planes acted together during this testing but future designs might consider maneuvering characteristics utilizing only forward or aft dive planes, or unequal coupling between the dive planes.

In order to design and build the control system without knowing actual system characteristics, a simplified model of the plant was needed. A first order model approximation was made for the vessel motion in the vertical plane. Equation (1) shows the transfer function relation between dive plane angle,  $\delta$ , and pitch rate,  $\dot{\theta}$ .

$$K_y * \delta = (J_y S + B_y) * \dot{\theta} \quad (1)$$

As can be seen, the indirect hydrodynamic terms have been neglected as well as the bouyancy term which provides a resisting moment because of the offset between the center of gravity and the center of bouyancy along the vertical centerline. Based on the model vehicle design given in Chapter 3, an estimate of  $K_y$  was calculated by estimating the forces developed by the fore and aft dive planes and calculating the pitching moment that results. For a dive plane angle of 30 degrees and a vessel speed of 1 ft/sec, the lifting forces were calculated. The total forward dive plane area,  $A$ , is  $[9.50 * \sin(30)]$  square inches.

$$F_{bow} = \rho A V^2 \sin(\theta_{eff})$$

With  $\theta_{\text{eff}} = 15$  degrees,  $F_{\text{bow}} = 0.017$  lbf and  $F_{\text{stern}} = 0.48$  lbf. The forward moment arm was taken as 7.6 inches and the aft moment arm as 16.375 inches. This gives a total moment of about 0.9 in-lbf. Assuming linear response for dive plane moment vs. dive plane angle, the constant  $K_y$  is 0.14 ft-lbf/rad. Estimated values of  $J$  and  $B$  were determined. The closed loop transfer function  $G_\theta$  could then be formulated.

$$G_\theta = K_{py}K_y / \{J_y S^2 + B_y S + K_{py}K_y\}$$

$$\omega_n^2 = K_{py} * K_y / J_y$$

$$2\zeta\omega_n = B_y / J_y$$

Setting  $\zeta = 1.0$ , the value of  $K_{py}$  was determined to be 0.0107. This is a very small value of gain. The natural frequency gives an estimate of the period of 126 seconds. However, choosing a shorter period, say five seconds, yields a value for natural frequency of 1.2566, and a value of 6.8 for  $K_{py}$ .  $K_{py}$  relates pitch angle error to dive plane angle and must be selected based upon physical limitations of the plant. With  $K_{py}$  set equal to 0.7, which means a pitch angle error of 43 degrees calls for a dive plane angle of 30 degrees, the resulting value of circular natural frequency is 0.4 rad/sec and the period is 15.5 seconds. To change the natural frequency and hence, the period, the control variable  $K_y$  must be changed. This would require vehicle reconfiguration.

The value of damping coefficient estimated by linearizing about an angular rate of 1.0 rad/sec was 0.836 ft-lbf/rad. Since a larger value of damping means rate feedback may not be necessary, the control system design will assume that only a small amount of damping exists. A maximum limit on the magnitude of the rate feedback gain can then be set. When actual vehicle damping is determined the rate feedback gain can be adjusted

accordingly. Utilizing rate feedback ( $K_r$ ) around the plant, as shown in Figure 3, the transfer function now becomes:

$$G_\theta = K_{p_y}K_y / \{J S^2 + (B + K_r K_y)S + K_{p_y}K_y\} .$$

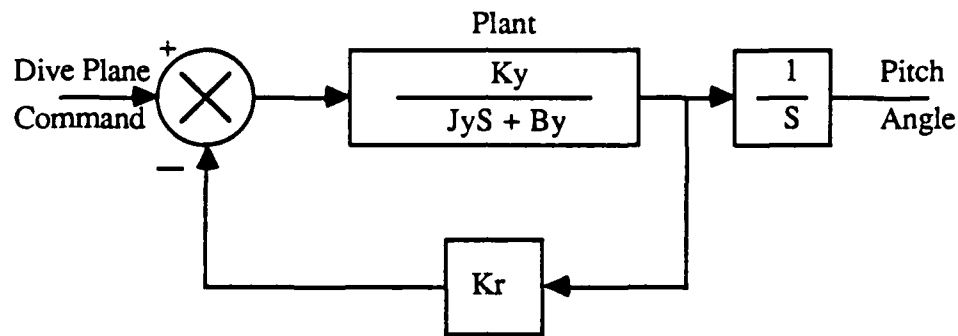


Figure 3 First Order Plant Model

For a damping ratio of 0.8, The value of  $K_r$  is found to be 2.31.  $K_r$  was set equal to 2.0. This gave an effective damping coefficient,  $B_{eff}$ , of 0.34 and a damping ratio of 0.708. The rate of change of depth is approximated as  $U \cdot \theta$ . Depth,  $z$ , can then be found by integration. The depth control system is shown in Figure 4.

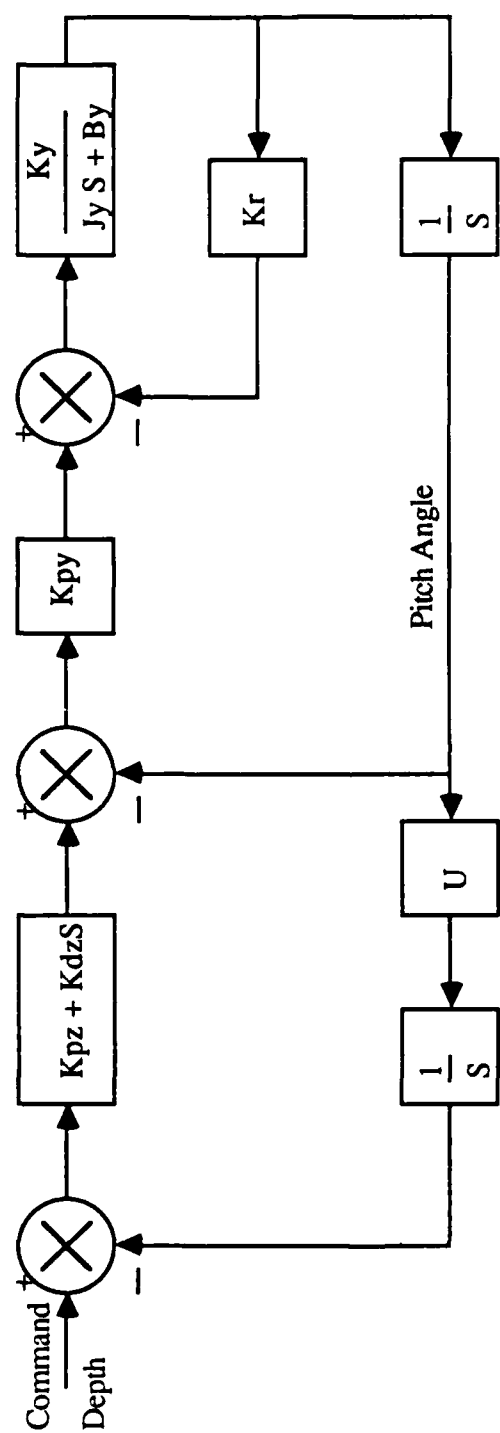


Figure 4 Closed Loop System Block Diagram

The effective damping coefficient,  $B_{eff}$ , is given by:  $B_y + K_r * K_y$ .

The closed loop transfer function is:

$$G_z = \frac{[K_{pz}K_yK_{py}U + (K_{dz}K_yK_{py}U)s]}{[Js^3 + B_{eff}s^2 + (K_{py}K_y + K_{dz}K_yK_{py}U)s + K_{pz}K_yK_{py}U]}$$

The steady-state error to a step input is zero. In order to meet the necessary conditions for stability the following requirements must be met,  $K_{dz} > -1/U$  and  $K_{pz} > 0$ . For  $K_{dz} = 0.0$ , Routh's Stability Criterion shows that  $K_{pz} < 2/U$ .

In order to gain an understanding of how stability would be affected by values of  $K_{pz}$  and  $K_{dz}$ , Root Locus plots, Figures 5 to 8, were made for two forward speeds and two values of proportional gain. The derivative gain,  $K_{dz}$ , was allowed to vary. These plots showed that increasing speed,  $U$ , or  $K_{pz}$  resulted in moving the poles closer to the imaginary axis. This indicates a reduction in system damping. A reasonable value of  $K_{pz}$  had to be chosen. This gain provides the proportional gain between the depth error and a command pitch angle. For a three foot depth change corresponding to a 45 degree pitch angle, a value of 0.26 for  $K_{pz}$  results.  $K_{pz}$  was set equal to 0.25. Root locus plots corresponding to this value of proportional gain are shown in Figures 9 to 10. A derivative gain of about 0.5 for a forward speed of 1.0 ft/sec indicates a damping ratio of about 0.4. The system is more complicated than a simple second order system because of the addition of the zero in the numerator. The position of the zero is determined by the ratio of  $K_{pz}$  to  $K_{dz}$ .

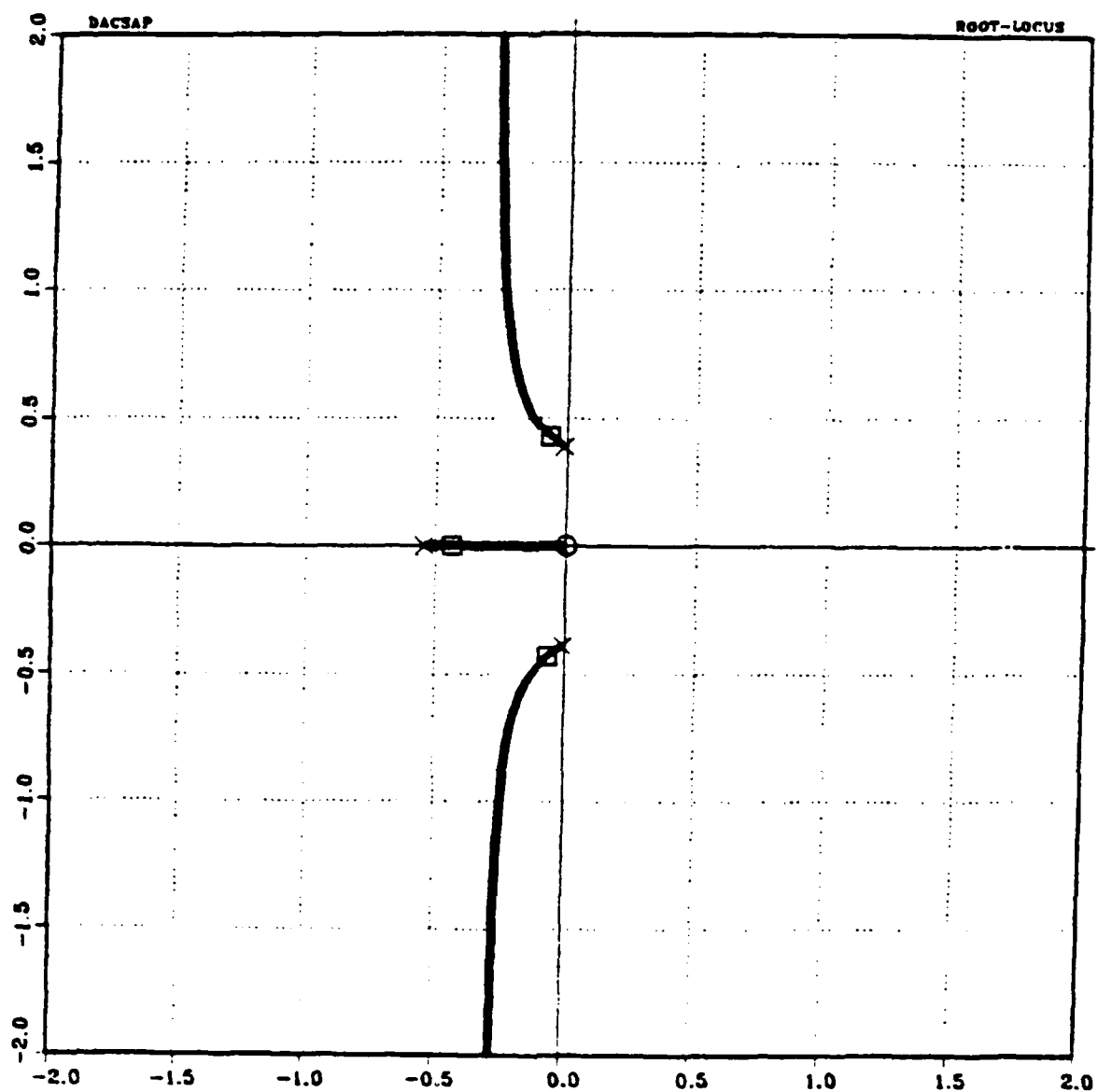


Figure 5 RLP[ $K_{pz}=1, U=0.5, K_{dz}$  Varied 0.0 to 100.0]

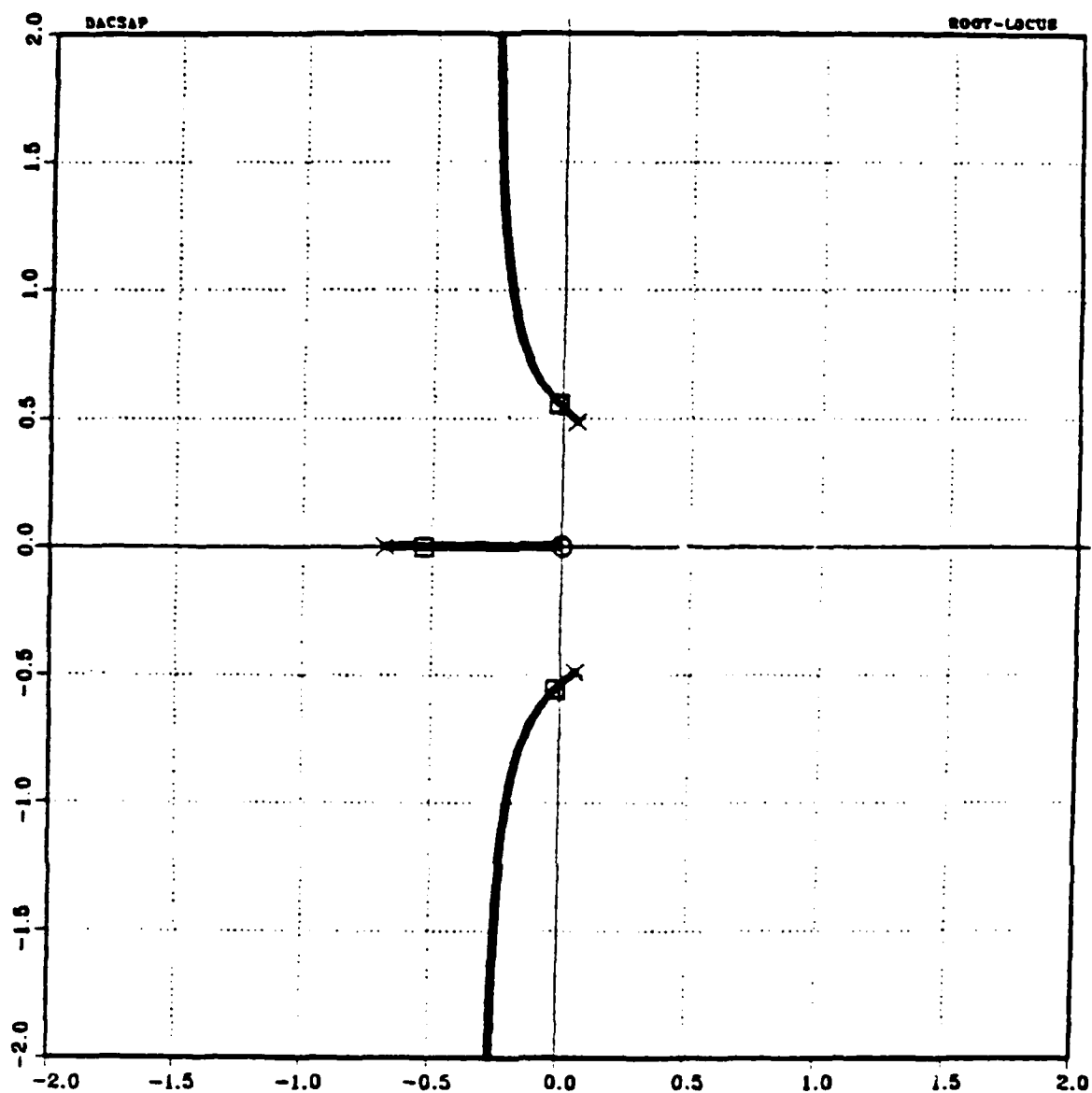


Figure 6 RLP[ $K_{pz}=1, U=1, K_{dz}$  Varied 0.0 to 100.0]



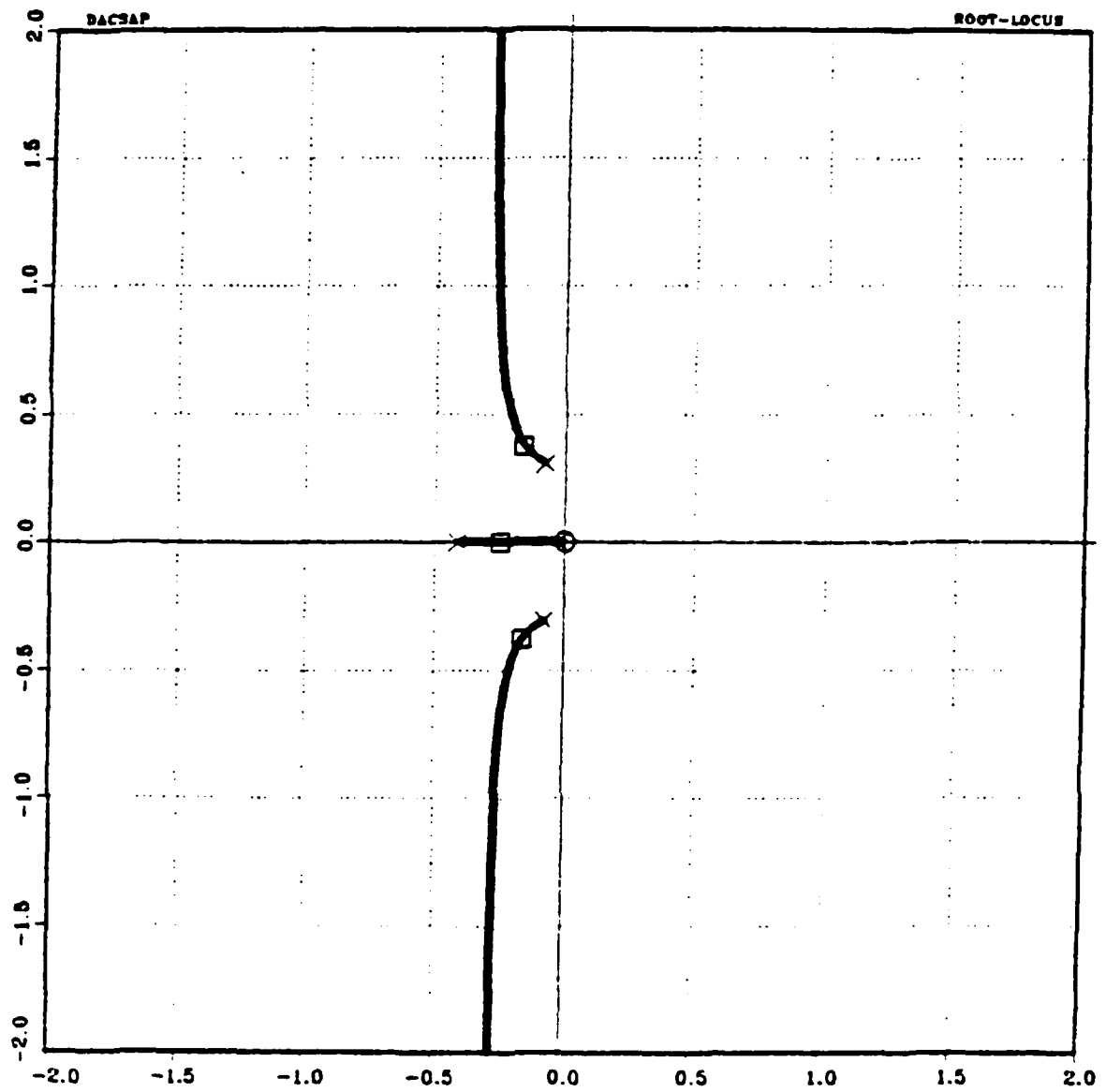


Figure 7 RLP[ $K_{pz}=0.5, U=0.5, K_{dz}$  Varied 0.0 to 100.0]

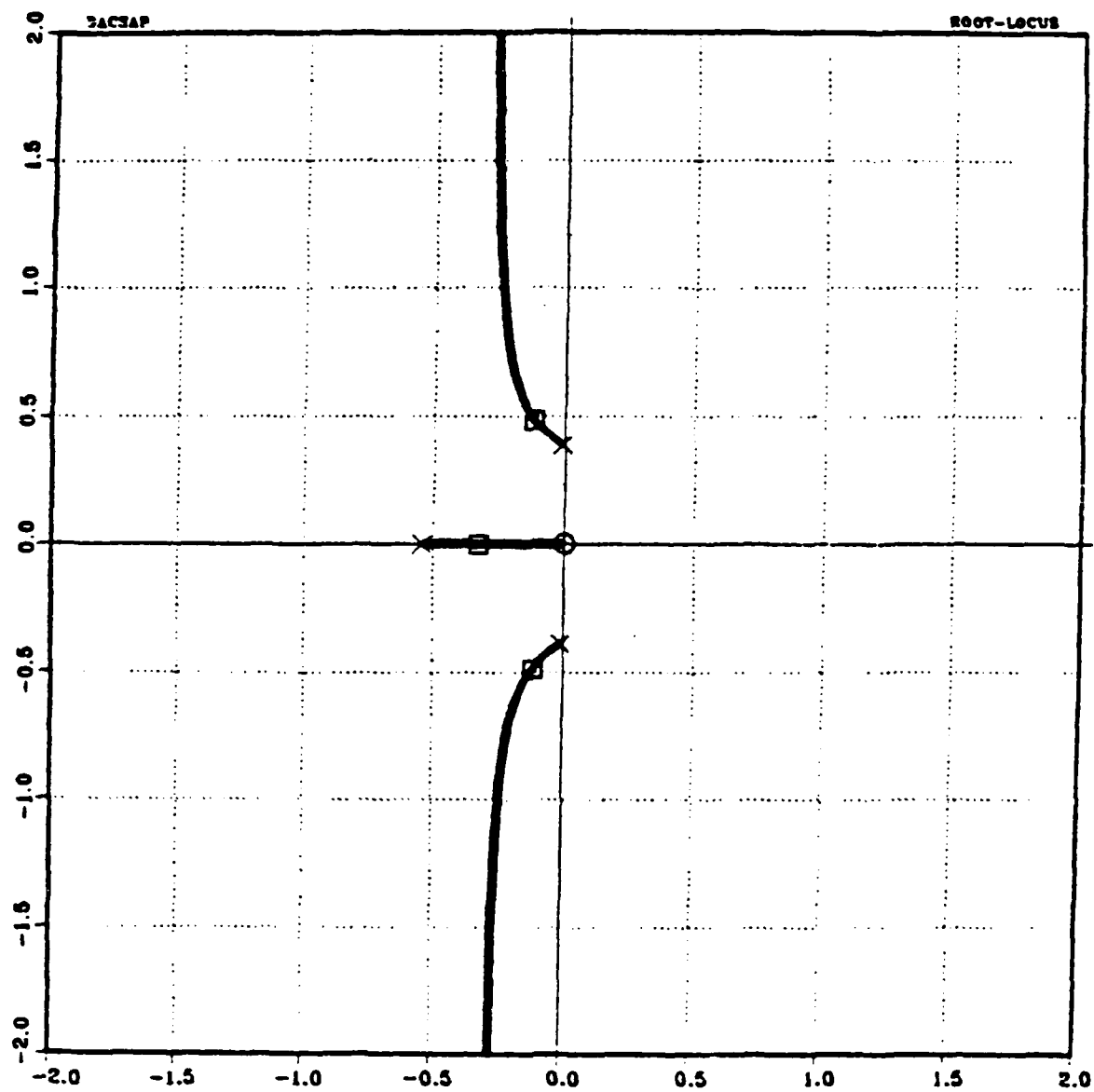


Figure 8 RLP[ $K_{pz}=0.5, U=1, K_{dz}$  Varied 0.0 to 100.0]

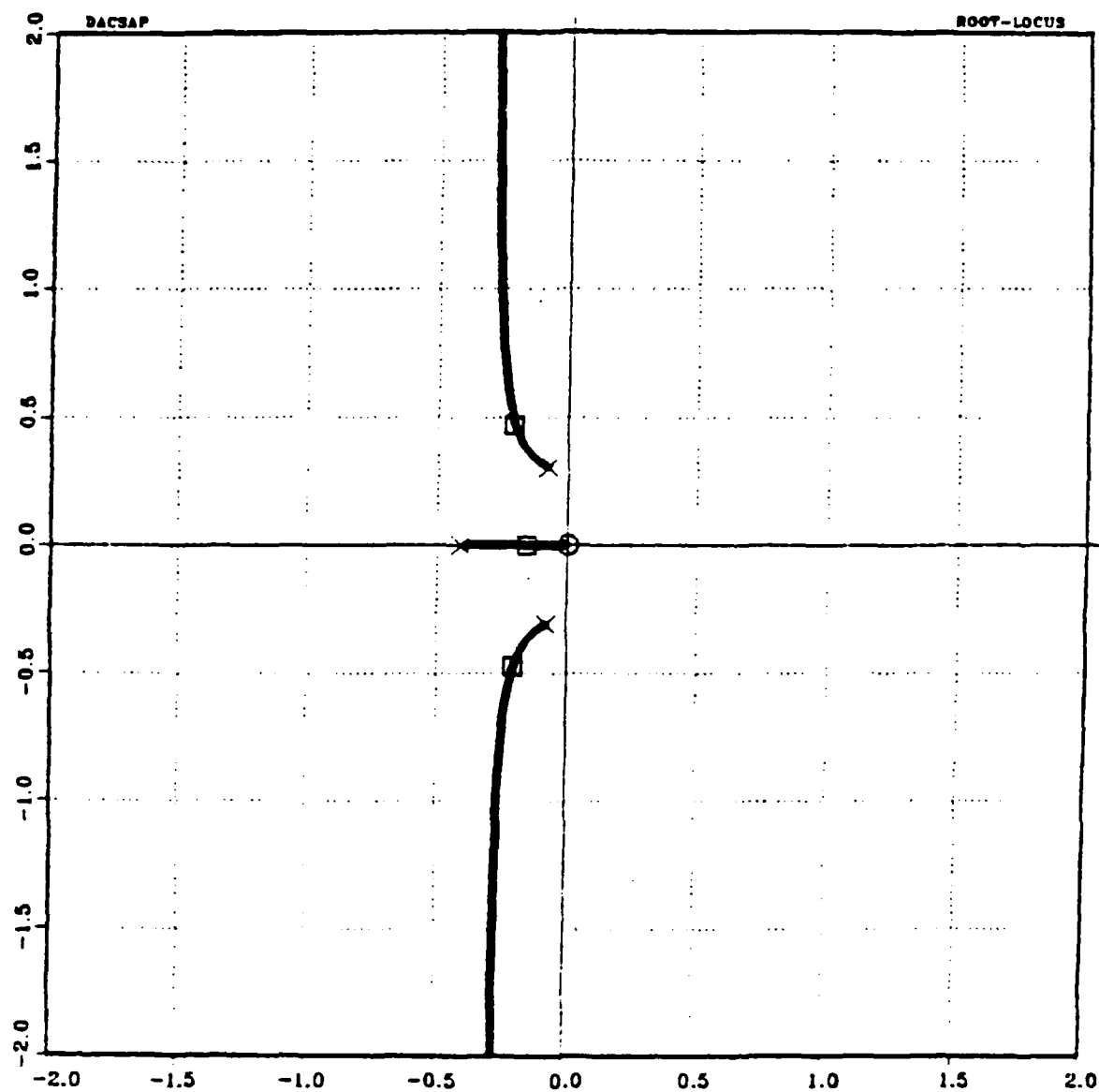


Figure 9 RLP[ $K_{pz}=0.25, U=1, K_{dz}$  Varied 0.0 to 100.0]

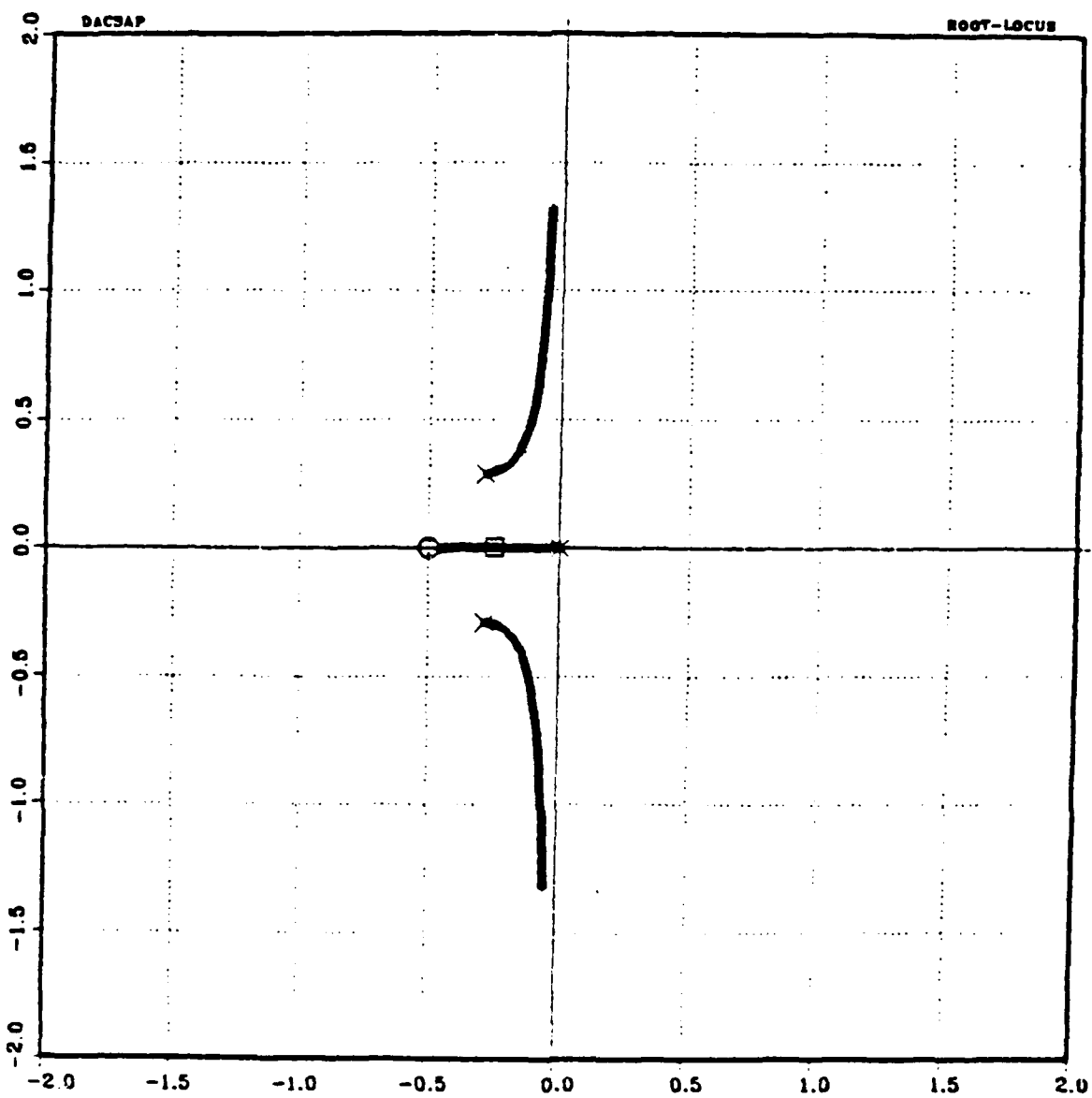


Figure 10 RLP[ $K_p=0.25, K_d=0.5, U$  Varied 0.0 to 20.0]

To get a better insight into the system response, the time responses were plotted for various values of derivative gain and forward speed. Figures 11 and 12 show that a larger derivative gain improves the response by reducing settling time, although overshoot increases. Without derivative gain the system model is unstable at speeds approaching three ft/sec as shown in Figure 13. Greater system damping is accomplished by adjustment of the rate feedback gain. Analysis of the vehicle equations of motion which follows later in this chapter, indicated that damping might actually be on the order of two times larger. A value of the effective damping coefficient was increased from 0.34 to 0.72. This corresponds to a value of rate feedback of about 4.71. A value of 1.50 for the damping ratio coefficient results. The root locus plot for the resulting transfer function is shown in Figure 14. Note the significant change in the character of the root locus. With the increase in system damping it is now possible to select a value of derivative gain which will provide a system damping ratio between 0.5 and 1.0. For a speed of one ft/sec, the derivative gain for zero overshoot is  $\cong 1.5$ . At a higher speed of three ft/sec, this value of derivative gain allows some overshoot. Figures 15 and 16 show the expected time responses to a step input of three feet in depth.

As expected, in classical control techniques the values of gain must change as the plant conditions change if optimum vehicle performance is to be maintained. This demonstrates the frequent need for adaptive control techniques or model based controller designs. For the purpose of model testing the classical controller is sufficient. A suitable set of gain values can be selected for the vehicle test speed. For completeness, the system root locus plot for zero derivative gain was considered. The simplest control system would consist only

of a proportional gain. Figure 17 shows that at high speeds, as expected, the system becomes unstable. A lower value of proportional gain gives a greater range of stability. Figure 18 shows the basic depth controller block diagram along with the corresponding analog controller.

### C. ROLL CONTROL

This section describes the method of approach for the design of the roll control system. Figure 19 shows the basic block diagram of the roll control system along with the analog equivalent. The output of the roll gyro is integrated for comparison to a command signal. The command signal would in most cases be equal to zero reference which is the horizontal plane. The error signal is then multiplied by a proportional and derivative gain. The derivative gain gives the desired anticipatory dynamic response. The output signal is the forward dive planes differential angle order. The dive plane response may be considered as analogous to the ailerons of an airplane. Rate feedback could also be used to provide a satisfactory system response. The system model was approximated by a first order system. Equation (2) shows the transfer function relation between forward dive plane angle,  $\beta$ , and roll rate,  $\dot{\Phi}$ .

$$K_X * \beta = (J_X S + B_X) * \dot{\Phi} \quad (2)$$

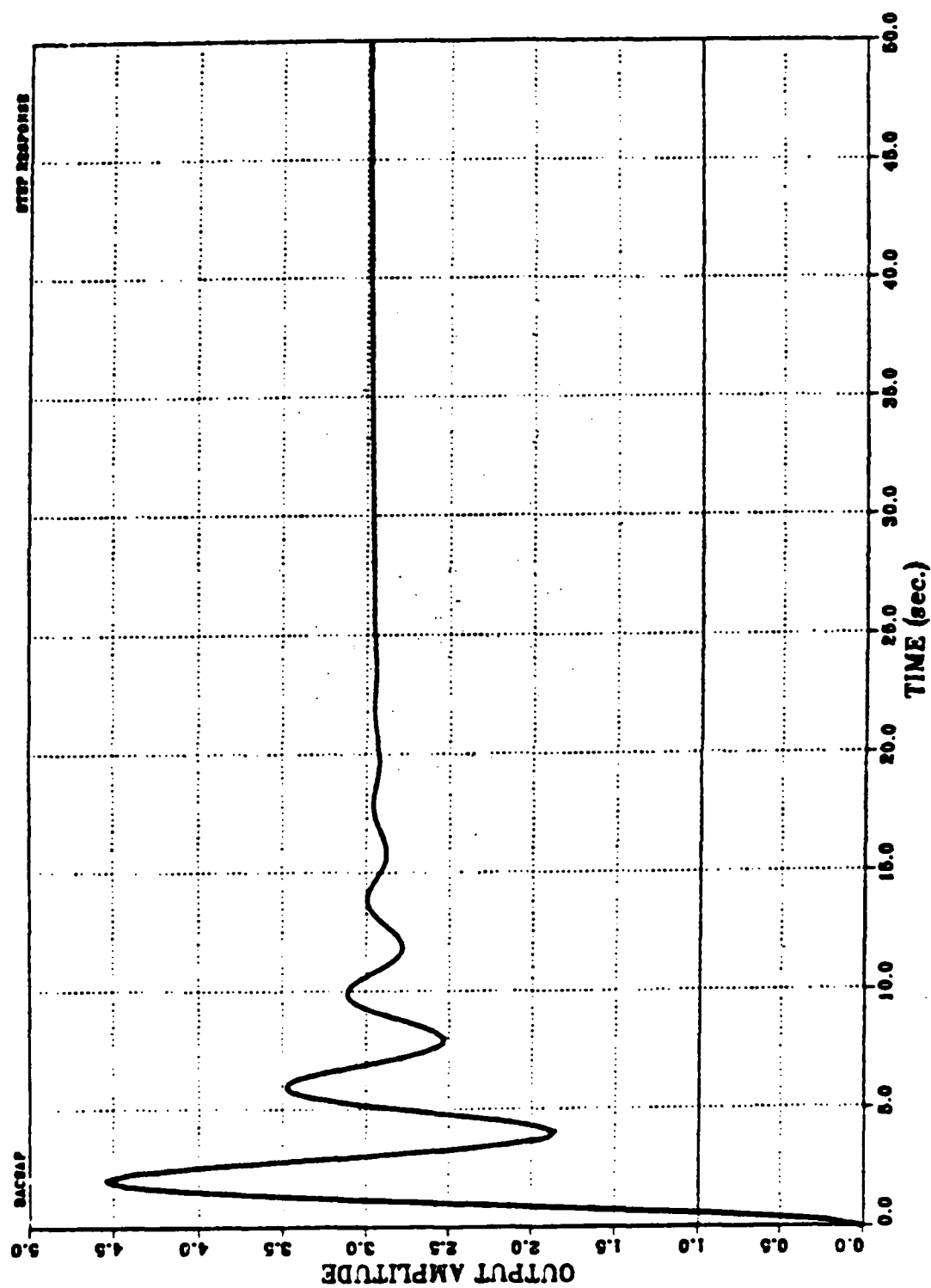


Figure 11 TR[Kpz=0.25,Kdz=5,U=3.0]

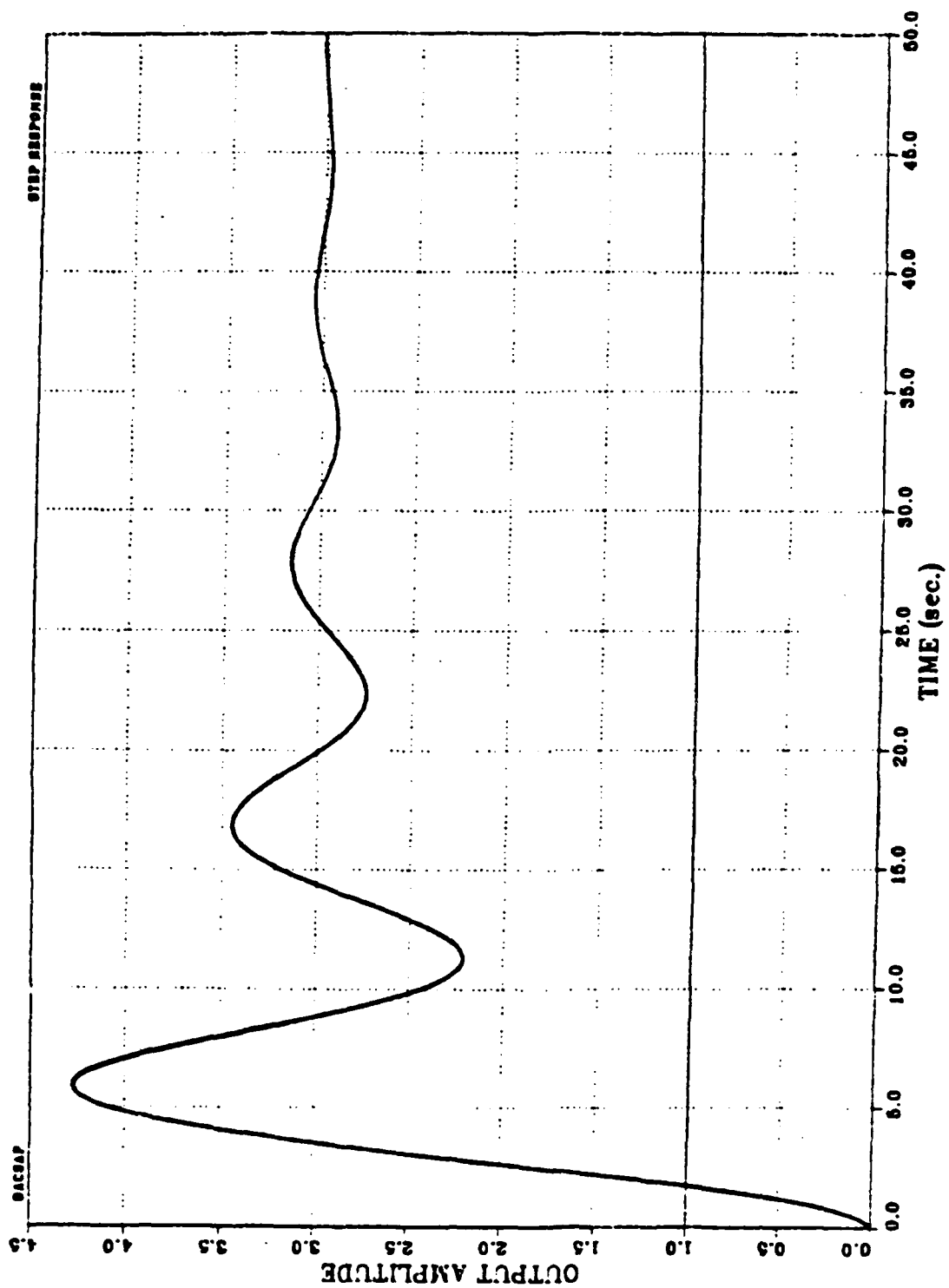


Figure 12 TR[Kpz=0.25,Kdz=0.5,U=3.0]



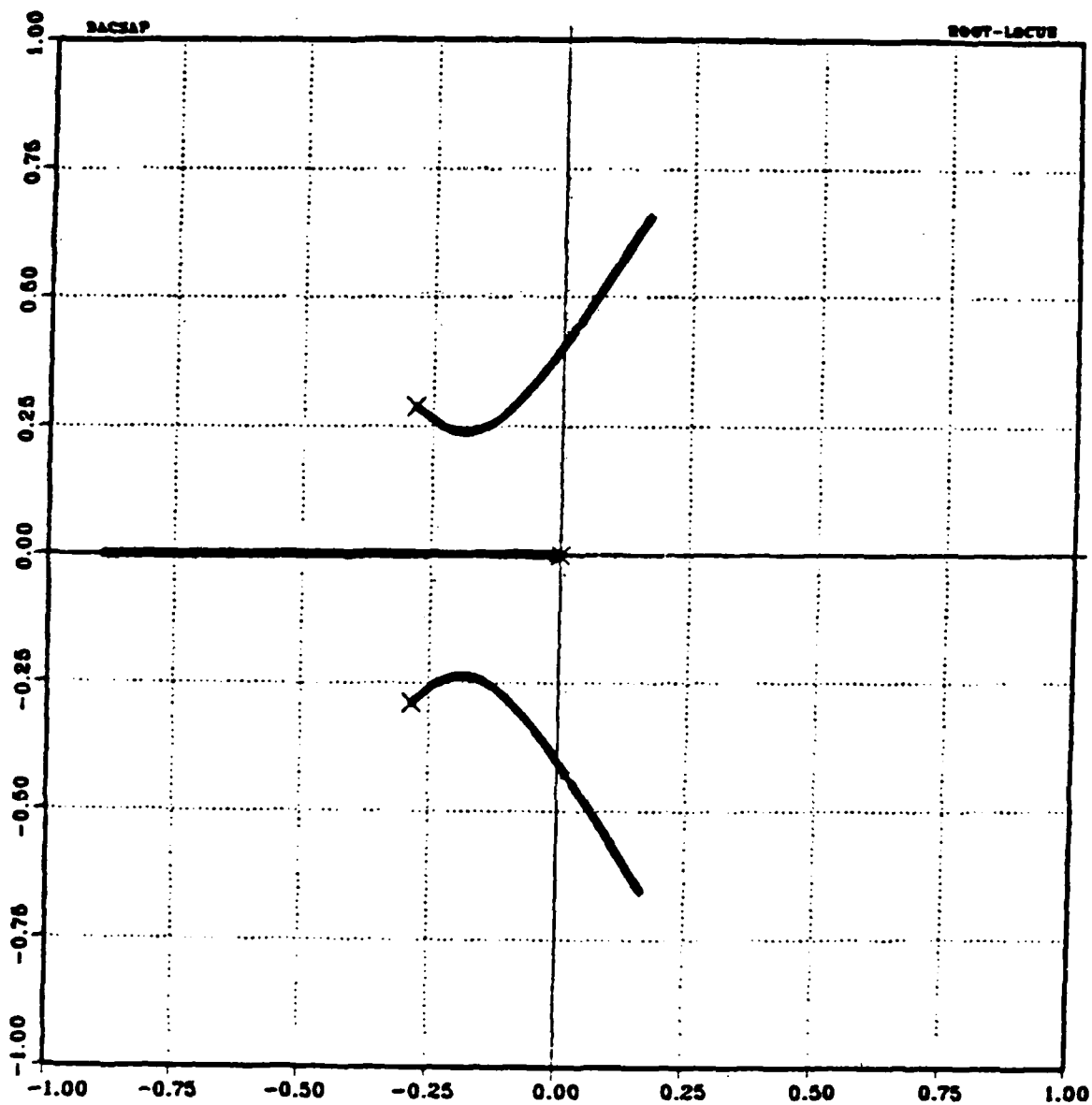


Figure 13 RLP[ $K_{pz}=0.25, K_{dz}=0, U$  Varied 0.0 to 10.0]

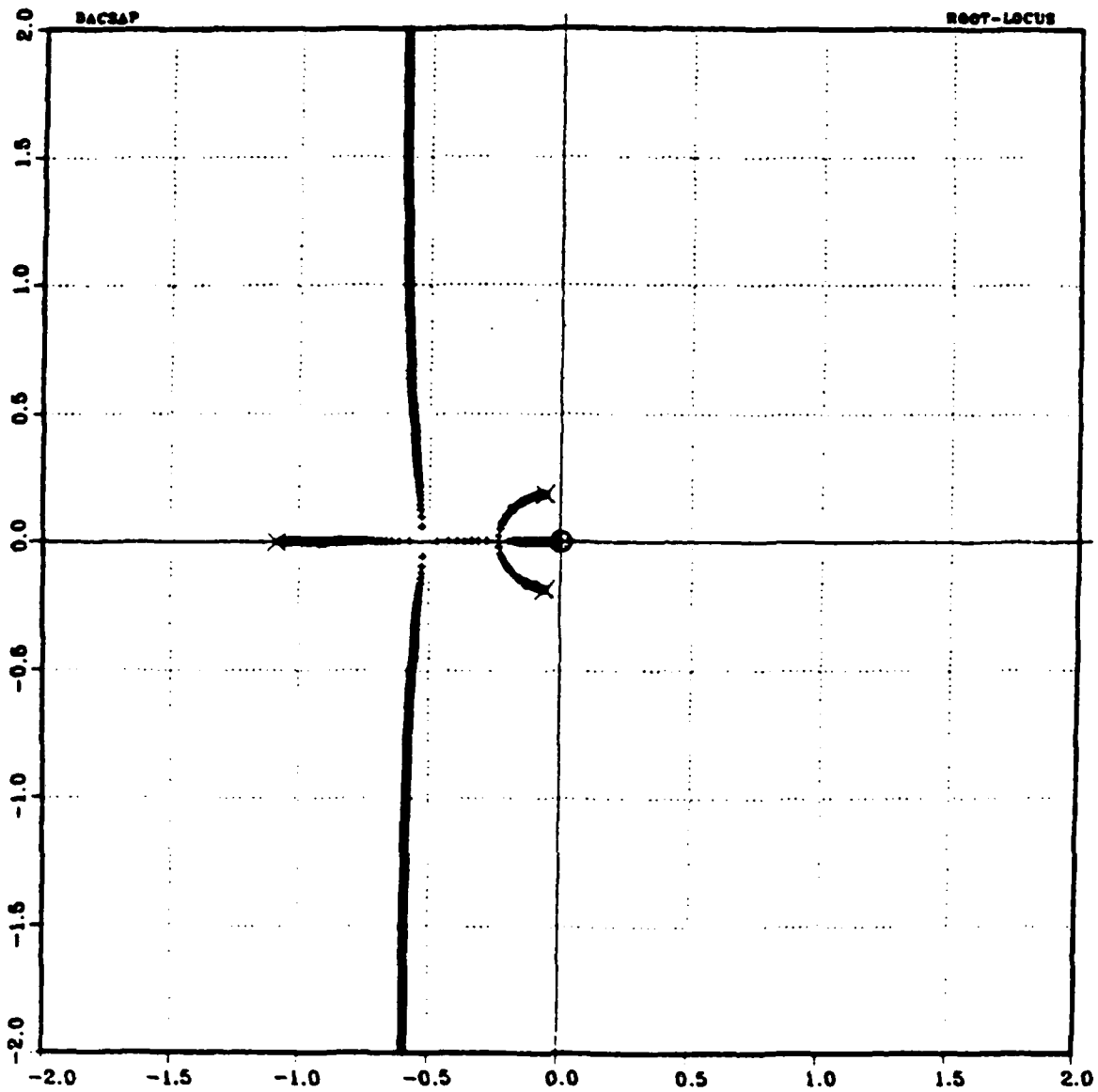


Figure 14 RLP[ $K_{pz}=0.25, U=1.0, K_{dz}$  Varied 0.0 to 100.0,  $B=0.72$ ]

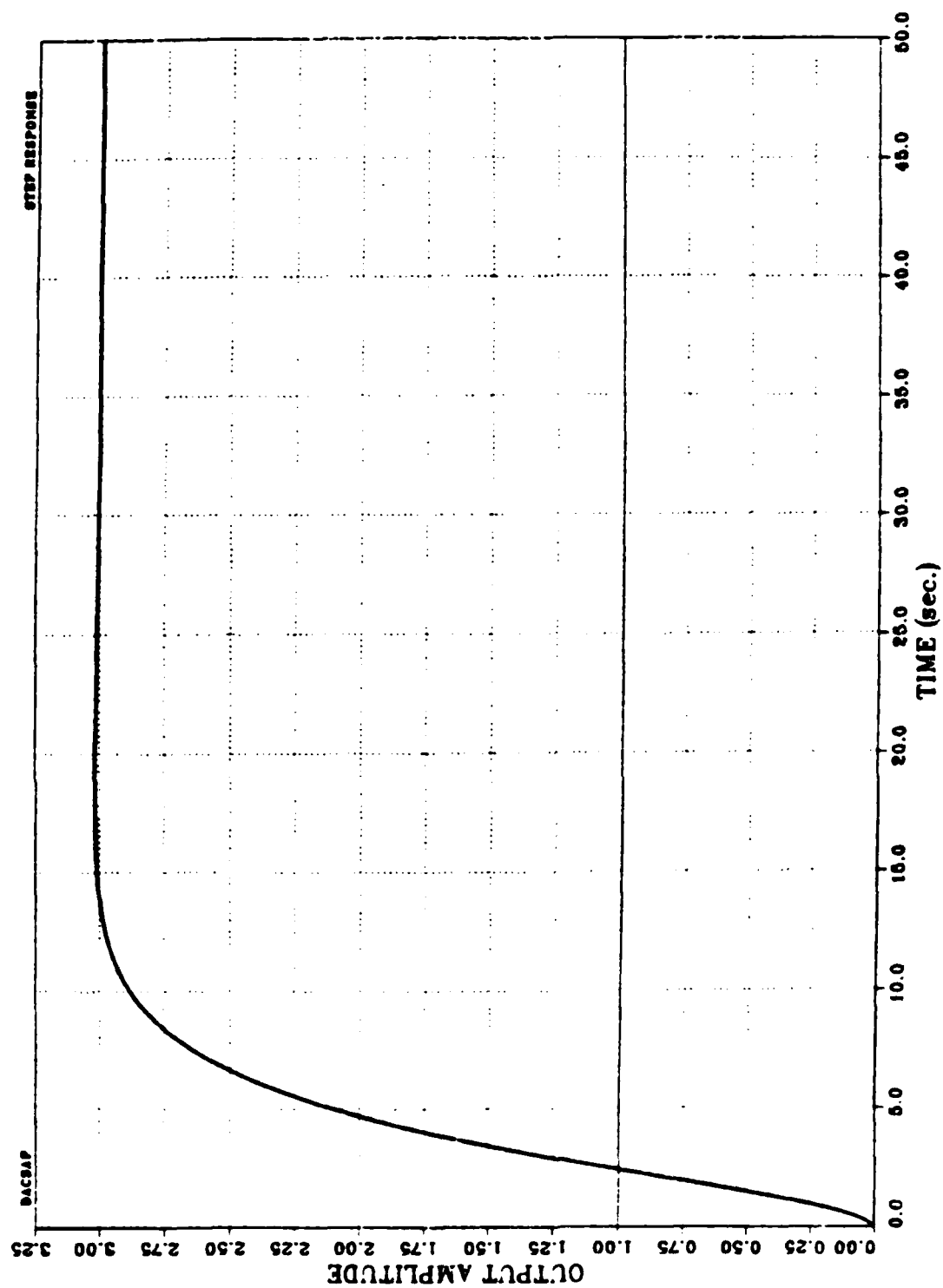


Figure 15 TR[Kpz=0.25,Kdz=1.5,U=1.0,B=0.72]

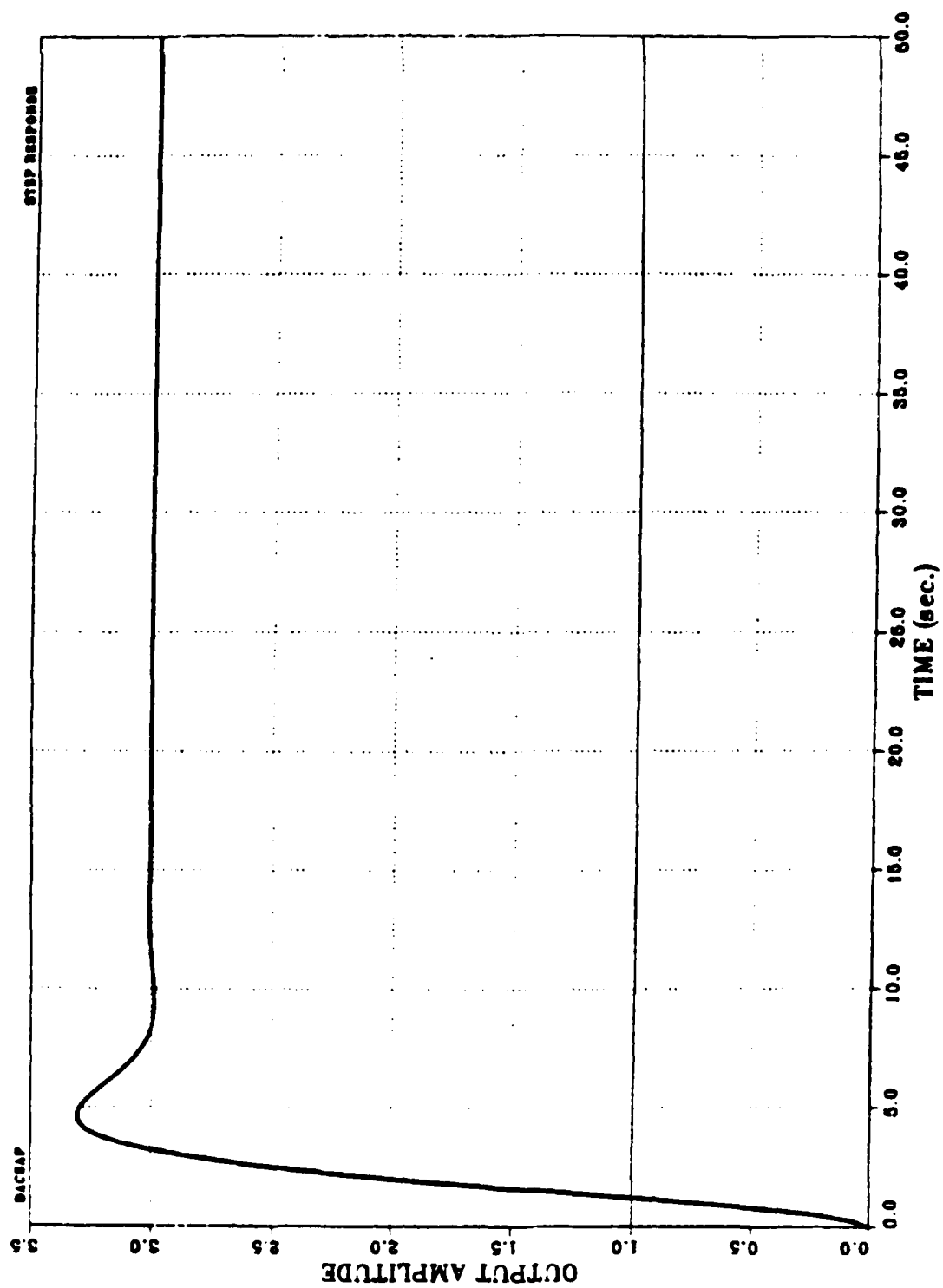


Figure 16 TR[Kpz=0.25,Kdz=1.5,U=3.0,B=0.72]

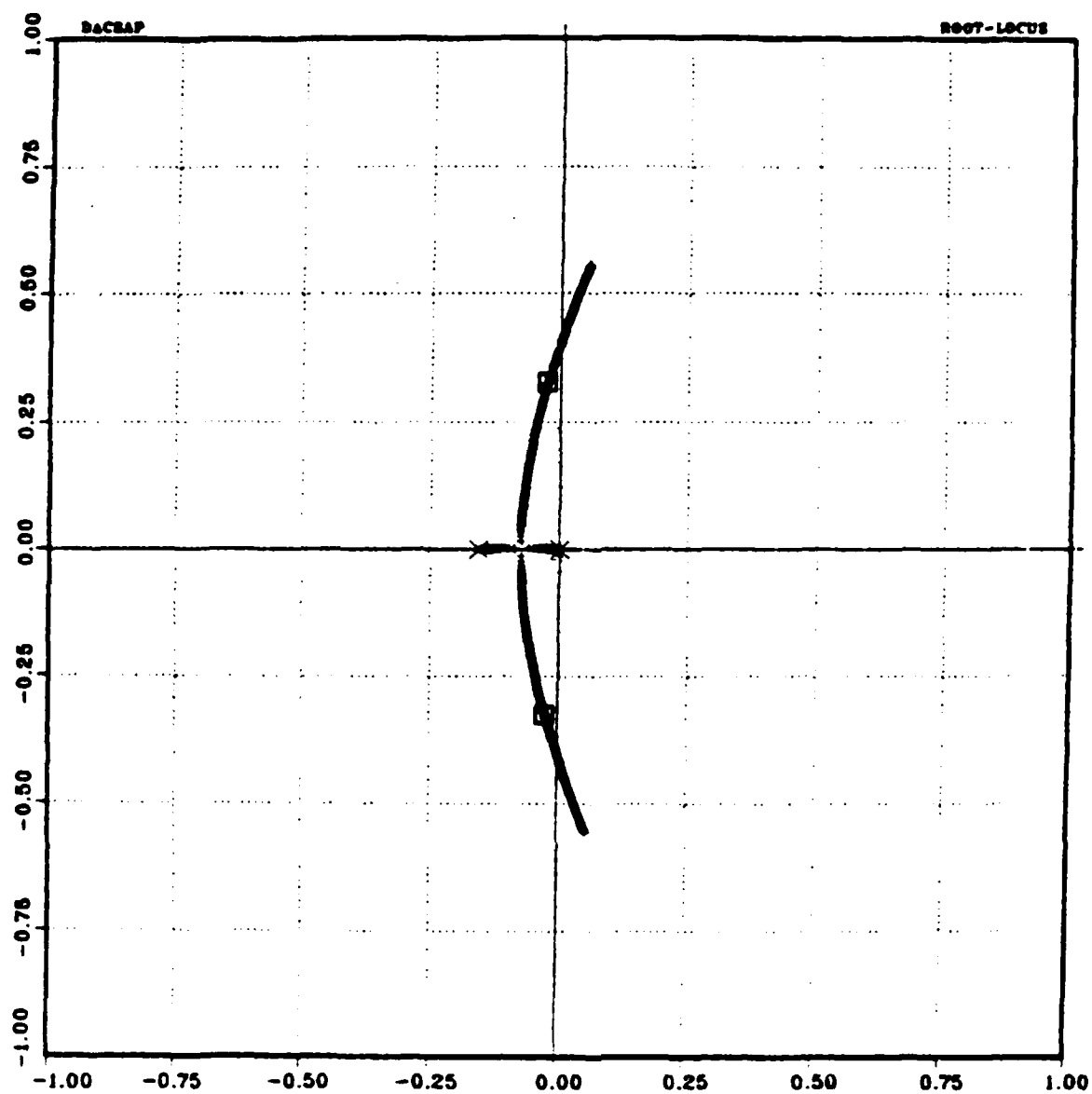
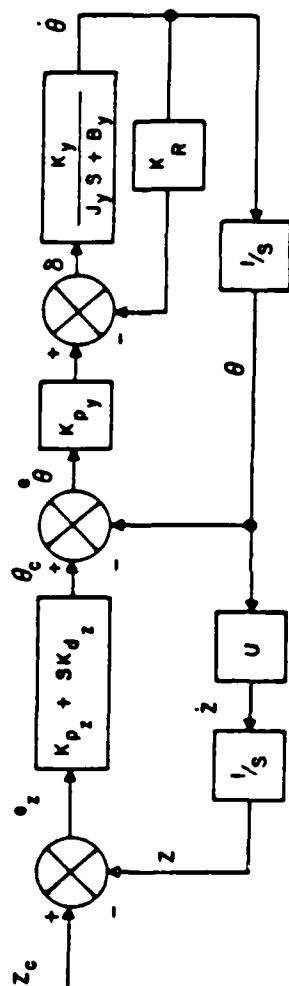


Figure 17 RLP[ $K_{pz}=0.25, K_{dz}=0.0, U$  Varied 0.0 to 10.0,  $B=0.72$ ]

# DEPTH CONTROL SYSTEM BLOCK DIAGRAM



## ANALOG CONTROLLER

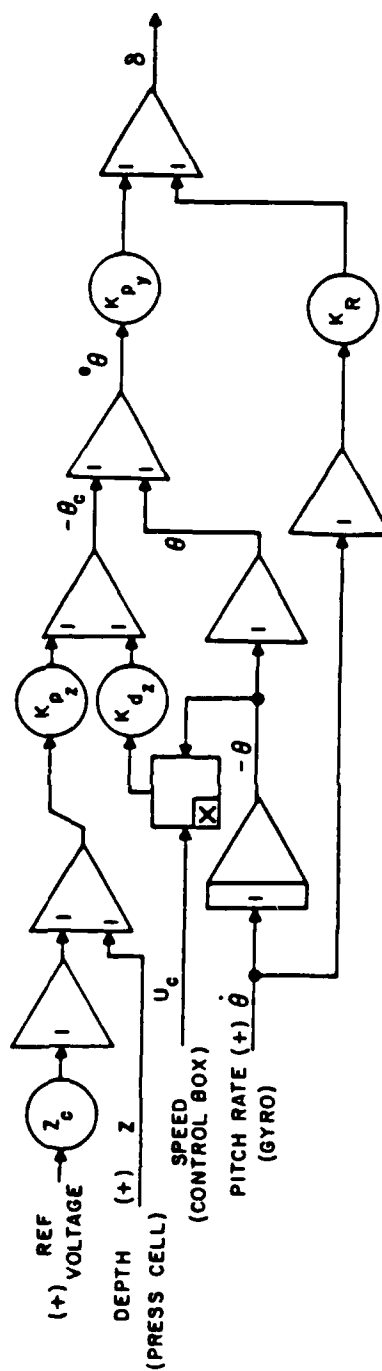
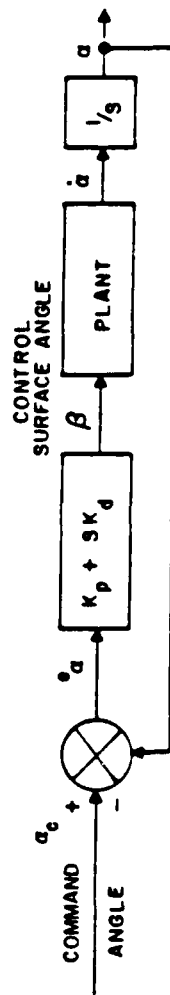


Figure 18 Depth Controller

# ROLL/YAW CONTROL SYSTEM BLOCK DIAGRAM



## ANALOG CONTROLLER

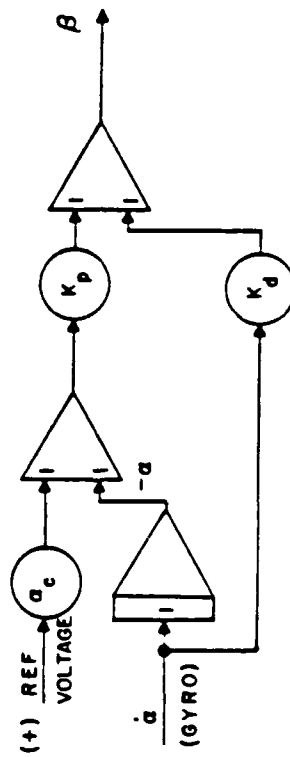


Figure 19 Roll/Yaw Controller

An estimate of  $K_x$  was made by assuming a linear relation between the dive plane angle and the roll moment. Assuming a forward dive plane total area of four in<sup>2</sup>, the force produced by a 30 degree dive angle while traveling at one ft/sec is approximated as:  $F = \rho A V^2 \sin(\Theta/2)$ . This gives a value of 0.014 lbf. With a moment arm of about nine inches, the moment produced is  $\cong 0.0105$  ft-lbf. Assuming torque is equal to a constant,  $K_x$ , times the angle  $\beta$ ,  $K_x$  is determined to be 0.02 ft-lbf/rad. With the plant now determined, the controller gains could be selected. The closed loop transfer function becomes:

$$G_{\Phi} = [K_x K_{p_x} + K_x K_{d_x} S] / [J_x S^2 + (B + K_x K_{d_x}) S + K_x K_{p_x}]$$

A reasonable value of  $K_{p_x}$  was selected. For a one degree roll error, a ten degree plane angle was chosen. Thus,  $K_{p_x} = 10$ .  $K_{d_x}$  could then be solved for as follows.

$$\omega_n = \sqrt{K_x K_{p_x} / J_x}$$

$$\zeta = B_{eff} / (2 \sqrt{K_x K_{p_x} J_x})$$

$$t_s = 4 / \zeta \omega_n$$

For a damping ratio,  $\zeta$ , of 0.9,  $B_{eff}$  was found to be 0.16. As a result,  $K_{d_x}$  is found to be  $\cong 8$ .  $K_{d_x}$  was set equal to 10.0. This gives an effective damping value of 0.201 and a damping ratio of 1.12. The natural circular frequency is 5.0 rad/sec. Utilizing a 2% settling time criterion, the settling time is about 0.7 seconds. When the restoring moment is added to the plant model,  $B_{eff}$  becomes 0.2,  $K_{d_x}$  equals 10.0, the natural frequency is 2.739 rad/sec, and the resulting settling time is 1.6 seconds. A root locus plot is shown in Figure 20.



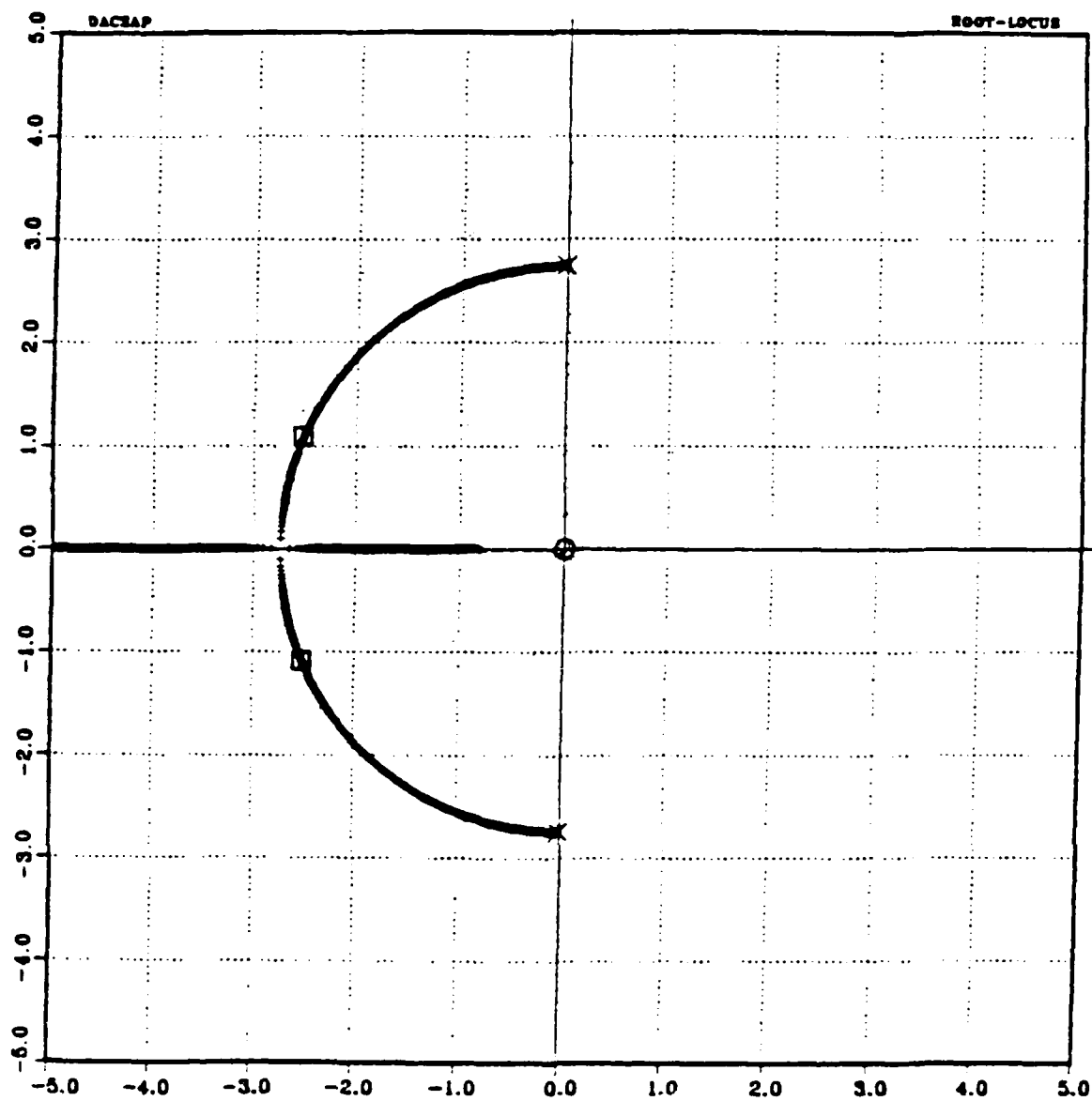


Figure 20 RLP Roll [ $K_{px}=10.0, M_{\theta}=0.1, K_{dx}$  Varied 0.0 to 20.0]

#### D. COURSE CONTROL SYSTEM

The course control system is similar to the roll control system. See Figure 19. The output of the rudder gyro is integrated to give course relative to an initial reference axis. The signal is compared to the command course signal and the error then provides the input to a proportional plus derivative controller just as in the roll control circuit.

The plant is again approximated as a first order system and is given by the following transfer function relating rudder angle,  $\delta_r$ , to yaw rate,  $\dot{\psi}$ .

$$K_z \times \delta_r = (J_z S + B_z) * \dot{\psi} \quad (3)$$

The rudder area is about the same as the aft dive plane area but the amount of rudder which is within the propellor propwash is less. The rudder force was only roughly estimated at about 0.03 lbf. The moment arm was estimated at 14 inches. Assuming a linear relation between rudder angle and force, a value of  $K_z$  was calculated to be about 0.07 ft-lbf/rad. Now, as before, the control system gains can be determined. The closed loop transfer function is given by:

$$G_\phi = [K_z K_{p_y} + K_z K_{d_y} S] / [J_z S^2 + (B_z + K_z K_{d_y}) S + K_z K_{p_y}]$$

A gain value of one was selected for  $K_{p_y}$ . Thus, for a one degree course error, a one degree rudder order would be generated. A higher gain would probably be desirable at lower speeds. For the purpose of estimating controller gains, a value of one was used. Using the same methods as before with a damping ratio of 0.9 arbitrarily selected,  $K_{d_y}$  was found to be 3.3.  $K_{d_y}$  was set at 3.0. This gives a value of damping of 0.828 and a 2% settling time of 10.0 seconds. A root locus plot is shown in Figure 21.

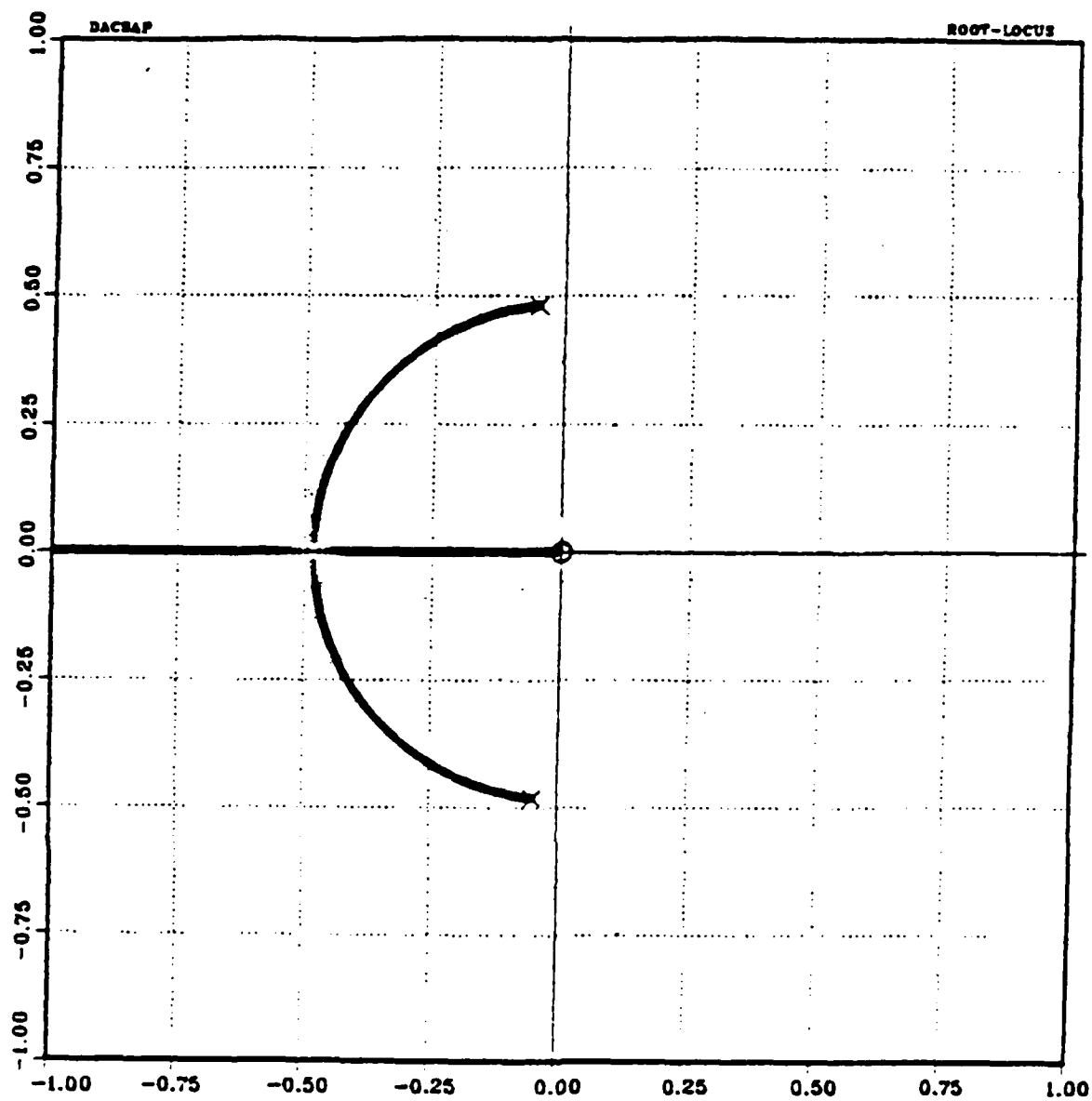


Figure 21 RLP Yaw[ $K_{py}=1.0, K_{dy}$  Varied 0.0 to 20.0]

## E. SPEED CONTROL

A speed regulator control system was designed to maintain a desired command speed. Figure 22 shows the basic block diagram. Command speed is compared to actual speed and an output error generated which is then amplified by a proportional gain. The amplified error signal is then summed with the command speed to produce the control input signal to the electronic speed control box. The electronic speed control was purchased from Vantec Inc. which specializes in speed controls for radio controlled models. It is fully proportional and designed to operate on 12 VDC input. Based upon the input signal voltage, the voltage applied to the drive motors is proportionally adjusted.

## F. EQUATIONS OF MOTION

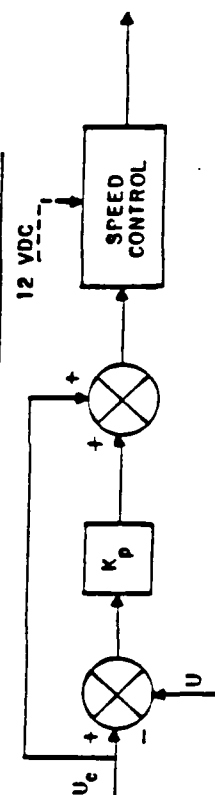
The following section concerns the theoretical calculations of the hydrodynamic coefficients for the vertical plane equations of motion for the model vehicle. Also, a comparison will be made between results of this simulation and the simplified model controller simulation previously conducted. The effects of discarding certain hydrodynamic derivatives from the simulation will be looked at. The equations of motion are given below.

The prime superscript indicates nondimensional values.

$$-Z'_w w' + (m' - Z'_{\dot{w}}) \dot{w}' - (Z'_q + m') q' - Z'_{\dot{q}} \dot{q}' = Z'_{\delta} \delta$$

$$-M'_w w' - M'_{\dot{w}} \dot{w}' - M'_q q' + (I'_y - M'_{\dot{q}}) \dot{q}' - M'_{\theta} \theta = M'_{\delta} \delta$$

# SPEED CONTROL SYSTEM BLOCK DIAGRAM



## ANALOG CONTROLLER

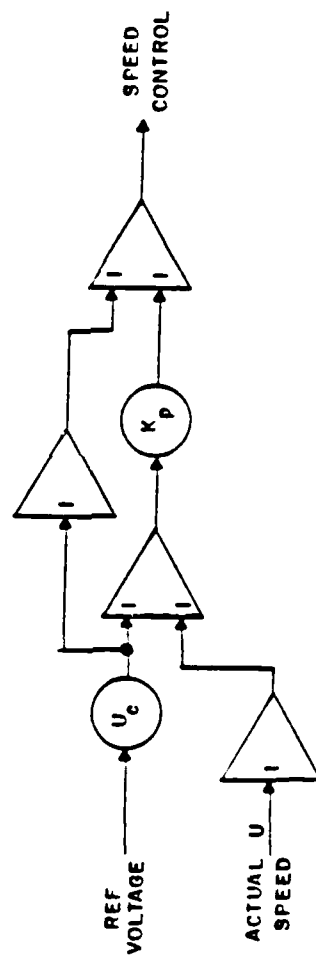


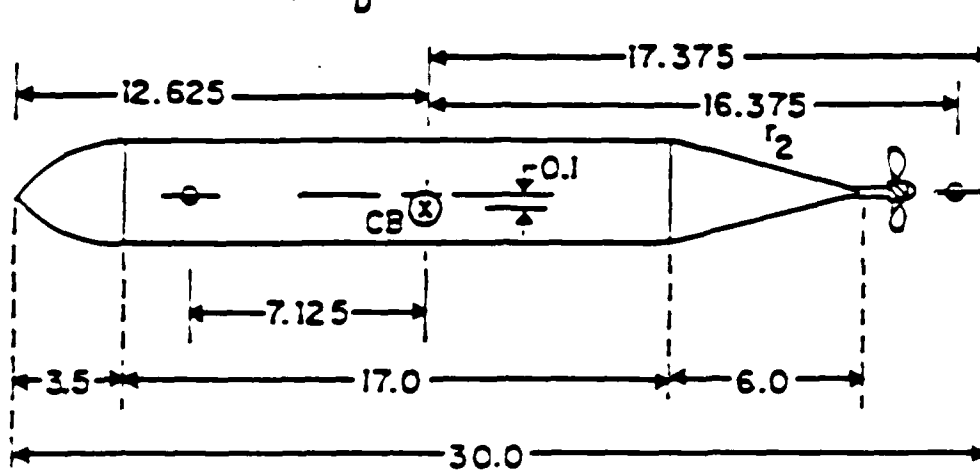
Figure 22 Speed Controller

The hydrodynamic derivatives in the vertical plane were estimated using the techniques described in Reference 8, Principles of Naval Architecture. The reference quantities used are given in Table 2 later in this section. The principle model dimensions are shown in Figure 23. Once the equations of motion were known, a Dynamic Simulation Language (DSL) program was written to provide a simulation of a depth maneuver for a given step change on the dive control planes. Several modifications to the general program were made. Various hydrodynamic coefficients were set equal to zero or adjusted in value in order to assess their importance. The principle program, T2, and the modified programs are shown in Appendix A.

A step change of +30 degrees at  $t=0+$  was input for 10 seconds and then removed. The first maneuver was carried out using both the heave equation and the pitch equation with all nonnegligable derivatives included. The program was then modified by removing the heave degree of freedom from the simulation. This left only the rotary inertia, damping and restoring moment hydrodynamic derivatives in the pitch equation. This is program T3 in Appendix A. Program T4 provides a simulation when only the rotary inertia and damping coefficients exist. The simplified control system analysis performed in the previous section assumes this type of plant. Program T5 is a simulation with both equations and all nonnegligable derivatives acting, but the rotary damping term is reduced by a factor of ten. The DSL simulation figures are located in Appendix B.

# PRINCIPLE DIMENSIONS

MODEL : WEIGHT,  $W = 19.6$  lbs  
 MASS,  $M = 0.609$  slugs  
 LENGTH,  $L = 30$  inches  
 BREADTH,  $B = 7.0$  inches  
 HEIGHT,  $T = 3.5$  inches  
 RESTORING ARM,  $BG = 0.1$  inch  
 DISPLACED VOLUME,  $V_D = 543$  in<sup>3</sup>



## DIVE PLANES:

### *FWD*

MOMENT ARM,  $r_1 = 7.6$  inches  
 MEAN CHORD,  $\bar{c} = 1.9$  inches  
 MEAN SPAN,  $b = 2.5$  inches  
 AREA (EACH),  $A = 4.75$  in<sup>2</sup>  
 GEOMETRIC ASPECT RATIO,  $a_g = 1.316$   
 EFFECTIVE ASPECT RATIO,  $a = 2.63$

### *AFT*

MOMENT ARM,  $r_2 = 16.375$  inches  
 MEAN CHORD,  $\bar{c} = 1.6$  inches  
 MEAN SPAN,  $b = 2.0$  inches  
 AREA (EACH),  $A = 3.2$  inches<sup>2</sup>  
 GEOMETRIC ASPECT RATIO,  $a_g = 1.25$   
 EFFECTIVE ASPECT RATIO,  $a = 2.5$

Figure 23 Principle Dimensions

1. Program T2 (All Derivatives)

Figures B1 through B3 show that the vehicle is directionally stable and is well damped. The step input in control planes produces a large initial angular acceleration with a corresponding rapid rise in linear and angular velocities. This results in a fairly rapid change in depth and angular position. Depth changes one foot in four seconds. The final depth reached is 2.61 feet. The oscillations apparent in angular position as well as linear and angular accelerations is a result of the restoring moment. This moment results from the offset along the vertical axis of the center of gravity from the center of bouyancy. Any angular inflections resulting from control plane action or distubances are resisted by this moment. Thus, when the control planes are restored to zero angle of attack, the vessel reacts to the restoring moment and returns to a level condition with respect to the horizontal. At low speeds this *restoring moment is significant*. If large, a considerable dive plane angle will be necessary to counter this moment and the pitch angle reached will be considerably less than if this moment were reduced. The moment is always there but at higher speeds it is less dominant in relation to the other hydrodynamic derivatives. These derivatives have a dependency on speed, while the restoring moment is a static effect. The nondimensionalized restoring moment coefficient becomes smaller as velocity increases because it is nondimensionalized with respect to velocity squared in the denominator. Steady-state conditions are reached in about four seconds from the step input in control plane movement.



## 2. Program T3

Figures B4 and B5 show the results of a maneuver when only the pitch equation is considered. The heave equation is neglected. Figure B5 shows that the angular velocities and accelerations seem not to be affected. The same response patterns occur as previously. The pitch angle achieved is slightly greater than that reached before. When the heave equation was considered a pitch angle of about -4.2 degrees was reached as was shown in Figure B1. Without the heave equation a pitch angle of about -4.4 degrees was reached as shown in Figure B4. This is because of the absence of the  $M'_{ww}$  term in the pitch equation.  $M'_{ww}$  is the derivative providing the moment which results as a consequence of linear velocity. The sign of this coefficient is positive while the sign of the restoring moment term is negative. This means these terms are working against each other; although  $M'_{ww}$  is small in relation to  $M'\theta$ . Thus,  $M'_{ww}$  could be adjusted by design of control planes and hull structure to partially offset  $M'\theta$ . The final depth achieved is about 1.77 feet. This demonstrates a 32% reduction in depth for the same dive plane movement. Figure B2 shows clearly that the linear velocity,  $w$ , is of significant proportion. This velocity is represented in the equation for rate of depth change,  $ZDOT$ , by the term  $wg \cdot \cos(\alpha)$ . Refer to computer programs of Appendix A. This linear velocity is a positive value; therefore, it adds to the velocity component which results from the forward velocity and the pitch angle.

## 3. Program T4

In this case the dive planes were held at +30 degrees for only one second. This was necessary to prevent the vessel from performing a loop

maneuver. With the restoring moment term removed, a steady state pitch angle cannot be attained as long as the control planes are at an angle of attack. This situation could be compared to a vehicle which has its center of gravity coincident with its center of bouyancy. With reference to Figure B6, although the dive planes are held at 30 degrees for only one second, a -27.5 degree dive angle is achieved. This shows that once the control plane angle is removed the vessel will stabilize as a result of damping to a steady pitch angle and continue to decrease in depth. This shows straight line stability but no directional stability as expected. Comparing the angular velocity and acceleration in Figure B7 to those reached in the case presented in Figure B3 indicates an increase in magnitude of at least a factor of two. This demonstrates the significance of the restoring moment. A vehicle whose design requirements might include stationkeeping (hovering) while maintaining other than a horizontal position may require this type of character to minimize power consumption. Careful control over position of the center of gravity in relation to center of bouyancy is needed to ensure adequate vehicle controllability.

#### 4. Program T5

In this program all hydrodynamic coefficients were restored but the value of damping was reduced by a factor of ten. A small value of damping had been assumed in the initial controller design. Figures B8 through B10 show the results. The same steady state depth is reached as expected. With the reduced damping, significant oscillations in pitch angle,  $\Theta$ , and in all velocities and accelerations are evident. The oscillations in depth will mean wasted power in a real vehicle and may hamper its operations as well. If

damping was a problem, an adequate control system must be designed to compensate for this by using techniques such as rate feedback and derivative control.

### 5. Calculation of Hydrodynamic Derivatives

Horizontal plane equations of motion were used as the source of the vertical plane equations used here. The direction of positive pitch angle,  $\Theta$ , is opposite in sense to positive yaw angle,  $\Psi$ , with respect to the 'z' and 'y' axes respectively. This requires sign changes in the indirect hydrodynamic coefficient equations. Table 1 is a listing of the coefficients. The indirect derivatives,  $Z'_{\dot{q}}$  and  $M'_{\dot{w}}$ , are generally quite small for most bodies. They have been assumed to be zero.

TABLE 1. HYDRODYNAMIC COEFFICIENTS

<u>Normalized Coefficient</u>	<u>Nondim Value</u>	<u>Dimensional Value</u>
$Z'_w$	-1.295	-0.8541 lbf-sec/ft
$Z'_{\dot{w}}$	-0.65	-1.00 lbf-sec <sup>2</sup> /ft
$Z'_q$	-0.20	-0.3078 lbf-sec
$Z'_{\dot{q}}$	0.0	0.0
$Z'_{\delta}$	+0.095	+0.0627 lbf
$M'_w$	+0.088	+0.1354 lbf-sec
$M'_{\dot{w}}$	0.0	0.0
$M'_q$	-0.20	-0.718 ft-lbf-sec
$(I'_y - M'_{\dot{q}})$	+0.072	+0.6 ft-lbf-sec <sup>2</sup>
$M'_{\theta}$	-0.106	-0.163 ft-lbf
$M'_{\delta}$	-0.184	-0.283 ft-lbf

In order to nondimensionalize the equation coefficients, reference dimensions must be selected. Although the model length is 30 inches overall, a value of 28 inches was used as the reference length. This length had been used during preliminary research of this vehicle shape to account for the rounding of the vehicle nose and the open spacing of the tail section in the vicinity of the rudders and dive planes. The reference mass is 1.539 slugs. The reference force is 0.6596 lbf. Table 2 and Figure 23 give a listing of principle dimensions and reference parameters.

TABLE 2. REFERENCE PARAMETERS

<u>Parameter</u>	<u>Value</u>
length, L	28.0 inches
mass, m	1.539 slugs
fwd velocity, U	1.0 ft/sec
height, T	3.5 inches
breadth, B	7.0 inches
force, F ( $m \cdot U^2 / L$ )	0.6596 lbf
moment, M ( $F \cdot L$ )	1.539 ft-lbf

a. Rotary Moment of Inertia Coefficient, ( $I_y - M \dot{q}$ )

From initial calculations, and verified by swing test data, it was determined that the moment of inertia in air was 0.2 ft-lbf-sec<sup>2</sup>. The added mass contribution was about 0.4 ft-lbf-sec<sup>2</sup> giving a total value of 0.6 ft-lbf-sec<sup>2</sup>. The nondimensional value becomes 0.072.

b. Drag Coefficient,  $Z_w$ , and Coupled Moment Coefficient,  $M_w$ , for Bare Hull

When a linear velocity in the 'z' direction exists in unison with a forward velocity in the 'x' direction, the hull will act as an airfoil under an angle of attack to the fluid stream. This is because the total velocity vector will be acting at an angle of attack to the hull. The aspect ratio of the hull was taken as the breadth to length of the bare hull, or  $B/L = 7.0/26.5 = 0.264$ . The Jones Formula was used to estimate the derivative of the lift coefficient. There will be some error at this value of aspect ratio when using this formula but it was considered sufficiently accurate for this simulation. Figure 41 of Reference 8, pg. 501, shows that the Jones Formula begins to lose accuracy at values of about 0.2 for aspect ratio. The force which results from a velocity in the positive direction of 'z' will be a resisting force and hence, negative in sign.  $Z'_w$  was found to be -0.83. For calculation of  $M'_w$ , equation 54 of Reference 8 was utilized. Approximating the model as an ellipsoid allows the determination of coefficients necessary to calculate the Munk moment. This moment is a result of the fact that an elongated ellipsoid body at some angle of attack in a nonviscous fluid will experience a couple which tends to increase the angle of attack. An equivalent diameter for the vessel was determined from the value of the cross-sectional area at the mid-section. This was taken as the length of an ellipsoid's minor axis. The bare hull length of 26.5 inches was taken as the length of the major axis. In this particular case, the point at which the force resulting from  $Z'_w$  acts is assumed to be aft of the mid-position of the hull. This is where it acts for a deeply submerged ellipsoid. The reason for this is the assumption that vortices will only be

formed on the downstream side of the tail section of the body, as is the case for the deeply submerged ellipsoid. For surface ships, the position at which the force acts is often taken to be forward of the mid-section. The sharpness of some ship's bows may generate vortices in a manner similar to the stern. The value of  $M'_w$  determined in this manner was +0.12. Alternately, the hull could be treated as an airfoil. This is not too bad of an assumption when considering the hull form of this particular vehicle. The distance aft of the nose at which the vertical force acts is assumed to be one quarter of the hull length. This results in a value of  $M'_w$  of +0.18. Since the value of +0.12 is more conservative, it was used in the simulation. The positive value indicates that downward (+z') motion results in a counterclockwise rotation.<sup>1</sup>

In the determination of  $Z'_w$  and  $M'_w$  for the control planes, values of the lift coefficient derivative were calculated by using equation 23 of Reference 8. The large values of aspect ratio for the control planes necessitates use of this method since the Jones' Formula can only be used with accuracy at values of aspect ratio less than about 0.2. The values of  $(Z'_w)_{f \text{ aft}}$  and  $(Z'_w)_{f \text{ fwd}}$  were added directly to the bare hull value. This gave a total value of -1.295. The moment coefficients which result from the fins were calculated by multiplying the direct derivatives by the moment arms through which they act. These moment arms were assumed to act from the center of gravity of the model to the center of pressure for the fins. The centers of pressure were assumed to be at one quarter of the mean span distance from the leading edge. The forward fins create a positive moment and the aft fins a

---

<sup>1</sup>Right hand coordinate system with positive 'x' axis moving to the right.

negative moment. The total value of  $M'_w$  is +0.088. The positive sign indicates this will be a stabilizing moment.

c. Rotary Damping Coefficient,  $M_q$

The method of estimating this term was to assume the vessel to have a block shape and was rotating about its centerline. Details of this approach are shown in the following chapter. The forces acting were found by assuming a  $V^2$  drag law where 'V' is the average velocity acting. The forces were assumed to act at the centroids of the velocity triangles thus giving a moment arm equal to two thirds of the length, L. A plot of moment vs. angular rate was made. This curve was quadratic in nature and was approximated with a linear curve. The slope of this line was taken to be the damping. This resulted in -0.06 ft-lbf-sec/rad, a very small value of damping. Nondimensionalized, this gives -0.02. The derivative of the quadratic curve evaluated at some point would also give a value of the damping coefficient. The question to answer is where on the curve should the derivative be evaluated. For the simplified controller simulation it was not critical since rate feedback was used in the control scheme to give adequate plant performance. For the DSL simulation the value of  $M'_q$  was found using the methods of naval architecture engineering as described in Reference 8. The value of the prismatic coefficient, needed to approximate the position where the bare hull linear force coefficient,  $Z'_w$ , is acting, was calculated to be 0.7915. A total nondimensional rotary damping coefficient of -0.20 results. This is a factor of 10 greater than the value found by the previous over-simplified method. For this reason, the DSL simulation was conducted for two values of  $M'_q$ .

d. Restoring Moment Coefficient,  $M'\theta$

This is a very important coefficient because of its effect in counteracting control plane induced moments. It also acts to return the vehicle to an upright, horizontal position when control induced moments are removed. The restoring moment arm which results from an angle of inclination,  $\Theta$ , will be the distance between the center of bouyancy and the center of gravity ( BG ) multiplied times  $\sin\Theta$ . A small angle approximation was used. This allows dropping the sine function. Taking the derivative with respect to the angle of inclination gives a value of the coefficient equal to the distance, BG. After nondimensionalizing,  $M'\theta$  equals -0.106.

e. Linear Added Mass Coefficient,  $Z'\dot{w}$

Reference 3 gives formulae for determining values of added mass for various 3-dimensional bodies. By assuming the model consisted of various shapes, the added mass values were approximated. The value of added mass,  $Dm$ , was calculated to be about 1.0 slug. This gives a value of  $Z'\dot{w}$  of -0.65.

f. Rotary Lift Coefficient,  $Z'q$

This term consists of components from the Munk moment, bare hull damping coefficient and the fin damping coefficients. It describes the net effect of applying a rotary motion to the model.  $Z'q$  was calculated to be -0.20. The minus sign indicates that positive rotary motion tends to lift the vehicle in the negative 'z' (upward) direction. This is an important result. When the vessel rotates in the negative pitch direction, such as when diving to



increase depth, the resulting linear force will be in the downward sense giving rise to an acceleration and velocity in the desired direction.

#### G. SIMPLIFIED CONTROLLER SIMULATION

The simplified controller simulation assumes a plant where the only hydrodynamic derivatives acting are  $(I'_y - M'\dot{q})$  and  $M_q$ . This plant is controlled using proportional plus derivative control techniques. Program T6 of Appendix C is a DSL simulation program that describes this controller. The proportional gains  $K_{pz}$  and  $K_{py}$  are set by design considerations of maximum desired commanded pitch angle and maximum dive plane angle available. Table 3 gives the correlation between variable names and values. Figure C1 shows the system block diagram and Figures C2 through C9 present the effects of varying the derivative gain,  $K_{dz}$ , from a low value of 0.25 to a high value of 1.0. The optimum value appears to be about 0.6. No overshoot occurs and the depth remains within 3.5% of command depth subsequent to the rise time of about 12.5 seconds.

TABLE 3. SIMPLE MODEL COEFFICIENTS

Controller Simulation	Value	Hyd Deriv	Value
$K_y$	-0.14	$M_\delta$	-0.283
$J_y$	0.6	$(I'_y - M'\dot{q})$	0.6
$B_y$ ( $B_{eff} = -0.34$ )	-0.06	$M_q$	-0.718

The simulation shows that the proposed controller technique should be adequate for this vehicle configuration. The next logical step in the

simulation is to add to the equations of motion the restoring moment, a stabilizing effect, and the heave equation contribution to depth change. This may remove the requirement for rate feedback and lower the value of derivative gain needed to prevent overshoot. Although the restoring moment will tend to reduce the achieved pitch angle for a given dive plane rotation, the value of  $M'\delta$  calculated using the techniques of Reference 1 is about twice as large as the value used in the controller simulation. As a consequence of substituting this larger value of  $M'\delta$  into the simulation equations, some compensation for the negative effect of the restoring moment term will occur. Further simulation studies are not necessary at this point since actual vehicle characteristics are expected to vary from theoretical predictions. It is noted that the DSL simulation presented in Appendix B indicated oscillations in pitch angle, accelerations and velocities even when all hydrodynamic coefficients were considered. Refer to Figures B1 through B3. Actual damping is expected to be larger than any calculated simulation value and along with the inertia coefficient, dominate vehicle response.

With the restoring moment acting, the revised closed loop transfer function becomes:

$$G_z = \frac{Z(s)}{\delta(s)} = \frac{(K_y K_{p_y} U)(K_{p_z} + K_{d_z} S)}{\{J_y S^3 + B_{eff} S^2 + [(K_y K_{p_y} + M_{\theta}) + K_{d_z} K_y K_{p_y} U] S + K_{p_z} K_y K_{p_y} U\}}$$

### III. DESIGN OF TEST MODEL AND FACILITY

#### A. INTRODUCTION

This chapter describes the methods used to determine the size and construction of the test model. The size of the test model was directly influenced by the availability and size of the test facilities. Some approximations were made with regard to design parameters and will be noted where appropriate.

#### B. MODEL SIZE

In order to facilitate handling and minimize construction costs, it was desirable to limit the size to something which was carryable by hand. The test tank size was the most important controlling parameter. To minimize the influence of tank sidewalls on the model hydrodynamic characteristics it was necessary for the model to have a maximum width not more than eight inches. The test model width, not including forward dive planes, was chosen to be seven inches. With forward dive planes the model width was eleven inches. The basic vehicle shape was chosen to be similar to that already being studied in related research. The breadth was set at twice the height and the length at roughly 7.5 times the height not including the screws, rudders or aft dive plane. Thus, the ratio of body dimensions,  $T * B * L$ , is  $1 * 2 * 7.5$ .

#### C. HULL FABRICATION

A durable but easily workable material was needed to build the hull. Several possible materials were: aluminum, wood, fiberglass, plastic. It was

decided that wood was not satisfactory since the vehicle has several penetrations and the main access cover would be removed periodically for controlling the operation and performing maintenance or adjustments. Because of ease of construction, and adaptation if weight became a problem, it was decided to use aluminum.

Hull thickness was determined by approximating the hull surfaces as flat plates under a uniform pressure distribution. Utilizing the following equation for stress,  $S = kwL^2/t^2$ , where;

$S$  = stress

$k$  = constant ( $\cong 0.5$ )

$w$  = uniformly distributed load

$L$  = length of plate

$t$  = plate thickness

with a design pressure of 5 psi ( $\cong 10$  ft. water depth) and a shear stress of 30,000 psi for aluminum, the minimum plate thickness could be calculated [Ref. 1]. The largest surface areas of uniform thickness are the upper and lower surfaces of the midsection. Because of bulkhead and joint construction needed to join the sidewalls to the upper and lower surfaces and to join the model sections together, an area less than actual vehicle dimensions was assumed. The length,  $L$ , was selected to be 16 inches and the width,  $b$ , 6 inches. Based upon the value of the ratio,  $L/b$ , of 2.67 the value of the constant,  $k$ , was chosen as 0.5 by rough interpolation of 'k' values in Table 20, pg 5-69, of Reference 1. Solving the above stress equation for 't' results in a thickness of 0.146 inches. Because of the already conservative design limit for depth of 10 feet, a slightly smaller but standard dimension of 1/8

inch was selected. From a fabrication viewpoint this thickness would also be relatively easy to work with.

A flexure formula for a flat plate with fixed sides was then used to determine maximum centerline deflection under load [Ref. 1].

$$\text{deflection, } \delta = k_1 w b^4 / E t^3, \quad k_1 = 0.028$$

Using  $E = 10 \times 10^6$  psi, the maximum flexure is about 0.01 inches. A 1/2 inch long boss is used for each forward dive plane. To prevent deflections of more than 0.001 inch at the boss, centerline deflection must be limited to 0.007 inches. The 0.001 inch is a design limit to minimize possible binding of the control shafts. The top of the midsection is the access cover for which deflection is not critical. There are no components mounted to it. As an added precaution to prevent midsection bottom deflection with corresponding possible component misalignment problems, strengthening beams were added. Utilizing the deflection equation for a beam with fixed supports from Reference 2, and assuming all load carried by the beams, the beam dimensions could be determined.

$$y = w L^3 / 384 E I, \quad y = 0.007 \text{ in.}$$

$$I = b h^3$$

$b$  = beam width

$h$  = beam height

$$E = 10 \times 10^6 \text{ psi}$$

$$L = 6 \text{ inches}$$

$$w = \text{load} = 5 \text{ psi} \times 6'' \times 16'' / (n+1), \text{ where}$$

$n$  = the number of beams

The variables are:  $n$ ,  $b$  and  $h$ . It was desirable to keep the height,  $h$ , of the beam as small as possible to minimize loss of internal space. The height selected was 0.25", or 1/8" thickness in addition to the skin thickness of 1/8". This results in a beam width of about one inch. Various numbers of beams were analyzed. As ' $n$ ' increases ' $b$ ' decreases, but the total beam cross-sectional area, and hence volume, increases. Since the design is already conservative, there was a desire to minimize weight. Two beams of cross-sectional area equal to 0.25" x 1.00" were added.

#### D. CALCULATION OF DISPLACEMENT AND FIRST-ORDER SYSTEM COEFFICIENTS

The forward section has parabolic plane sections as viewed from top and side. An approximation of the volume was made by assuming a prismatoid shape. Thus,  $V_f = h(B_1 + 4M + B_2)/6$  where;

$V_f$  = volume of forward section

$B_1$  = area of lower base

$M$  = area of midsection

$B_2$  = area of upper base

resulting in a volume of approximately  $37 \text{ in}^3$ . The midsection volume was  $17 * 7 * 3.5 = 416.5 \text{ in}^3$ . The stern has a triangular cross-section, as viewed from the side, and has a volume of  $73.5 \text{ in}^3$ . This gives a total volume of  $527 \text{ in}^3$ . Using a specific weight of water of  $62.4 \text{ lbf/ft}^3$ , the displaced weight is about 19 lbf. With the weight of each section and the point through which it acts known, the center of bouyancy, CB, was estimated for the model. The CB was found to be 0.7 inches aft of the geometric center of the midsection.

An initial approximation of the model mass moments of inertia in air were made by assuming the basic shape of a rectangular parallelepiped. The formula for this shape is:  $J = m(b^2 + l^2)/12$ . The following values were obtained using effective dimensions of 3.5" \* 24" \* 7". The length of twenty-four inches was selected in order to account for the rounded nose section and the low mass per unit area of the last four to five inches of the stern section.

$$J_{ym} = 0.201 \text{ ft-lbf-sec}^2$$

$$J_{xm} = 0.021 \text{ ft-lbf-sec}^2$$

$$J_{zm} = 0.213 \text{ ft-lbf-sec}^2$$

Added mass values for each axis of rotation were determined by approximating the model as a rectangular box in each plane of motion. Reference 3 gives added mass equations for three-dimensional rectangular shapes. When determining pitch moment a value of twenty-eight inches was assumed for the length. This helps to account for the dive planes. For a square plate of side length, A, and thickness, B, the added mass equation is  $\Delta m = k\rho A^2 B$  where 'k' is dependent upon the ratio B/A.

<u>B/A</u>	<u>k</u>
0.5	1.32
1.0	0.70
2.0	0.35

The added mass in pitch was calculated by assuming four blocks of 7" \* 7" \* 3.5". This gives each block a B/A ratio of 0.5. The total added mass value for the four blocks was calculated to be 1.016 slugs. An added mass moment of inertia value for pitch was then calculated to be about 0.490 ft-lbf-sec<sup>2</sup>. This gives a total mass moment of inertia,  $J_y$ , of 0.691 ft-lbf-sec<sup>2</sup>.

Because of the crude approximations and expecting the actual vehicle shape to have an added mass below this value,  $J_y$  was set equal to 0.60 ft-lbf-sec<sup>2</sup>.

The added mass terms for the other two axes were determined in the same manner. Results are summarized in Table 4.

TABLE 4. TOTAL INERTIA FOR 'X' AND 'Z' AXES

Axis	Block Dimensions	B/A Ratio	# Blocks	$\Delta M$ (slugs)	J (ft-lbf-sec <sup>2</sup> )
z	3.5*3.5*7.0	2.0	7	0.236	0.30
x	3.5*3.5*3.5	1.0	14	0.472	0.04

Values of viscous damping were calculated by assuming flat plates in uniform flow streams. A drag coefficient for a plate normal to the flow was assumed to be 1.2 [Ref. 4]. The drag force for a plate rotating about its centerline was assumed to be of the form  $\frac{1}{2}\rho AV^2 C_D$ . The average plate velocity was used in this equation. The rotation is assumed to produce a couple acting through the centroids of the triangular velocity distributions located on each side of the center of rotation. This gives a moment arm, 'r', equal to two thirds of the plate length. In terms of the angular velocity,  $\alpha$ , the linear velocity is  $r*\alpha$ . This results in an expression for the moment due to viscous damping of the form;  $N = C * \alpha^2$ . Then the damping term is equal to  $C * \alpha$ . For a first approximation of damping, the value of  $\alpha$  is determined by plotting the moment vs. angular rate and then approximating the resulting quadratic relation by a linear one. The slope of the linear approximation is



the value of damping. The average value of velocity used in the drag force equation is given by  $v_{avg} = \frac{L}{4} * \alpha$ . This gives a final form for the moment equation in terms of the angular rotation rate,  $\alpha$ .

$$N = \frac{\rho C_D A L^3 \alpha^2}{96}$$

The variable 'A' is the total plane area. As shown in Figures 24 through 26 the resulting values of damping will be quite small. The damping coefficients are the values of slope for the linear curve approximations, divided by 100 to account for the scale factors. This is a crude method of approximating damping.

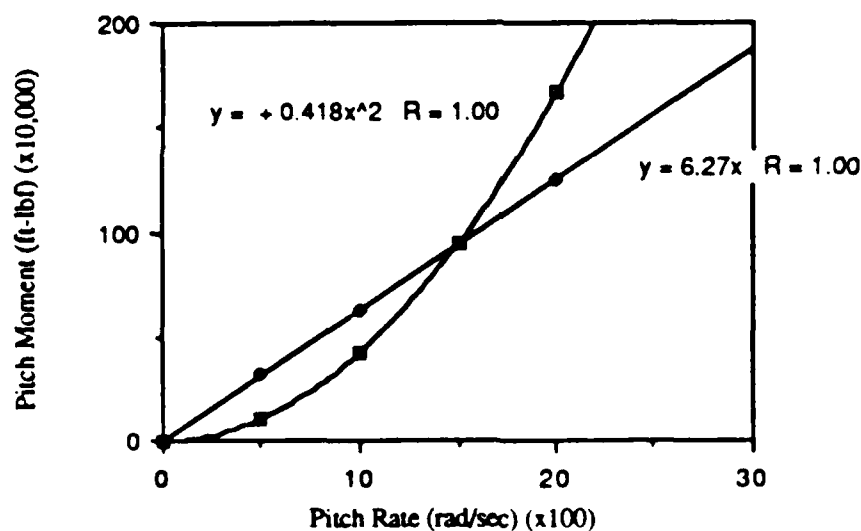


Figure 24 Damping About 'Y' Axis

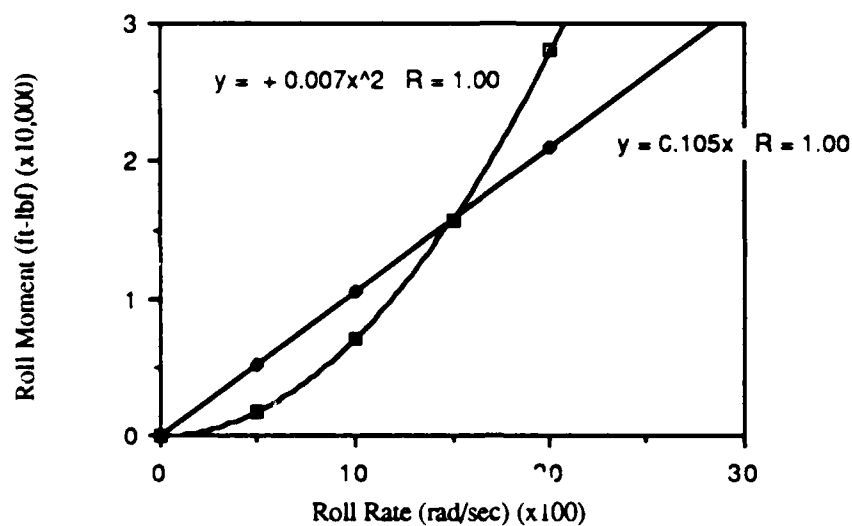


Figure 25 Damping About 'X' Axis

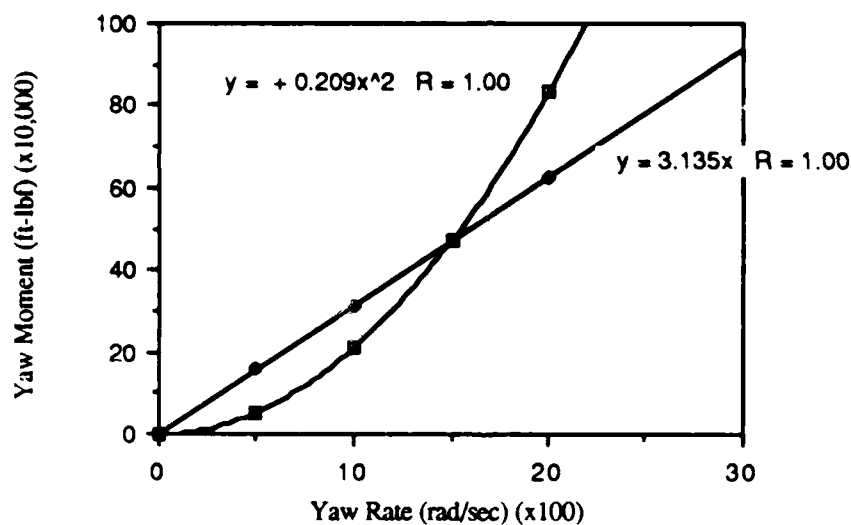


Figure 26 Damping About 'Z' Axis

The values of the damping coefficients are:  $B_x = 0.001$ ,  $B_y = 0.06$  and  $B_z = 0.03$  ft-lbf-sec/rad. If the equations relating angular rates to damping moments are linearized about a particular point and then evaluated at that

point, the hydrodynamic derivative  $M_q$  associated with rotational velocity in the pitch equation will result. For example; if the pitch equation is linearized about  $\alpha = 0.15$  and  $1.0$  rad/sec the following values for  $M_q$  result:

$$N = 0.418 \alpha^2 = f(\alpha)$$

$$M = f(a) + f'(a)(\alpha - a)$$

$$M = f'(a)\alpha + \text{Constant}$$

$$\frac{\partial M}{\partial \alpha} = f'(a) = M_\alpha = M_q$$

$$a = 0.15 \quad M_q = 0.1257$$

$$a = 1.0 \quad M_q = 0.836$$

Nondimensionalizing gives values of  $0.035$  and  $0.233$ . This indicates that the point at which the hydrodynamic derivative is evaluated strongly impacts the value. This is as expected. The value used for simulation studies must be chosen carefully.

## E. MOTOR REQUIREMENTS

The determination of power requirements for the model were based upon an approximation of the drag forces acting on the vehicle. The speed range of the vehicle was selected as  $0.0$  to  $5.0$  ft/sec. The drag forces were calculated in several ways. The possible conditions assumed were:

- 1) Skin friction dominant
  - a) Laminar flow
  - b) Turbulent flow
- 2) Pressure drag dominant
- 3) Model approximated as  $8:1$  ellipsoid
- 4) Model approximated as blunt nosed elongated cylindrical body in longitudinal flow

Equations for drag coefficients were taken from Reference 5. Table 5 lists the variables used and their definitions.

TABLE 5. DRAG COEFFICIENT DEFINITIONS

$C_{db}$	Base drag coefficient
$C_f$	Skin friction drag coefficient
$C_{fb}$	Forebody drag coefficient
$S_{fb}$	Forebody wetted surface area (460 in <sup>2</sup> )
$S_w$	Total wetted surface area (672 in <sup>2</sup> )
$A_b$	Cross-sectional area (24.5 in <sup>2</sup> )
$Re_l$	Reynolds number based on model length

Reynolds number calculations were based on flat plate approximations. For a speed of 5 ft/sec and plate lengths of 17", 20.5" and 28", Reynolds number varied between  $5 \times 10^5$  and  $10 \times 10^5$ . The following equations were used:

$$C_f = 1.33/\text{SQRT}[Re_l] \quad C_f = 0.043/[Re_l]^{1/6}$$

$$C_{fb} = C_f S_{fb}/A_b \quad C_{db} = 0.029/\text{SQRT}[C_{fb}]$$

Table 6 gives values of drag coefficients for Reynolds number based upon a plate length of 21 inches.

TABLE 6. VALUES OF DRAG COEFFICIENTS

V(ft/sec)	$Re_l(\times 10^5)$	$C_f(\text{lam})$	$C_f(\text{turb})$	$C_{db}$	$C_{fb}$
1.0	1.4	0.004	0.006	0.09	0.11
2.0	2.8	0.003	0.005	0.10	0.09
3.0	4.2	0.002	0.005	0.10	0.09
4.0	5.6	0.002	0.005	0.10	0.09
5.0	7.0	0.002	0.005	0.10	0.09

For laminar flow a maximum power of about 1.6 watts results. Turbulent flow gives 3.9 watts at five ft/sec. Combining forebody drag and base drag coefficients, which are based on the base area, along with the turbulent flow skin friction coefficient acting over the wetted surface area of the stern, a power requirement of about 6.5 watts results. Using a coefficient of drag of 0.2, which seems reasonable based upon Figure 3.18 of Reference 5, or for an 8:1 ellipse as given in Reference 6, the total power requirement is about 5.8 watts. It was desired that the motor power be able to compensate for induced drag from control surfaces along with the frictional or pressure drag. For this reason, the size of the control surfaces must be known. Control surface sizing is dependent upon the maximum expected rate of maneuvering. In order to arrive at a rough approximation of the maneuvering speed, some simple idealizations were made. Assuming for the moment that the motion along the 'z' axis is acting after the input, or disturbing force, has died away; the governing equation is given by:

$$m\ddot{z} + b\dot{z} + kz = 0$$

The value of damping was considered negligible. Solving for the linear acceleration and substituting with equivalent angular acceleration,  $[X\ddot{\Theta} = -\ddot{z}]$ , the following relation results:  $\ddot{\Theta} = \omega^2 Z/X$ . The natural frequency,  $\omega$ , can be written in terms of the period of the maneuver. This gives a final form of the equation as:  $\ddot{\Theta} = Z(2\pi)^2/UT^3$ . The period of the maneuver was set equal to the distance traveled divided by the forward velocity, U. The moment arms through which the forward and aft dive plane surfaces were acting were set at 16.375 inches (1.36 feet) for the aft dive

plane and 7.6 inches (0.63 feet) for the forward dive planes. This gives a governing equation of the form:

$$0.63F_1 + 1.36F_2 = J_y Z (2\pi)^2 / UT^3 \quad (4)$$

$F_1$  is the force generated by the forward dive planes and  $F_2$  is the force generated by the aft dive planes. To perform a 1.5 foot depth change in a horizontal distance of 8 feet, at a velocity of 1 ft/sec, the required moment was 0.07 ft-lbf with  $T = 8$  seconds. In order to solve this equation, one of the forces had to be estimated. The control plane areas were based on a freestream velocity of one ft/sec. The power requirement for a propeller may be approximated as  $\rho Q(V_p - V_f)V_f$  [Ref 6]. This equation was then set equal to the drag force on the vehicle in steady state forward motion.  $A_p$  is the cross-sectional area swept by the propeller and  $Q = [A_p(V_f + V_p)]/2$  where  $V_f$  is the free-stream velocity and  $V_p$  is the velocity downstream of the propeller. For a velocity of one ft/sec, the drag force was found to be about 0.05 lbf. At this stage of the design the propeller diameters were not known. Therefore a reasonable diameter of one inch was assumed. For the two screws, the total area was  $1.571 \text{ in}^2$ . The total deflected area was assumed to be one half of this,  $A_o = 0.7854 \text{ in}^2$ . Solving the propeller power equation for  $V_p$  gives the downstream velocity as 3.23 ft/sec. This velocity was considered to act upon the aft dive plane.

The forces acting on the dive plane positioned at some angle,  $\theta$ , to the horizontal were then approximated from the expressions:

$$F_y = \rho A_o V_p^2 \sin \alpha \quad (5)$$

$$-F_x = \rho A_o V_p^2 \cos \alpha - \rho A_o V_p \quad (6)$$

The area,  $A_0$ , is the cross-sectional area of the jet which has been deflected. The angle  $\alpha$  is the effective deflection angle. This angle can be found using simple geometry. The velocity leaving the plane surface is taken as the propeller velocity and is added vectorily to the free stream velocity. For a deflection of 15 degrees on the control plane, an effective angle of about 11.5 degrees results. Solving equation (5) for  $F_y$  gives 0.022 lbf. Solving equation (4) for  $F_1$ , with  $F_2$  set equal to  $F_y$ , yields a forward dive plane force of about 0.064 lbf. The forward dive plane area was approximated by utilizing the equation of force due to a momentum change;  $F_1 = \rho A V_f^2 \sin(\theta/2)$ . Solving this equation for area gives  $A = 18.4 \text{ in}^2$ . This is the total area of the two forward planes. This seems unacceptably large. If the forward velocity was to remain the same, the amount the dive plane was allowed to rotate had to be increased. {Note: Adding the force which results from the area of the aft dive plane which does not see any propeller thrust, but is acted upon by the freestream velocity, will change the required forward area by only a small percent, therefore, it was not included in the calculations. In the final design the aft dive plane consisted only of two rectangular sections located directly aft of the screws.} The angle of attack for the control planes was increased to 30 degrees. This gives an effective angle of attack,  $\alpha$ , of about 23 degrees. In this case,  $F_2 = 0.048 \text{ lbf}$  and  $F_1 = 0.007 \text{ lbf}$ . This gives a forward control area of about two square inches. A design goal was established to allow 30 degree dive plane movement. The size of forward dive planes was not crucial for dive control but will effect the capability of roll control. A search for prefabricated control surfaces and screws for model submarines resulted in the discovery of components which had potential for use.

Forward dive planes of roughly  $4.75 \text{ in}^2$  each and screws with a diameter of about one inch were located. These components, along with associated shafting, stuffing tubes and control links were adapted to the test model.

With the control surface sizes set, the induced drag could be calculated. For the forward dive planes; a drag force of about 0.009 lbf was calculated using equation (6), with a total cross-sectional area given by  $(9.5 \sin 30) \text{ in}^2$  and  $V_p$  set equal to a freestream velocity of one ft/sec. The drag due to the aft dive plane is calculated in the same manner but with a jet velocity of 3.23 ft/sec and an area of  $1.571 \text{ in}^2$ . The resulting drag is  $\cong 0.03 \text{ lbf}$  (2.8 watts). A total drag force of 0.039 lbf exists at one ft/sec freestream velocity due to control planes at maximum deflection. Assuming power is directly proportional to velocity cubed, the power at five ft/sec is equal to the power at one ft/sec times 125. This gives a power of 4.875 ft-lbf/sec, or equivalently, about 6.6 watts. Added to the 6.5 watts calculated previously, a sub-total requirement of 13.1 watts is needed. To this was added 2.8 watts for rudder deflection. Since the efficiency of the propellers is not known but is expected to be relatively low, say 50%, the total power needed to maintain maximum design speed with all control surfaces at full deflection is about 36 watts. This is a relatively small power requirement and can easily be met. Two standard size motors specifically designed for radio controlled models were selected. Although rated significantly above what was needed, it was decided to use them since it is good practice to operate well below rated voltage and current. Also, and most importantly, the amount of frictional load from the stuffing tubes was unknown. These motors were each rated for



8 amps at 12 volts DC. If weight became a significant problem, smaller motors might have been utilized.

#### F. GYRO SELECTION

In order to measure the maneuvering characteristics of the vehicle a suitable motion sensing system was needed. Various alternatives were looked at. Because of the slow rate of motions, accelerometers would have to be sensitive to very low accelerations such as 0.05 to 0.2 ft/sec. Some low frequency accelerometers were located; however, their size and cost were prohibitive.<sup>2</sup> For a larger scale model or prototype vehicle, inertial sensors were the preferred sensing devices because of their sensitivity, accuracy and reliability. Rate gyros had been considered first, and because of the availability of low cost radio controlled model gyros, accepted as the most likely device to meet the test requirements. Various RC model companies produce gyros as well as the associated radio control equipment such as transmitters, servos and speed control equipment. To ensure compatibility, all components were purchased from the same company with the exception of the motor speed controller. Three gyros were purchased and mounted in positions to allow monitoring of angular rate around each coordinate axis. In the test model installation, the gyro output signal is amplified and transmitted off the vehicle to the recording equipment via the data link cable. The gyro is used only as a sensor. It has no direct control function. The gyro system as purchased was a closed loop system within which the gyro signal was fed back to a control box. The control box also had the input reference signal

---

<sup>2</sup>High quality inertial sensors are available from Systron Donner Corporation

from the receiver. The receiver received the radio control signal from the radio control transmitter. Any movement sensed by the gyro produced an output signal which was then compared to the reference signal. A gain setting on the control box allowed adjustment of the gyro sensitivity. A servo control signal was generated that would then feed a control servo. Movement of an operating lever (joy-stick) on the radio transmitter would also generate an output signal for control of vehicle movement.

#### G. PRESSURE INSTRUMENTS

Two differential pressure cells were installed in the model. One cell was utilized for depth measurements and the other cell was used for speed measurements by sensing the differential pressure from a pitot tube mounted in the nose. The cell used for measuring depth has a range of 0 -100 cm of water. The pitot tube cell has a range of 0 - 2 cm of water.

The depth was initially determined by sensing outside water pressure through a port located 17.5 inches aft of the bow. The port was located on the bottom centerline of the vessel. This pressure was sensed at the pressure cell high pressure port. The low pressure port is vented to the vessel interior. It became evident during testing that the location of the pressure port was inadequate. This could have been foreseen. Maneuvering of the vehicle in the vertical plane caused pressure gradients to develop which were of sufficient magnitude to cause errors in depth readings. Thus, two pressure ports were installed, one centered on each side of the model located 14.5 inches aft of the bow. This is close to the vehicle midpoint. The ports were connected through tubing to a junction box which was connected to the high pressure side of the

depth cell and the low pressure side of the speed cell. The original port was plugged.

Initially, the vessel speed was sensed by a pitot tube located in the nose of the vessel. The pitot tube design proved to be less than satisfactory. Because of the method of construction, the stagnation pressure port was too small and the nose was rounded vs. square cut. This limited the dynamic sensitivity of the pitot tube. A thin walled sleeve was machined to fit over the original design. This created a larger stagnation port opening and reduced the sensitivity of the cell to any pitot tube misalignment. The static pressure ports were not the recommended distance from the stagnation port and were too close to the vessel body. Although the pitot tube would not accurately indicate speed, it was hoped it would still be useful to indicate vessel motion. Pitot tube operation and basic theory of design is given in Reference 7. During initial vehicle testing it was discovered that the small porting of the pitot tube prevented the proper sensing of speed. The pitot tube was removed and replaced with a stagnation pressure port. This port was connected to the high pressure side of the speed DP cell. This arrangement appeared effective in providing an indication of vehicle speed during level flight, however; the cell was sensitive to pitch angle. The sensing tubes did not fill with water because of their small size, and since the cell had a small range of only 0 - 2 cm, the cell output would saturate quickly. Lessons learned from this experience was that a higher range DP cell might prove effective in providing an indication of pitch angle provided the tubing between the sensing ports and the cell remained clear of water. The weight of the air columns would be negligible.

Speed was finally estimated by visual clocking of the model over a known distance by use of a stopwatch.

#### H. ELECTRONICS AND POWER

The Naval Postgraduate School Mechanical Engineering Electronics Lab constructed the necessary electronic circuits to provide power to the various internal components. Because of vehicle size, it became evident that a power source located on board would be too heavy. Small, but relatively high powered batteries were available for powering the electronic circuits, however, an external power source had to be used for the drive motors and it was decided to regulate this DC power source internally to the vehicle by use of small DC-DC voltage regulators for the electronics. The motors were rated for 12 volt DC. A six ampere rated DC power supply unit was adjusted to provide 12.0 volts under load to the vehicle. Batteries were not carried aboard the vessel. Figure 27 provides the layout of the electrical circuits. The 2.4 volt regulated DC supply, shown in the lower section of Figure 27, provided power to the gyro sensory circuits.

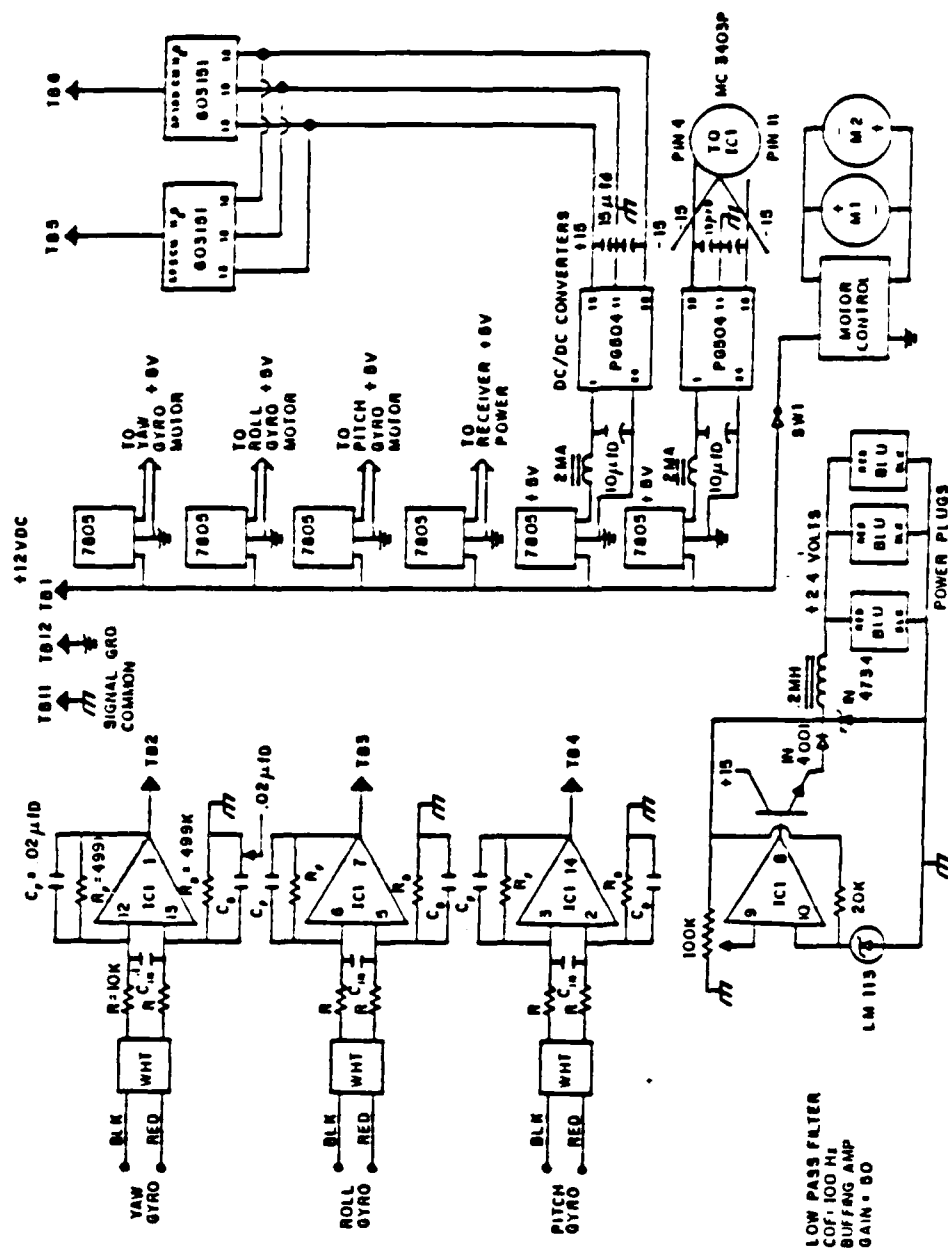


Figure 27 Electronic Circuit

## I. TEST TANK CONTROL STATION

A control station was set up next to the test tank. This station consisted of: 8-channel stripchart recorder, analog computer, digital computer, oscilloscope, multimeter, DC power supply and the radio control box. The control station allowed monitoring and recording of radio command and vehicle response signals. The oscilloscope and multimeter were used for monitoring of voltages at various locations of interest. Figure 28 indicates the station layout. The analog computer was used primarily as an output impedance buffer and signal conditioner between the radio control box and the digital data acquisition system.

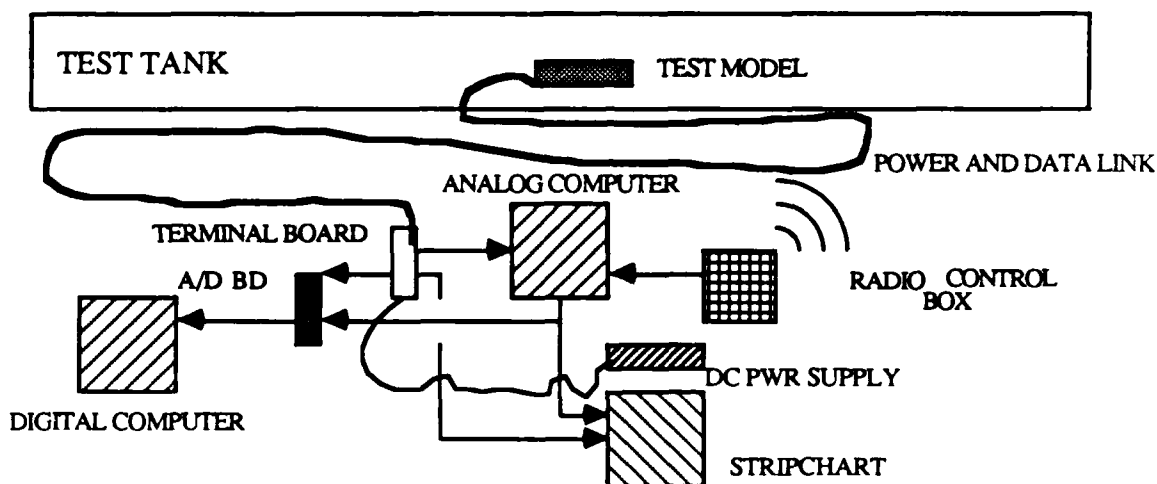


Figure 26 Station Layout

Further details concerning the development of the digital data acquisition system are provided in Reference 9.

## IV. CALIBRATION AND TEST PROCEDURES

### A. INTRODUCTION

This chapter describes the methods used to perform equipment and system calibrations as well as the test procedures used to acquire vehicle command and response data.

Testing and calibration of components utilized basic lab equipment such as multimeters, oscilloscope and stripchart recorder. An analog computer was used to provide buffering, amplification and integration of signals. The analog computer was a simple means of providing real time capability to perform operations on the vehicle response signals as well as the controller command signals. Several methods of filtering the rate gyro outputs were performed as a means of removing or minimizing the effects of a drifting bias signal. Both first order and second order filters were tested. A high pass filter can be produced on the analog computer by feeding the input signal to a summer. The summer output is then fed back via a potentiometer (pot), integrator and inverter to the input of the summing amplifier. Adjustment of the pot setting and the amplifier gains will control the value of the time constant. The filters seemed to be of limited value, because of the non-constant bias, and the final solution was the use of a relay comparator to provide a dead band.

Two test tanks were used. A small tank of about three feet in depth by four feet in length was utilized to adjust ballasting and to check the vehicle for initial leak tightness. A large water tank was utilized to perform

operational tests. This tank was about 4ft x 4ft x 40ft. Fresh water was used in the tanks.

## B. GYRO CALIBRATION

A calibration test was first needed to determine whether the gyros were sufficiently sensitive and could produce relatively clean signals. To accomplish this a flat circular board was prepared on which a gyro could be mounted. The board was then mounted on the handwheel of a mill machine. This allowed relatively fine control of the rotation rate. The rate was monitored by measuring the time required for a given amount of wheel rotation. For calibration purposes the reference signal was generated from a DC power supply. This signal was fed to the gyro control box. The gyro system output signal was then fed to an oscilloscope and multimeter for analysis and recording. Figures 29 through 31 show that for rotation rates of several rpm, the gyro output voltage is quite linear. These figures were obtained by measuring the output of a mixer circuit which included a signal processing gain. This mixer circuit was later removed so the results of Figures 29 through 34 were considered preliminary and were useful only in determining linearity and sensitivity of the low cost gyros.



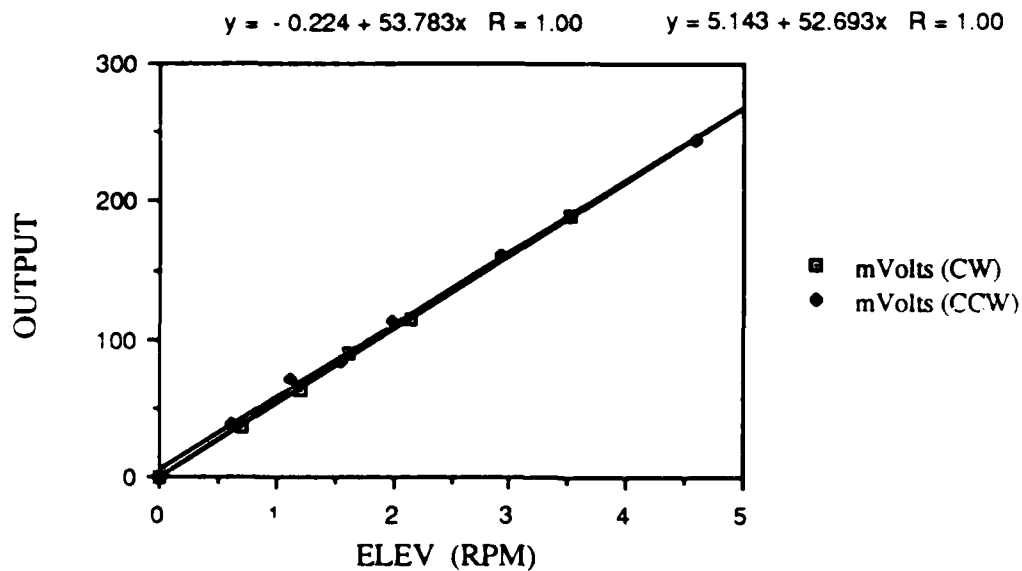


Figure 29 Pitch-rate Gyro

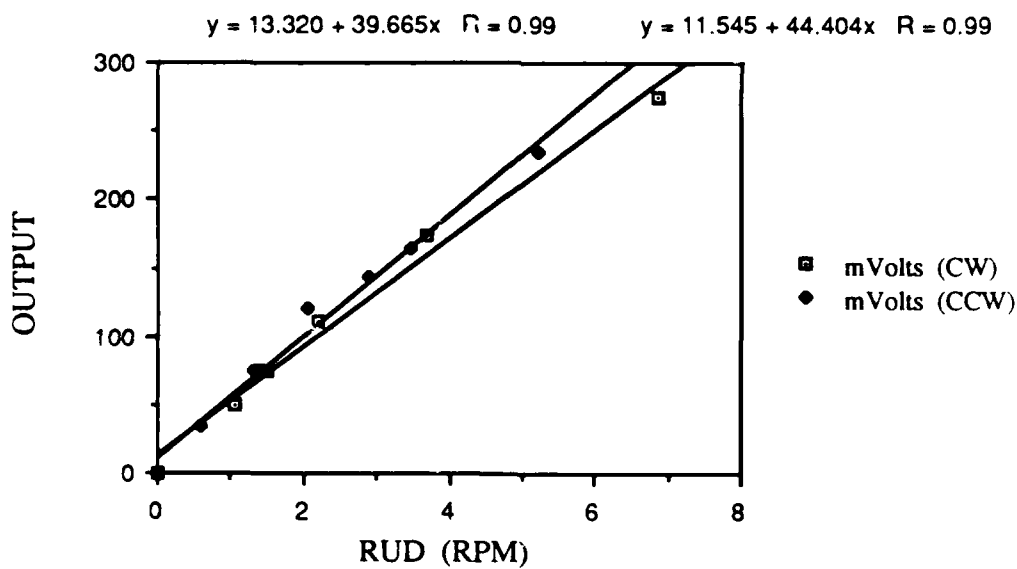


Figure 30 Yaw-rate Gyro

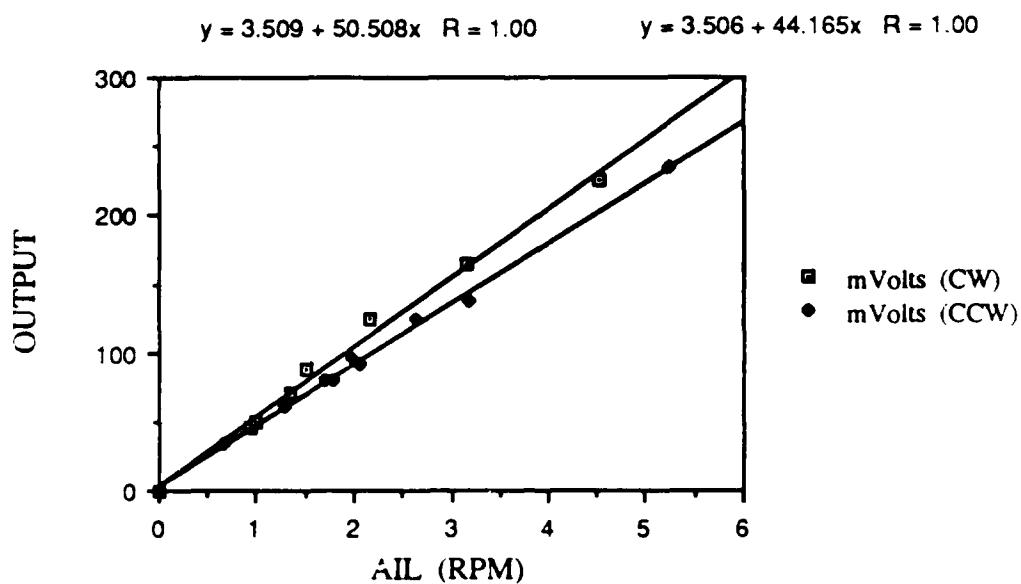


Figure 31 Roll-rate Gyro

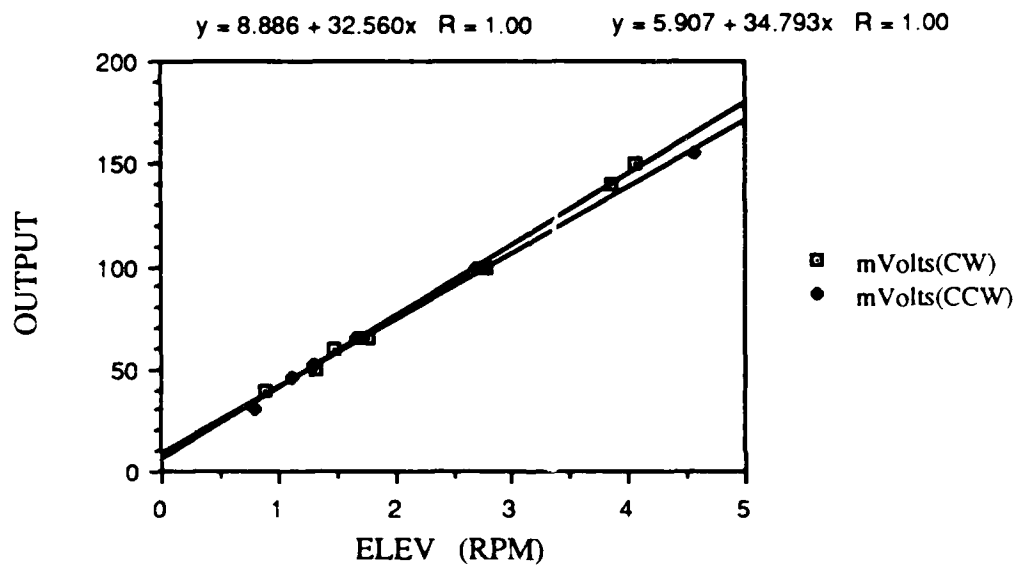


Figure 32 Pitch-rate Gyro at Low Ref. Voltage

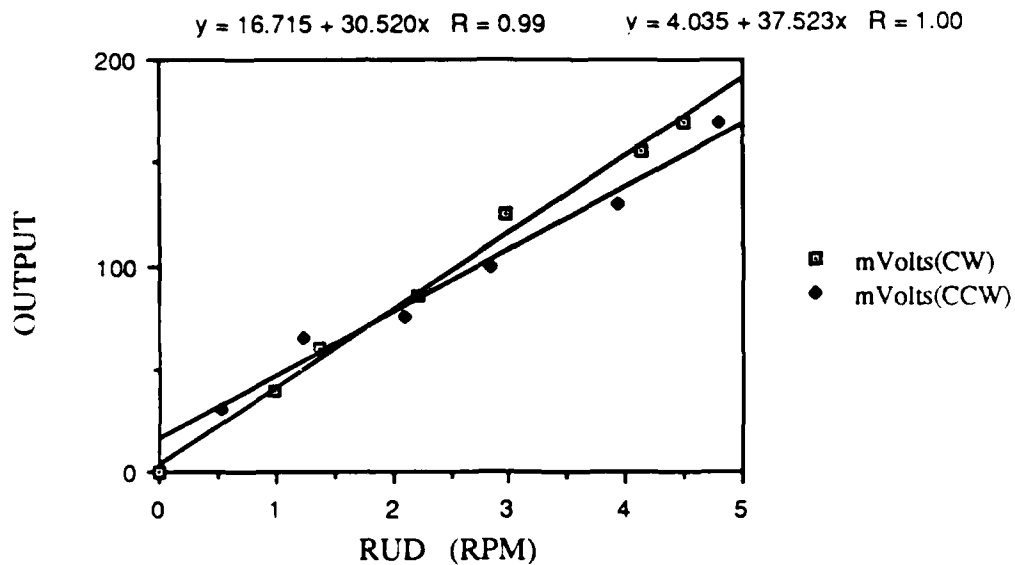


Figure 33 Yaw-rate Gyro at Low Ref. Voltage

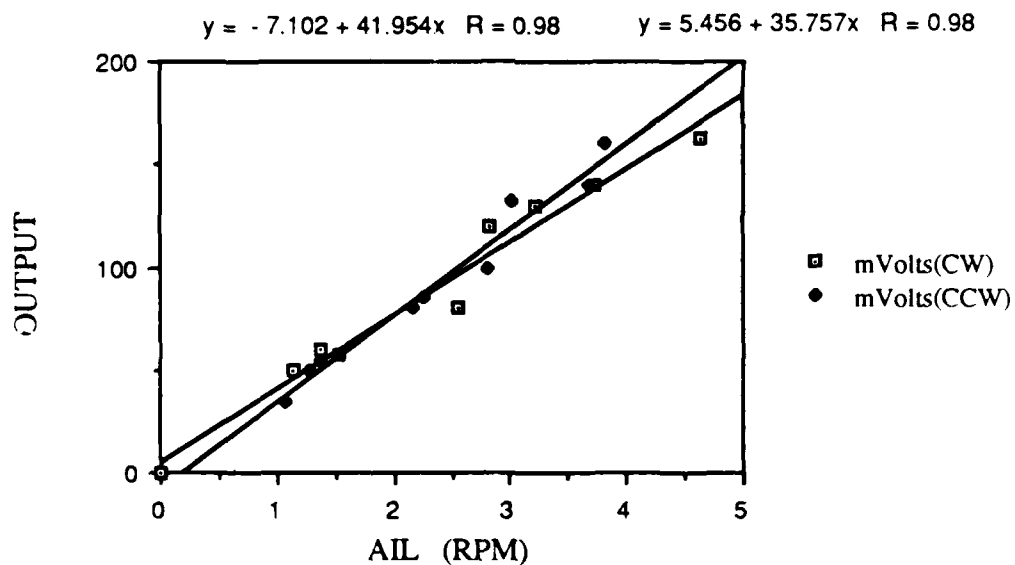


Figure 34 Roll-rate Gyro at Low Ref. Voltage

This data corresponds to a system design reference signal voltage of 4.8 volts. The same tests were done at a reference voltage of about 4.35 volts. The outputs were still measurable and linear as shown in Figures 32 through 34. By comparing the figures it can be observed that the gyro outputs are quite sensitive to reference signal voltage. In the design of the power supply system this fact had to be taken into account. If voltage fluctuations occurred during testing the calibration curves would not be usable for determining angular rates of motion.

It was determined during construction of the gyro power supply system that the mixer box component of the manufacturer supplied gyro system was in fact not necessary. The mixer box was needed when the gyro was operated as a closed loop system independent of the vehicle control circuits. It was part of the feedback network and supplied a gain amplifying the gyro output. With this component removed the previous gyro calibration was no longer valid and a new calibration of the entire gyro system as finally used was required. Since a swing test had been set up for mass moment of inertia determination, this test also provided the means for gyro calibration. By recording the output of the gyro on a stripchart the frequency of oscillation could easily be found. The vehicle was treated as a point mass and a small angle approximation was used. The equation of motion then becomes:

$\ddot{\theta} + \omega_n^2 \theta = 0$ . A solution of this equation is:  $\theta(t) = \theta_0 \sin \omega_n t$ . The amplitude of the velocity is  $\omega_n \theta_0$ . The initial angle,  $\theta_0$ , was measured prior to release of the vehicle. The period of oscillation was measured and it was observed that the value of damping was quite low. Thus,  $\omega_d \cong \omega_n = 2\pi/T$ . The period,  $T$ , was measured directly off of the stripchart recording. The voltage

corresponding to the maximum velocity was also measured from the stripchart recording. A relation between voltage output and rate is thus determined. The following values were calculated.

Pitch Rate Gyro: 12.5 mvolt-sec/degree

Roll Rate Gyro: 18.6 mvolt-sec/degree

### C. PRESSURE CELL CALIBRATION

Power was applied to the pressure cells for a period of about 20 minutes prior to calibration checks. This allowed the electronic circuits to reach normal operating temperature. The zeroes were set by adjustment of the zeroing potentiometers with all pressure sensing lines vented to atmosphere.

A 0 -10 inch Micromanometer Model 34 FB2TM was used for the 0 - 2 cm pitot tube pressure cell. The manometer level could be read to 0.001 inch water. The manometer water level was set at 0.8 inches ( $\cong 2$  cm) and the span adjust potentiometer adjusted to provide 10.0 volts output. The zero was then readjusted after venting the system. The micrometer level was adjusted every 0.1 inches and the voltage recorded. Figure 35 shows the expected linear output.

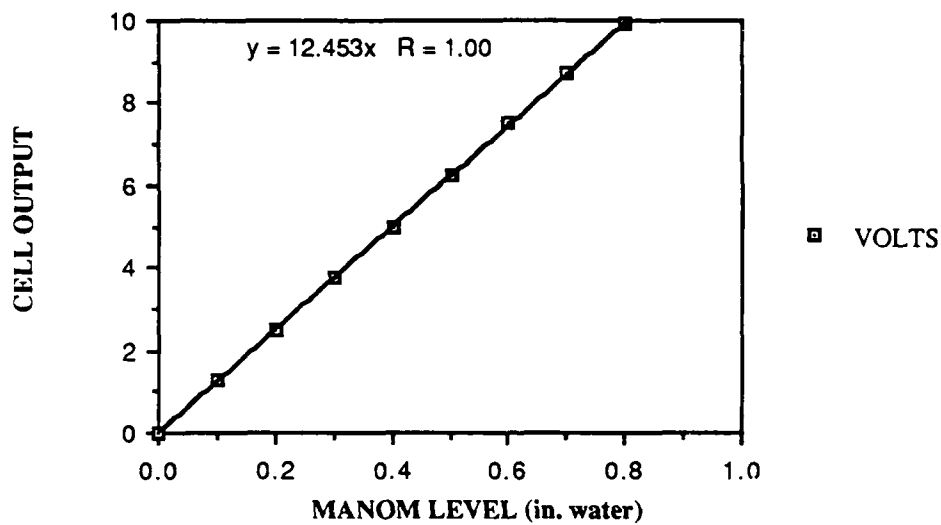


Figure 35 Velocity Cell Calibration Curve

A 0 - 120 inch manometer was used for calibration of the pressure cell used for depth measurement. The cell output was 0 - 100 centimeters. This corresponds to about 39 inches water. The same procedure used for the other cell was used. The zero was set, the range was set for a 10.0 volt output at 39 inches of water and then the zero reset. Water level was adjusted every five inches and the output voltage recorded. Figure 36 shows the linear behavior of the output. During operational testing it was determined that the cell operation was not satisfactory. Speed was measured by clocking the vehicle over a known distance. The motor voltage which corresponded to each speed was recorded. The resulting calibration curve is shown in Figure 37.

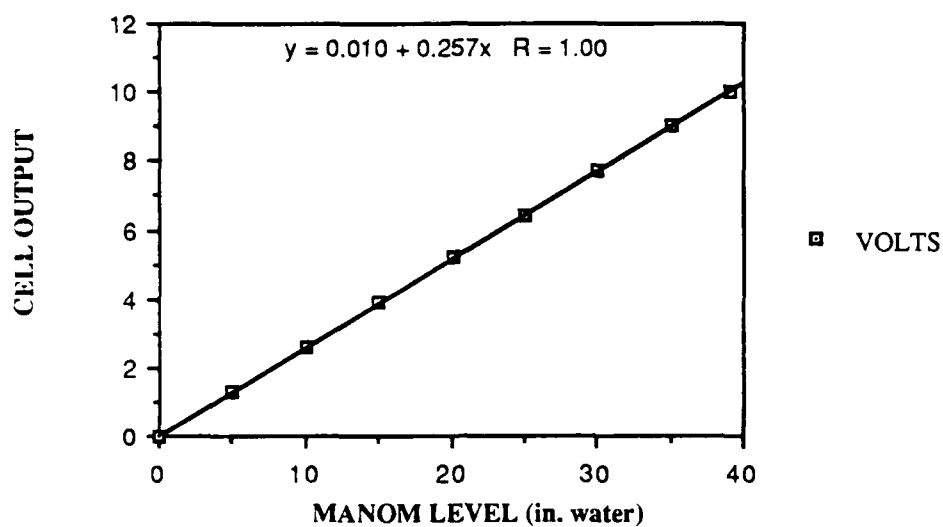


Figure 36 Depth Cell Calibration Curve (Bench Test)

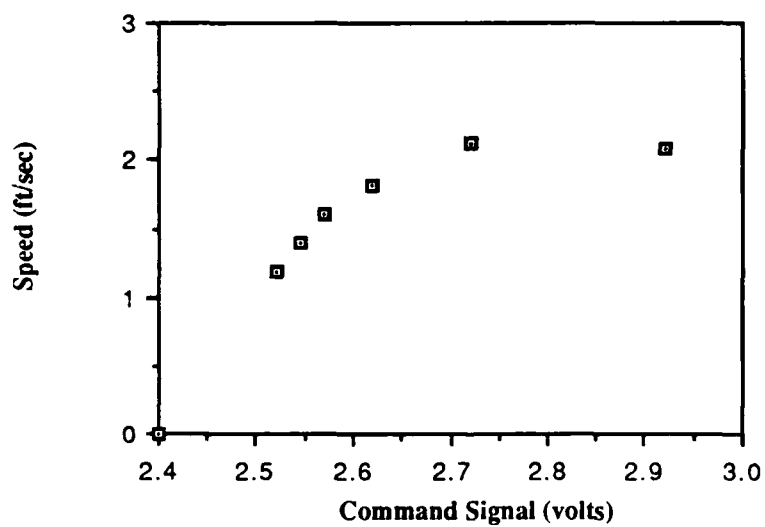


Figure 37 Vessel Speed vs. Command Signal Voltage

During operational testing, the pressure cell used for measuring depth was checked. This was performed with the vehicle in its final assembled form. The previous tests were bench tests. The vehicle was set in the test tank. The depth was varied and the output of the depth pressure sensor monitored on the multimeter. The results are plotted in Figure 38.

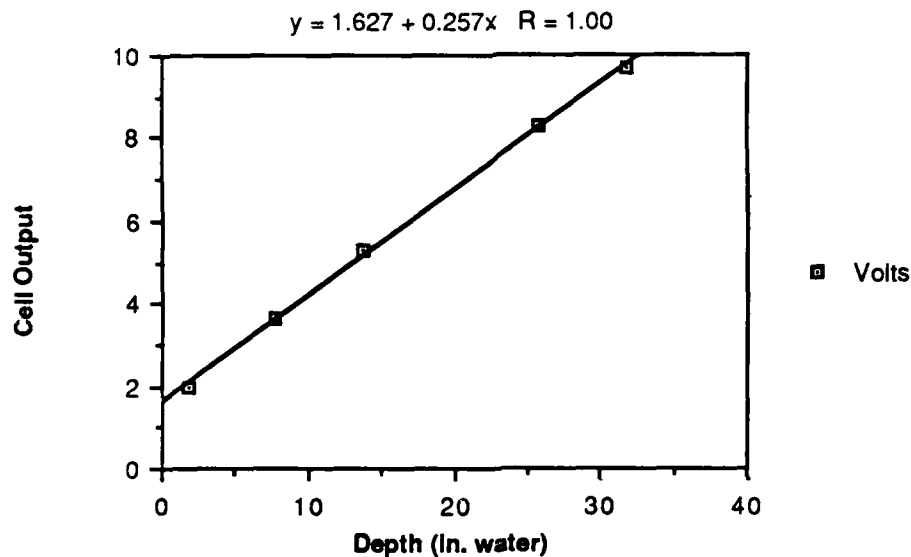


Figure 38 Depth Cell Calibration Curve

As can be seen in the above figure, the zero of the pressure cell has shifted. The slope of the curve has remained unchanged. This may be a result of a change in the power supply voltage or the zero adjust pot may have accidentally been moved. In future testing the pressure cell should be zeroed prior to performing data runs. This had been overlooked during the data runs performed here, but did not effect any of the dynamic response results.



#### D. BALASTING

Following vehicle assembly, all joints were visually checked for proper sealing. With the access cover removed, the model was then carefully lowered into a small water tank to check for signs of gross leakage from shafting and other hull penetrations. No leakage was noted. The access cover was then secured in place. The vehicle was then placed into the tank. When floating free, about 1/2 inch of freeboard forward and 1/16 inch aft was observed. The model had a slight list to port as expected because of the placement of servos. The initial displacement weight estimate of the vehicle was 19 pounds. This was determined from geometry and a specific weight for water of 62.4 lbf/ft<sup>3</sup>. Individual components were weighed prior to assembly. A total weight of 17.86 pounds was measured. In order to submerge the vehicle, about two pounds of weight had to be added to the model. About 1.5 lbs was hung from below and an additional 1/2 lb added above. The assembled dry weight of the model without ballasting is 8.215 kilograms or about 18 lbs. An accurate measurement of the vehicle plus the added weight for submergence indicated a total weight of 9.113 kg, or about 20 lbs. Thus, two pounds of ballasting was needed. Slightly more than one pound of ballast was prepared from lead bars, roughly 1/2 inch square by two inches long. The remaining ballast was in the form of small steel shot. The shot could be placed fore or aft into small tube sections which had been glued to the vehicle interior bottom. The vehicle was loaded with eight lead bars and placed in the water tank. A slight positive buoyancy was evident. Steel shot was added in an iterative process until the vessel was very close to

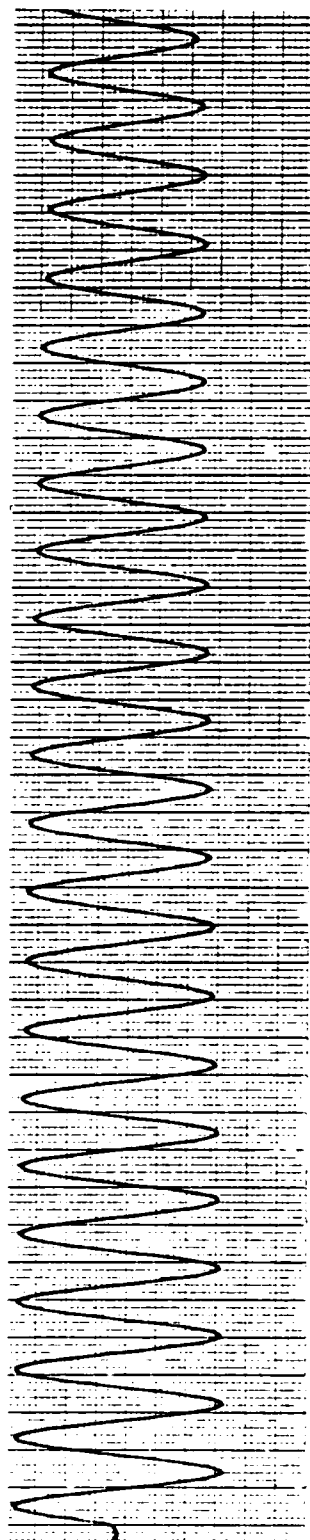
neutral bouyancy while maintaining a horizontal position. The resulting final displacement weight was 19.6 pounds.

#### E. MEASUREMENT OF $J_x$ AND $J_z$

The mass moments of inertia were estimated in Chapter 2. It was desired to perform experimental verification of these values. The experiment itself would also provide a means of monitoring gyro output due to actual vehicle motion. The test consisted of suspending the model from a pivot point thus allowing pendulum motion around the pitch axis and roll axis. This was done by suspending the model with four lines. Two lines were connected to the forward dive plane shafts and two lines were connected to the upper rudder support beams which extend from the fins. The four lines were fed through an eyebolt anchored in a 2 x 4 inch wooden beam. Turnbuckles were installed in each of the aft lines to allow for levelling about the 'x' axis. Levelling about the 'y' axis could be accomplished by lifting on one end of the vehicle allowing the support wires to slip through the support eyebolt. The support wires were passed through the eyebolt twice to prevent excessive slipping when the full weight of the vehicle rested on the wires. The equation of motion describing pendulum motion was used to solve for the mass moment of inertia. A small angle approximation was used. The governing equations are:

$$\begin{aligned} J_o \ddot{\theta} + mgL\theta &= 0 & \omega_n^2 &= mgL/J_o & \tau &= 2\pi/\omega_n \\ J_o &= mgL\tau^2/4\pi^2 & J_y &= J_o - mL^2 \end{aligned}$$

$J_0$  is the moment of inertia about the pivot point and  $J_y$  the moment of inertia about the 'y' axis. A reasonable value of 'L' was selected to be approximately one vehicle length, or about 30 inches. This results in a reasonable value for the period and ensures sufficient motion for gyro sensing. A 12 volt DC power source supplied power to the gyro motors and instrumentation. The output of the gyro being tested was connected to a strip chart recorder, multimeter and oscilloscope. The vehicle was positioned in the horizontal while hanging motionless. A level was used to ensure it was completely horizontal. The gyro bias was adjusted to bring it near zero. Motion was then initiated by pulling the vehicle along the desired axis and releasing. Sinusoidal motion was recorded on the strip chart as the gyro sensed movement about its reference axis. Thus, by measuring the period of the motion from the strip chart recording, the moment of inertia could be calculated. Several runs were performed. Figure 39 is the strip chart recording for the first run. During this run the length from the pivot point to the centerline of the vehicle was set at 31.1875 inches. The center of mass is 0.1 inches below the centerline. This gives a total length, L, of 31.2875 inches. The period measured was 1.816 seconds. The mass moment of inertia,  $J_y$ , was calculated to be about 0.13 ft-lbf-sec<sup>2</sup>. Another test was run the following day. The length of the pivot was slightly different since the model had been rerigged. The length from the pivot to the vehicle centerline was 30.375 inches. This gives a pivot length, L, of 30.475 inches. The period was measured as 1.80 seconds. The mass moment on inertia was again calculated and found to be 0.16 ft-lbf-sec<sup>2</sup>. The slight difference may be due to the error in reading the number of cycles on the strip chart and the



5 mvolt/div 5 mm/sec chart speed

Figure 39 Inertia Test

measurement of the pivot arm length. The first test was run with cotton string as the support wires and the second test used monofilament fishing line. Both of these values of inertia agree well with the original estimate. As expected, the estimate was slightly larger since it assumed uniform mass distribution while the experimental value is based on the actual mass distribution.

The test was also performed to measure the mass moment of inertia about the 'x' axis. A period of  $\cong 1.77$  seconds was measured from the stripchart recording. The length from pivot point to mass center was 30.475 inches. The value of  $J_x$  measured was  $\cong 0.02$  ft-lbf-sec<sup>2</sup>. The estimated value as calculated in Chapter 3 was also  $\cong 0.02$  ft-lbf-sec<sup>2</sup>. Less error between measured and estimated values exists, as compared to the 'y' axis values, because the assumption of uniform mass distribution about the 'x' axis is a closer approximation to the actual vehicle.

An additional test conducted was to integrate a gyro output and display it on the strip chart recorder. This test was to verify gyro output sensitivity and the quality of the integrated signal. For almost imperceptible visual motions the gyro produced clear sinusoidal output signals. The signal was also fed to an analog computer for integration. The vehicle was rotated about the pitch axis by hand allowing the suspension wires to slip through the pivot point eyebolt. The elevation of the forward dive planes and the propellor shaft penetrations with respect to the deck were then measured using a scale rule. Since the length between these points as measured along the vehicle axis was known, the angle of inclination could be determined using simple geometry. It was determined that integration was possible and could provide a means of

determining vehicle angular position; however, the problem of gyro bias integration would have to be solved. The gyro bias did not appear to remain at an initial value but drifted during operation. Gyro bias is a real problem and needs to be compensated for in precision control.

#### F. PRELIMINARY TESTING FOR STABILITY

Simulation studies showed the vehicle to be directionally stable. With the vehicle near neutral bouyancy it was a simple matter to check for directional stability. With the model ready for testing, the large test tank was filled. The model was launched at various speeds along a horizontal path. A dive plane angle was given to initiate a dive maneuver. After the model developed a pitch angle of at least ten degrees, the dive planes were returned to their zero position. A pitch rate opposite to that which had been initiated by the control action was immediately apparent and the vehicle began to return to a horizontal position. At slow speeds, as expected, this effect was more pronounced. This is because of the independence of the restoring moment from speed and its dominance over hydrodynamic dependent system coefficients at low speeds. At higher speeds the tendency existed but insufficient room in the tank prevented the vehicle from returning to the horizontal plane prior to collision with tank bottom.

From preliminary testing, when familiarization with the control system was in progress, it was evident that one person had difficulty providing adequate control over both the dive planes and rudder. Frequent collisions with tank sidewalls took place. It was desired to keep the model centered with respect to tank sidewalls. To allow a second person to take control of the

rudders, a separate potentiometer control box was connected to the radio control unit rudder control channel. The control box had sufficient cable length to permit the operator to remain at the end of the test tank in constant view of the model with respect to tank longitudinal centerline. This freed the other operator to concentrate on performing vertical plane maneuvers.

#### G. DIVE PLANE AND ROLL PLANE COMMAND SIGNAL CALIBRATION

In order to know the dive plane angle for data analysis, a calibration had to be done to determine the amount of voltage corresponding to each angle order. The control box output command signals for dive control, roll control (aileron), speed and rudder were measured and found to vary about 0.5 volts from a reference voltage of roughly 2.5 volts. In order to record these signals on the stripchart recorder it was necessary to reduce or remove the reference voltage. Insufficient zero adjust was available on the strip chart recorder to compensate for these voltages and still allow monitoring of the entire control signal range. Because of the low analog computer input impedance, a one megohm resistor was inserted at the operational amplifier (op-amp) input. The signal was then sent to a summer where a compensating voltage was added to the command signal. The compensating voltage was adjustable by using a potentiometer (pot) to provide the signal. This pot was adjusted to produce a 0.0 volt output from the summer with control planes at zero angle of attack. Since the dive command signal was of primary importance, only two pots were used. One was used to zero the speed signal and the other for dive plane command. The output of this second pot was also used for the remaining control signal summers for roll control and rudder

control. The outputs could then be monitored on the stripchart, although the signal values for roll (aileron) and rudder were not zero at zero angle order. Figures 40 through 43 show the signal curves for dive plane command and roll command with and without compensation voltage.

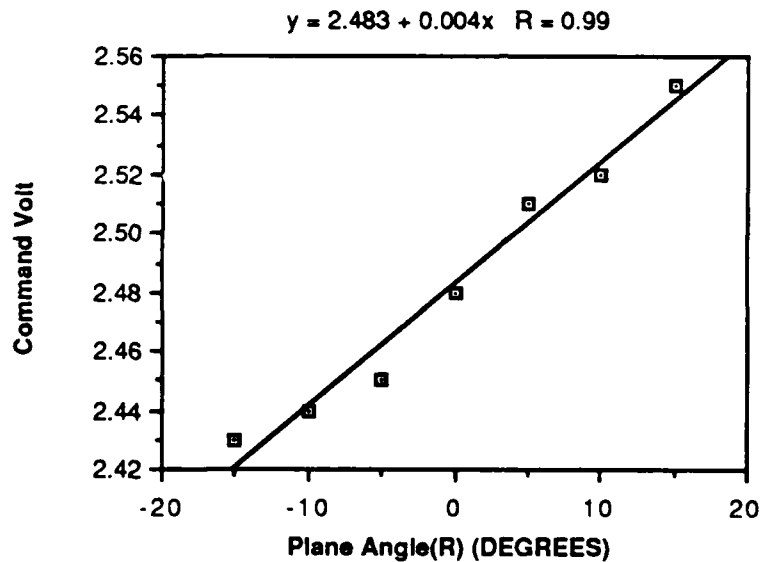


Figure 40 Uncompensated Roll Control Signal

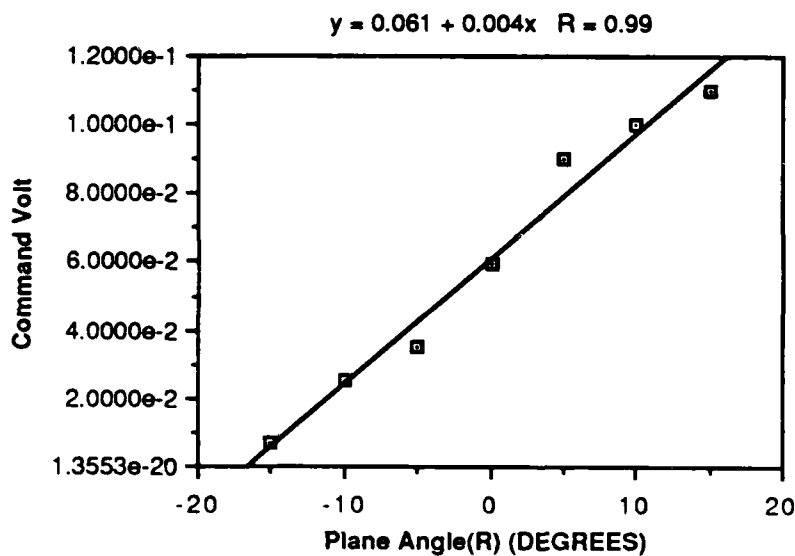


Figure 41 Compensated Roll Control Signal



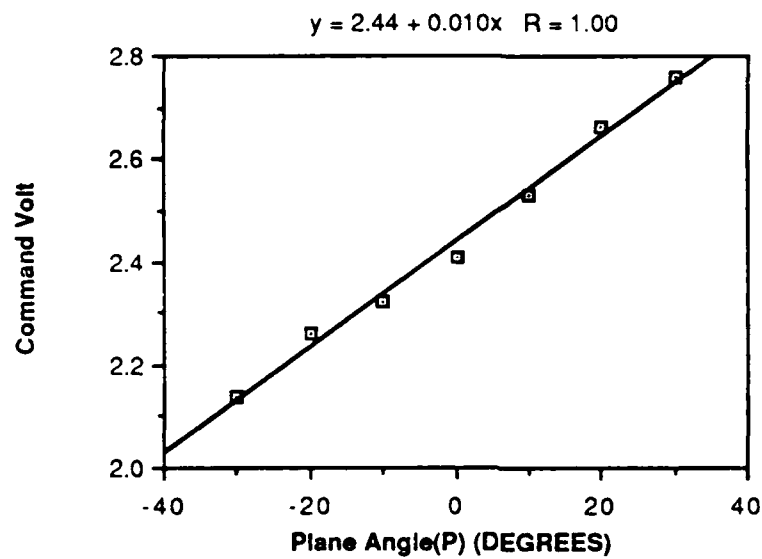


Figure 42 Uncompensated Dive Plane Control Signal

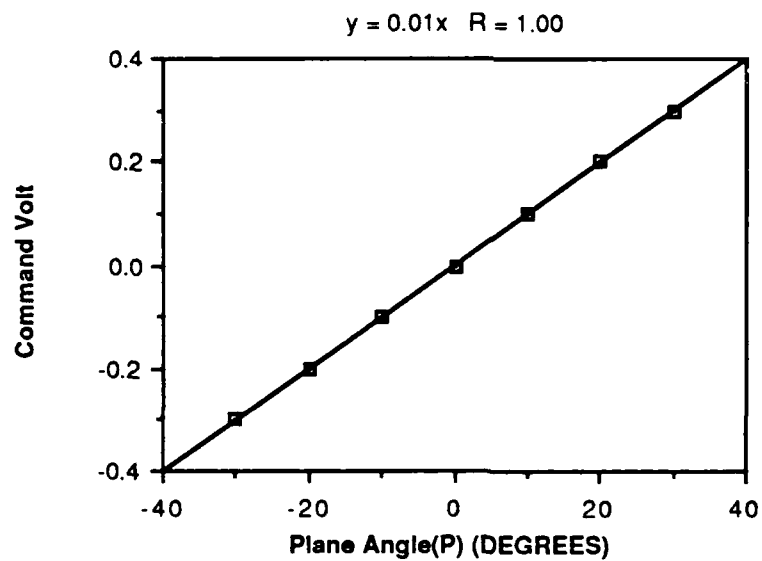


Figure 43 Compensated Dive Plane Control Signal

## H. DATA ACQUISITION

Five channels of data were transmitted from the vehicle by wire. Along with the positive and negative power lines, these wires were wrapped together to form the data and power cable. Spare wires and the radio receiver antenna line were also included. These wires were connected to a standard terminal board. Table 7 gives the pin number vs. data channel hookup.

TABLE 7. TERMINAL BOARD HOOKUP

<u>Pin Number</u>	<u>Channel</u>
1	Positive Power Lead
2	Yawrate Gyro
3	Rollrate Gyro
4	Pitchrate Gyro
5	Speed Pressure Cell
6	Depth Pressure Cell
7	Antenna
8	Spare
9	Spare
10	Spare
11	Signal Ground(connected to analog computer ground)
12	Negative Power Lead

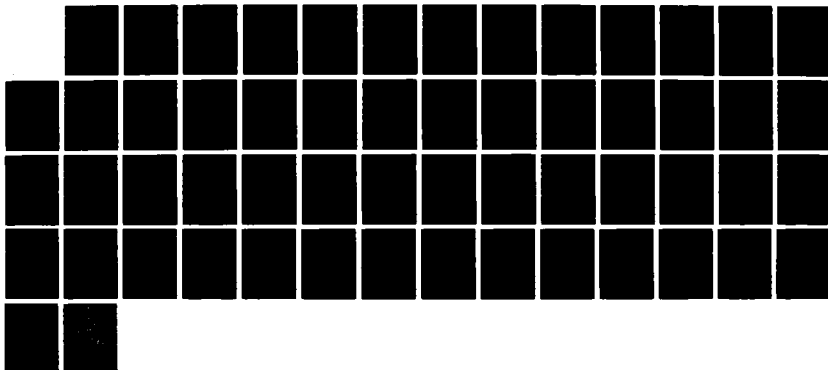
The terminal board was secured to a carriage assembly located above the tank. This carriage traveled the length of the tank. Sufficient cable was then run between the terminal board and the recording instruments and power supply to permit operation of the vehicle down the complete length of the test tank. A six ampere rated DC power supply, with floating ground, was used to

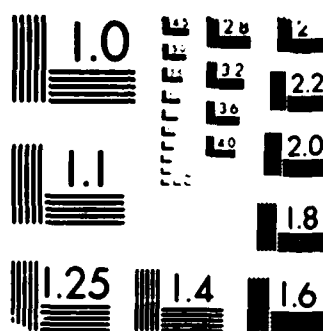
AD-A193 843

EXPERIMENTAL VERIFICATION OF AUV (AUTONOMOUS UNDERWATER  
VEHICLE) PERFORMANCE(U) NAVAL POSTGRADUATE SCHOOL 2/2  
MONTEREY CA G M BRUNNER MAR 88

UNCLASSIFIED

F/G 13/10 NL





MICROCOPY RESOLUTION TEST CHART  
 U.S. GOVERNMENT PRINTING OFFICE: 1963 O

supply the necessary 12.0 volts to the vehicle. Current drawn reached levels of nearly four amperes at full speed ahead on the throttle control with all other systems on line. The primary data signals of interest were the DP cell monitoring depth and the pitch rate gyro. These signals along with the yaw rate gyro and the DP cell monitoring speed were connected to an eight channel stripchart recorder. Four channels had been assigned to vehicle signal return lines. Roll rate was not monitored. The restoring moment acted against any inclination of the vehicle to roll. Mechanical adjustment of dive planes was performed to minimize any mismatch in dive plane action which would cause such a roll. Differences in friction in the forward dive plane shafting, as well as small variances in actual shape and size which resulted during manufacture, were countered by the restoring moment. No dive induced roll was observed. The other four channels of the stripchart recorder were connected to the output of the analog computer. The analog computer was used to modify the command signals for rudder, speed, roll and dive planes produced by the radio control box. One potentiometer was set to provide 2.19 volts for cancellation of a 2.19 volt bias in the dive plane command signal. This same voltage was applied to summers in conjunction with the roll and rudder signals to reduce the output voltages to levels within the range of the stripchart recorder. Another potentiometer was used to zero the command speed signal. The command signals monitored were speed, rudder and dive plane angle. Pitch was fed into the remaining stripchart channel. The pitch rate signal from the vehicle gyro was fed into the analog computer relay comparator. Two relay comparators had been installed in the computer but one of them was not operational. A second analog computer

also became inoperable. With only one relay comparator available, a plus-minus deadband about zero could not be provided. By careful adjustment of the pitch rate gyro zero pot the gyro bias could be maintained on the positive side of zero volts. The analog computer relay comparator was then set to perform switching at zero volts. A downward pitch of the vehicle produced a negative output signal from the pitch rate gyro. When a dive was performed the switch was set up to connect the rate signal to the input of an integrator. The output of the integrator was a signal proportional to pitch. Gyro bias tended to drift somewhat in a range of about 25 millivolts. This would introduce error in any final calibration relation between the actual angle and a corresponding voltage. This bias was the reason a deadband was required. Since it was not constant, it could not easily be compensated for.

The pitch rate signal, Depth DP cell signal, dive plane command signal and the Speed DP cell signal were connected to an Analog to Digital Converter (ADC) board so this data could be digitized. The data was then recorded by computer. By analysis of the data, a transfer function between the input, dive plane command, and output, depth, could be found by use of least square fit identification methods. Integration of the pitch rate data would also provide a means of determining pitch angle and allow calibration of the pitch signal generated by the analog computer integrator. Figure 44 shows the basic signal flow paths.

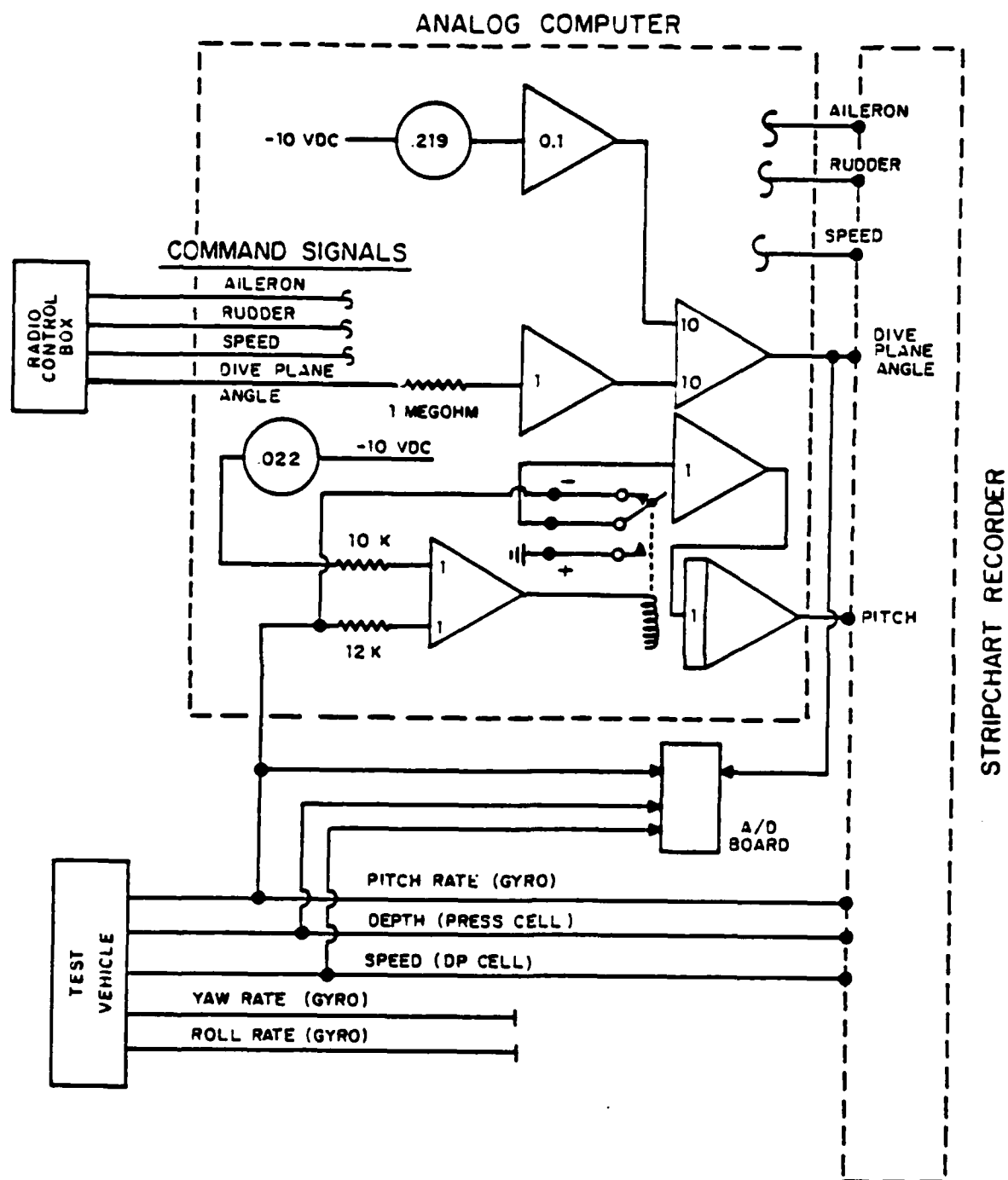


Figure 44 Signal Flow

## V. RESULTS

### A. INTRODUCTION

This chapter describes the technique used to evaluate the transfer functions for system identification and presents the results. Only motion in the vertical plane was analyzed. MATRIXX is the computer software program utilized to accomplish this. An estimate of the system transfer function was made as described in the previous chapters. Thirty-four data runs were performed. Model vehicle maneuvers were controlled through the use of a remotely operated radio control unit. The radio receiver was located aboard the vehicle. The radio control unit was operated manually, therefore, all tests were open-loop. Future implementation of the computer controller will provide closed-loop control.

Ten data runs were selected for computer analysis. Five of those runs were selected for presentation in graphical form. Refer to Figures 45 through 56. These runs were selected based on data quality and run performance. Important considerations were whether the test run was performed with minimal rudder operation, speed loss or any obvious outside disturbing influence present.

For both the theoretical and computer generated transfer functions a Single-Input-Single-Output (SISO) system was assumed. A Recursive Least Squares technique was used to fit the data. This technique has some inherent problems since it can not account for unmodeled disturbances or biases. An extended Kalman Filter technique might be able to compensate for these disturbances and biases in future work.



## B. PREDICTED TRANSFER FUNCTIONS

A first approximation was the simplified plant model incorporating only the pitch equation of motion with indirect hydrodynamic coefficients neglected. The system equations are:

$$\frac{\dot{\theta}}{\delta} = \frac{Cf_1 K_y S}{J_y S^2 + BS + M_\theta}, \quad \frac{z}{\dot{\theta}} = \frac{Cf_2 U}{S^2}$$

$$\begin{aligned} J_y &= 0.6 \\ B &= 0.72 \\ K_y &= -0.14 \\ M_\theta &= 0.16 \\ U &= 1.0 \\ Cf_1 &= 1.25 \\ Cf_2 &= 4.306 \end{aligned}$$

These equations were multiplied by the necessary conversion constants  $Cf_1$  and  $Cf_2$ , which were determined from the calibration tests, to give them dimensions of volts/volts. The second model utilized the equations of motion with all hydrodynamic derivatives acting. These equations were significantly more complicated to solve but transfer functions were derived. The coefficients of each term are comprised of various combinations of the hydrodynamic derivatives. The model equations are:

$$\frac{q}{\delta} = \frac{Es^2 + Fs}{As^3 + Bs^2 + Cs + D} \quad (7a)$$

$$\frac{z}{q} = \frac{N_1 s^3 + N_2 s^2 + N_3 s + N_4}{s^2 [D_1 s^2 + D_2 s + D_3]} \quad (7b)$$

where  $q = \dot{\theta}$  after nondimensionalizing.

These equations were also multiplied by necessary conversion factors to give them dimensions of volts/volts. The constants in Equations 7a and 7b correspond to the following hydrodynamic coefficients.

$$a1 = -M'_w$$

$$a2 = -Z'_w$$

$$b1 = -M'_q$$

$$b2 = m' - Z'_\dot{w}$$

$$c1 = (I'_y - M'_\dot{q})$$

$$c2 = -(Z'_q + m')$$

$$d1 = -M'_\theta$$

$$k2 = Z'_\delta$$

$$k1 = M'_\delta$$

$$A = b2 * c1$$

$$N1 = k2 * A$$

$$B = b2 * b1 + a2 * b1 + a1 * c2$$

$$N2 = k2 * B + E * [U * b2 - c2]$$

$$C = b2 * d1 + a2 * b1 - a1 * c2$$

$$N3 = \{k2 * C + F * [U * b2 - c2] + U * a2 * E\}$$

$$D = a2 * d1$$

$$N4 = U * a2 * F + k2 * D$$

$$E = k1 * b2$$

$$D1 = b2 * E$$

$$F = k1 * a2 - k2 * a1$$

$$D2 = a2 * E + b2 * F$$

$$D3 = a2 * F$$

These equations were then discretized to determine the 'z' domain transfer functions using a zero order hold. The order of the model is provided as an input to the program. A least-squares-fit method was then performed by the program to adjust equation coefficients until the best fit between input and output data was achieved. By using this approach to system identification, the system model equations could be adjusted to better simulate the actual vehicle characteristics. This allows better controller design.

### C. COMPUTER SOLUTION APPROACH

The basic method of solving for the transfer functions is as follows:

- 1) Load the data file for the particular run of interest.

- 2) Detrend data as necessary.
- 3) Enter the order of the transfer function numerator and denominator.
- 4) Perform recursive-least-squares (RLS) fit of the data.
- 5) With the computer generated transfer function, simulate the model's response to the input data.
- 6) Compare actual response to simulated response.

Detrending of data was not always performed. Caution had to be used in using this software capability. Detrending effectively removes constant bias signals; however, if applied to data files such as depth or dive plane command signals, the computer-generated fit may be poor. These signals necessarily contain a non-zero mean value. Detrending was performed on the gyro output since these gyros did exhibit a relatively constant bias for the duration of each run, although in theory, they should have had none.

#### D. RESPONSE OF PITCHRATE TO DIVE PLANE ANGLE

Ten data runs were analyzed to determine the transfer function between dive plane command signal and pitch rate. Excellent correlation for both a second order and third order transfer function was achieved for the runs conducted at the two higher speeds of 1.8 and 2.1 ft/sec. Correlation for the lower speed run conducted at about 1.2 ft/sec was not as good. Very little difference between second order and third order approximations was found. This seems to indicate the predominance of the inertia and damping coefficients over other system parameters. Thus, a simple second order system model provides adequate simulated responses with the restriction that

speed is sufficient to reduce the effects of the restoring moment and other system disturbances. At low speeds the drag from the data and power cord appears to cause a sufficient disturbing moment to affect vehicle movement. Also, the gyro signal is not quite as large with the slower motions taking place at lower speeds. The predicted discretized transfer functions are presented in Table 8. The different numerators in the fourth order model transfer functions for depth vs. pitchrate is because some of the coefficients in the numerator are functions of speed, U. The second order model for pitchrate vs. dive plane angle was found by simple estimations of damping, forces on dive planes, etc., assuming a vessel speed of one ft/sec. The higher order model was found using the nondimensionalized equations of motion which include the effects of angle of attack and the stability derivative,  $M_w$ .

TABLE 8. PREDICTED TF  
PITCHRATE vs. DIVE PLANE ANGLE

<u>Second Order</u>	<u>Third Order</u>
{U=1.0 ft/sec}	
$\frac{\dot{\theta}}{\delta} = \frac{0.0142z - 0.0142}{[z^2 - 1.9411 + 0.9418]}$	$\frac{\dot{\theta}}{\delta} = \frac{1.54U[-0.1191z^2 + 0.2313z - 0.1122]}{[z^3 - 2.8074z^2 + 2.6257z - 0.8181]}$

C.E. Roots : 0.9849, 0.9562      C.E. roots : 0.8888, 0.9593 ± j 0.0141

DEPTH vs. PITCHRATE

<u>Second Order</u>	<u>Fourth Order</u>
$\frac{Z}{\dot{\theta}} = \frac{0.0053825U[z+1.0]}{[z^2 - 2z + 1]}$	
{U=1.2 ft/sec}	$\frac{Z}{\dot{\theta}} = \frac{23.44[-0.0001z^3 + 0.0034z^2 - 0.0063z + 0.0029]}{U[z^4 - 3.8298z^3 + 5.4927z^2 - 3.4962z + 0.8332]}$
{U=1.8 ft/sec}	$\frac{Z}{\dot{\theta}} = \frac{23.44[0.0007z^3 + 0.0027z^2 - 0.0070z + 0.0036]}{U[z^4 - 3.8298z^3 + 5.4927z^2 - 3.4962z + 0.8332]}$

TABLE 8. continued

{U=2.1 ft/sec}

$$\frac{Z}{\dot{\theta}} = \frac{23.44[0.0010z^3 + 0.0024z^2 - 0.0073z + 0.0039]}{U[z^4 - 3.8298z^3 + 5.4927z^2 - 3.4962z + 0.8332]}$$

C.E. roots : 0.8529, 1.0, 1.0, 0.9769

## E. TRANSFER FUNCTION IDENTIFICATION

Results of the computer fit simulations are shown in Figures 45 through 56. The abscissa is the number of sampling periods. The sampling time was 0.05 seconds. The excellent fit between actual response and simulated response indicates that this is a rather good means of determining system models. That is, building a test model, recording rotational rates, depth, speed and linear accelerations to develop system transfer functions. It also demonstrates that the predicted theoretical models are often in error. It is difficult to accurately predict submarine motions through equations developed with assumed or roughly estimated hydrodynamic coefficients. The predicted transfer functions which relate depth to pitchrate differ significantly from the computer generated transfer functions. Table 9 gives a summary of the computer generated transfer functions. With some calculations or by an iterative process the hydrodynamic coefficients which are in error might be determined.

TABLE 9. CALCULATED TF		
<u>Run Number</u>	<u>Order</u>	<u>Transfer Function</u>
9/2	2nd	$\frac{\dot{\theta}}{\delta} = \frac{0.033 Z + 0.0758}{Z^2 - 0.7812 Z - 0.099}$ <p>C.E. Roots = 0.8922, -0.1110</p>
	3rd	$\frac{\dot{\theta}}{\delta} = \frac{0.0131 Z^2 + 0.1236 Z - 0.0222}{Z^3 - 0.7751 Z^2 - 0.0338 Z - 0.0669}$ <p>C.E. Roots = 0.8961, -0.0605 ± j 0.2664</p>

TABLE 9. continued

7/3

2nd

$$\frac{\dot{\theta}}{\delta} = \frac{0.0701 Z - 0.053}{Z^2 - 0.7397 Z - 0.2053}$$

C.E. Roots = 0.9547, 0.2136

3rd

$$\frac{\dot{\theta}}{\delta} = \frac{0.079 Z^2 - 0.0808 Z + 0.0174}{Z^3 - 0.76761 Z^2 - 0.3062 Z + 0.125}$$

C.E. Roots = 0.9513, -0.4658, 0.2821

7/5

2nd

$$\frac{\dot{\theta}}{\delta} = \frac{0.0196 Z + 0.0132}{Z^2 - 0.4239 Z - 0.4417}$$

C.E. Roots = 0.9095, -0.4857

3rd

$$\frac{\dot{\theta}}{\delta} = \frac{0.0198 Z^2 + 0.0195 Z - 0.0024}{Z^3 - 0.3082 Z^2 - 0.3171 Z - 0.2285}$$

C.E. Roots = 0.9215, -0.3066 ± j 0.3924

8/1

2nd

$$\frac{\dot{\theta}}{\delta} = \frac{0.0602 Z + 0.0875}{Z^2 - 0.4565 Z - 0.3950}$$

C.E. Roots = 0.8969, -0.4404

$$\frac{z}{\dot{\theta}} = \frac{0.03 Z - 0.056}{Z^2 - 1.8729 Z + 0.8727}$$

C.E. Roots = 1.0017, 0.8712

3rd

$$\frac{\dot{\theta}}{\delta} = \frac{0.1367 Z^2 - 0.1051 Z + 0.1579}{Z^3 - 0.343 Z^2 - 0.2446 Z - 0.2211}$$

C.E. Roots = 0.8936, -0.2753 ± j 0.4142

4th

$$\frac{z}{\dot{\theta}} = \frac{-0.076 Z^3 + 0.122 Z^2 - 0.0767 Z - 0.0429}{Z^4 - 0.8098 Z^3 - 0.8152 Z^2 + 0.0982 Z + 0.5267}$$

C.E. Roots = 1.0018, 0.984, -0.588 ± j 0.4343

TABLE 9. continued

9/1	2nd	$\frac{z}{\dot{\theta}} = \frac{0.1151 Z + 0.0832}{Z^2 - 0.6302 Z - 0.3103}$
		C.E. Roots = 0.9565, -0.3245
	3rd	$\frac{z}{\dot{\delta}} = \frac{0.1266 Z - 0.1213}{Z^2 - 1.697 Z + 0.6957}$
		C.E. Roots = 1.0041, 0.6928
	4th	$\frac{\dot{\theta}}{\delta} = \frac{0.0641 Z^2 + 0.2092 Z - 0.0629}{Z^3 - 0.5989 Z^2 - 0.2345 Z - 0.1077}$
		C.E. Roots = 0.9600, -0.1806 ± j 0.2821
	5th	$\frac{z}{\dot{\theta}} = \frac{-0.0291 Z^3 + 0.0252 Z^2 + 0.0431 Z - 0.0572}{Z^4 - 1.1377 Z^3 - 0.291 Z^2 + 0.06 Z + 0.3683}$
		C.E. Roots = 1.0059, 0.9646, -0.4164 ± j 0.4541
	6th	$\frac{z}{\dot{\delta}} = \frac{0.0811 Z - 0.0952}{Z^4 - 1.1415 Z^3 - 0.284 Z^2 + 0.0577 Z + 0.3699}$
		C.E. Roots = 0.9996, 0.9709, -0.4145 ± j 0.4552

## F. DISCUSSION

### 1. Run 7/3

The forward speed was 1.2 ft/sec. Figure 45 shows the pitchrate response of the vehicle to the detrended dive plane command input, UD, shown in Figure 46. The actual response is curve 1. The computer generated fit for a second order and third order transfer function are shown as curves 2 and 3 respectively. The response predicted by the 2nd order theoretical model equation is also shown. This run was performed at a relatively slow speed of 1.2 ft/sec. It is apparent that outside disturbances were taking place which were not accounted for in the models. These disturbances are

attributed to the power and data cord, noise, and a drifting bias in the gyro sensors. The cord caused a slight negative bouyancy on the stern section of the vehicle. (Future tests might consider the use of a neutrally bouyant cord.) Gyro bias is a serious problem which the models could not predict.

## 2. Run 7/5

The forward speed was 1.2 ft/sec. Figure 47 shows the pitchrate response to the square wave input, Y4, shown in Figure 48. The pulse width of the input command signal is longer than in the previous run. A better fit to the actual output, curve 1, is evident. Curve 2 is the second order transfer function and curve 3 is the third order fit. For this run the data was not detrended but rather adjusted to begin at zero. The RLS technique requires zero initial conditions for best data correlation.

## 3. Run 8/1

Speed for this run was measured to be 2.1 ft/sec. Figure 49 shows the pitchrate output, curve 1, and computer fit curves for a second and third order transfer function. Curves 2 and 3 lie directly on top of each other indicating that the second order transfer function accurately predicts the vehicle output. The excellent fit for this data run is believed to be the result of operating at higher speed which minimizes the effect of the data cord and other minor disturbances. The depth is plotted in Figure 50. Curve 1 is the actual output. Curve 2 is the second order computer model. It can not accurately predict the depth response since it lacks the two required integrations relating pichrate to depth. The fourth order model, curve 3, does provide a reasonable prediction of depth, however, the initial condition



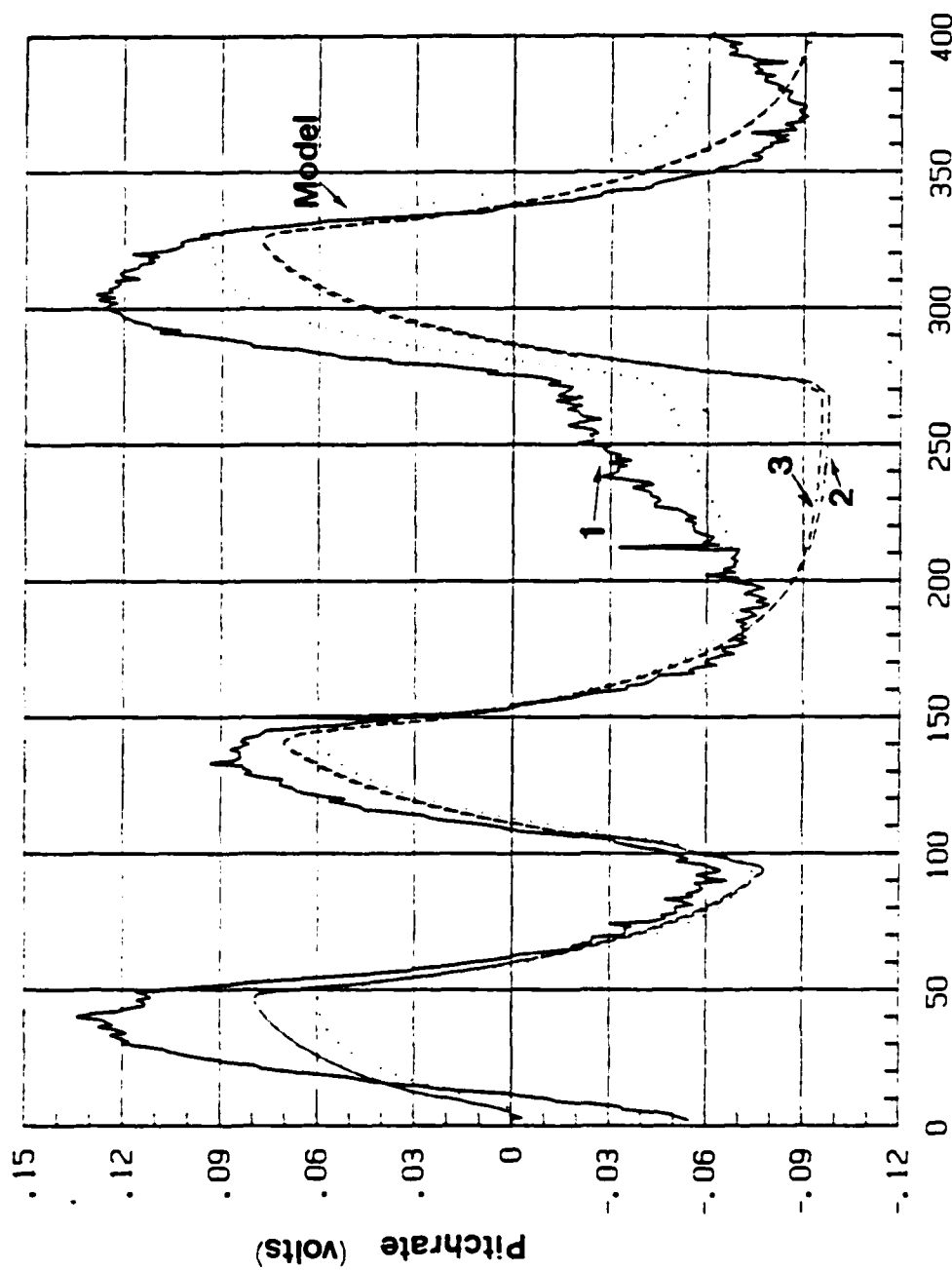
for rate of change of depth is not zero as required for proper data correlation when using RLS. Figure 51 shows the dive plane command input, Y4.

#### 4. Run 9/1

This run was conducted at 1.8 ft/sec. A reasonable second and third order fit to the output, curve 1, was achieved. Curves 2 and 3 lie very close together indicating that the second order fit can accurately predict pitchrate output. Depth correlation could not be achieved for this run. Figure 53 demonstrates the effect of varying the order of the transfer function. Curve 2 is the second order fit between depth and pitchrate and curve 3 is the third order fit. Curve 4 is the transfer function relating dive plane command to depth. This seems indicative of the disturbing influence of the data and power cord on depth. Other difficulties arise from the fact that initial conditions are not all zero. Figure 54 shows the input dive plane command signal, Y4, with bias offset removed.

#### 5. Run 9/2

This run was performed at 1.8 ft/sec but, the dive plane command signal was rapid sinusoidal shaped versus the short pulse width input of Run 9/1. Figure 55 shows the actual output, curve 1, and the second and third order fits, curves 2 and 3 respectively, in response to the input shown in Figure 56. An excellent fit is achieved here since the rapid cycling of dive plane command signal provided a rapid and relatively large gyro output. This masked the effects of bias and noise.



ROW-INDEX  
**Figure 45**    **Run 7/3A**

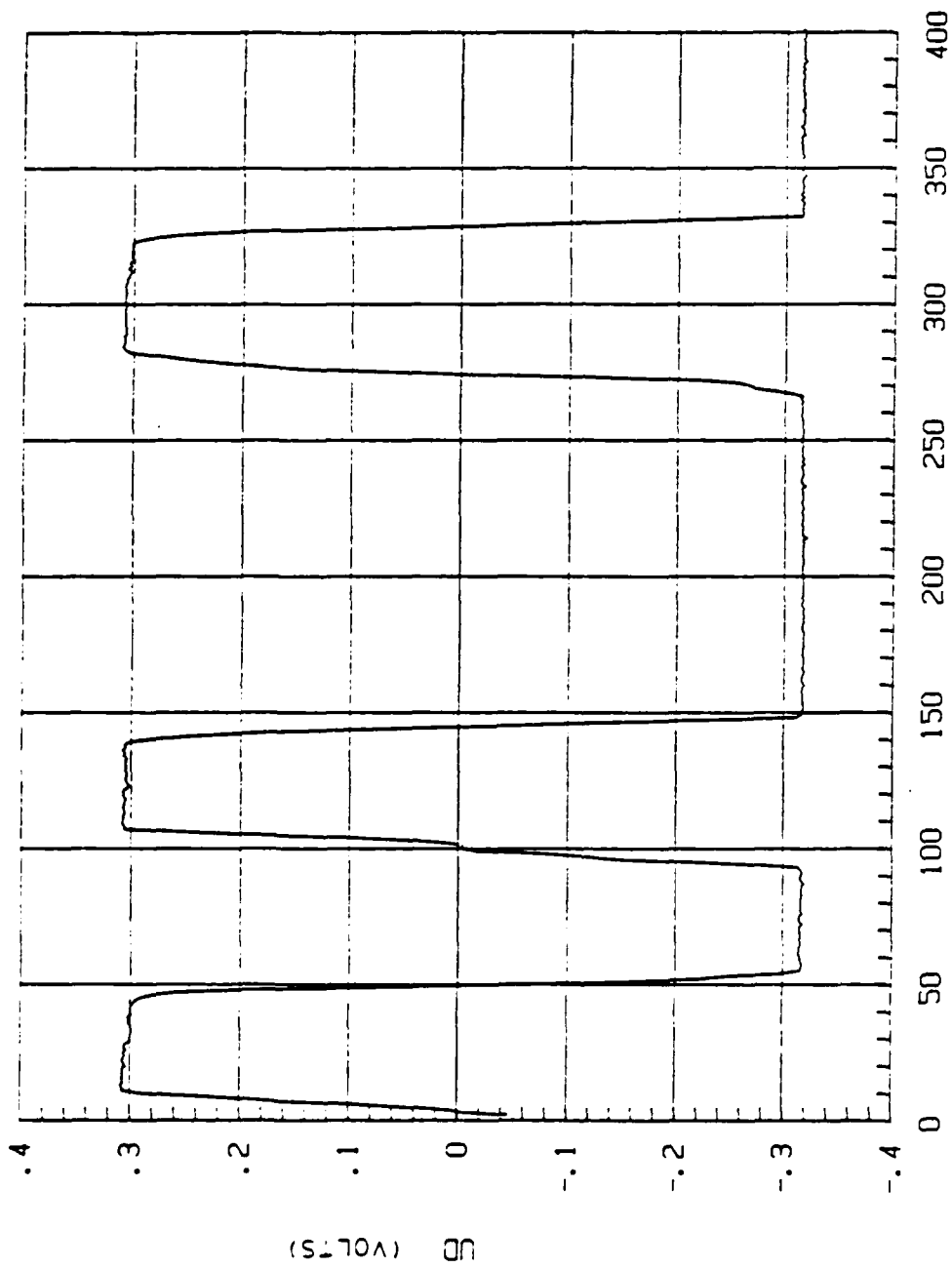


Figure 46 Run 7/3B

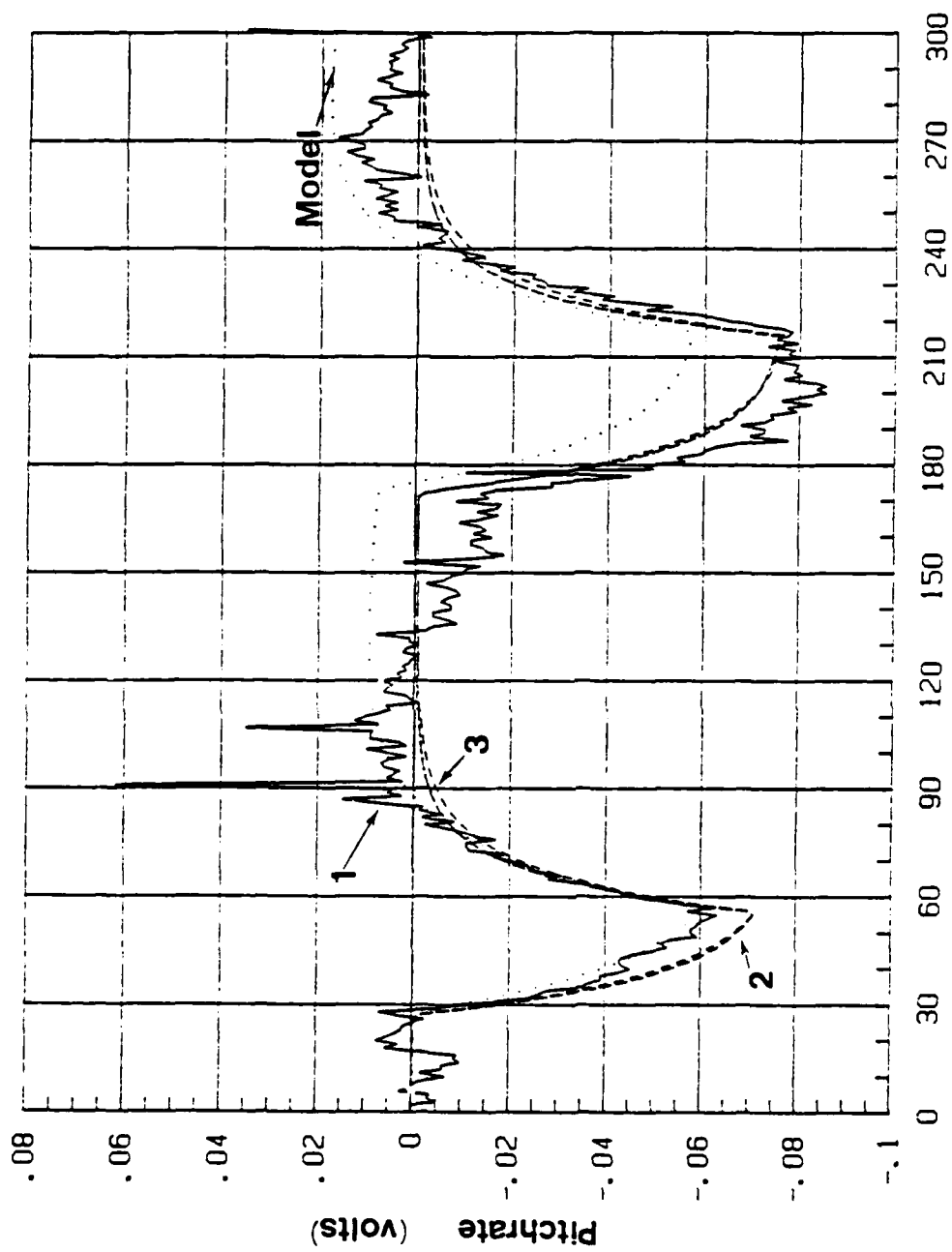
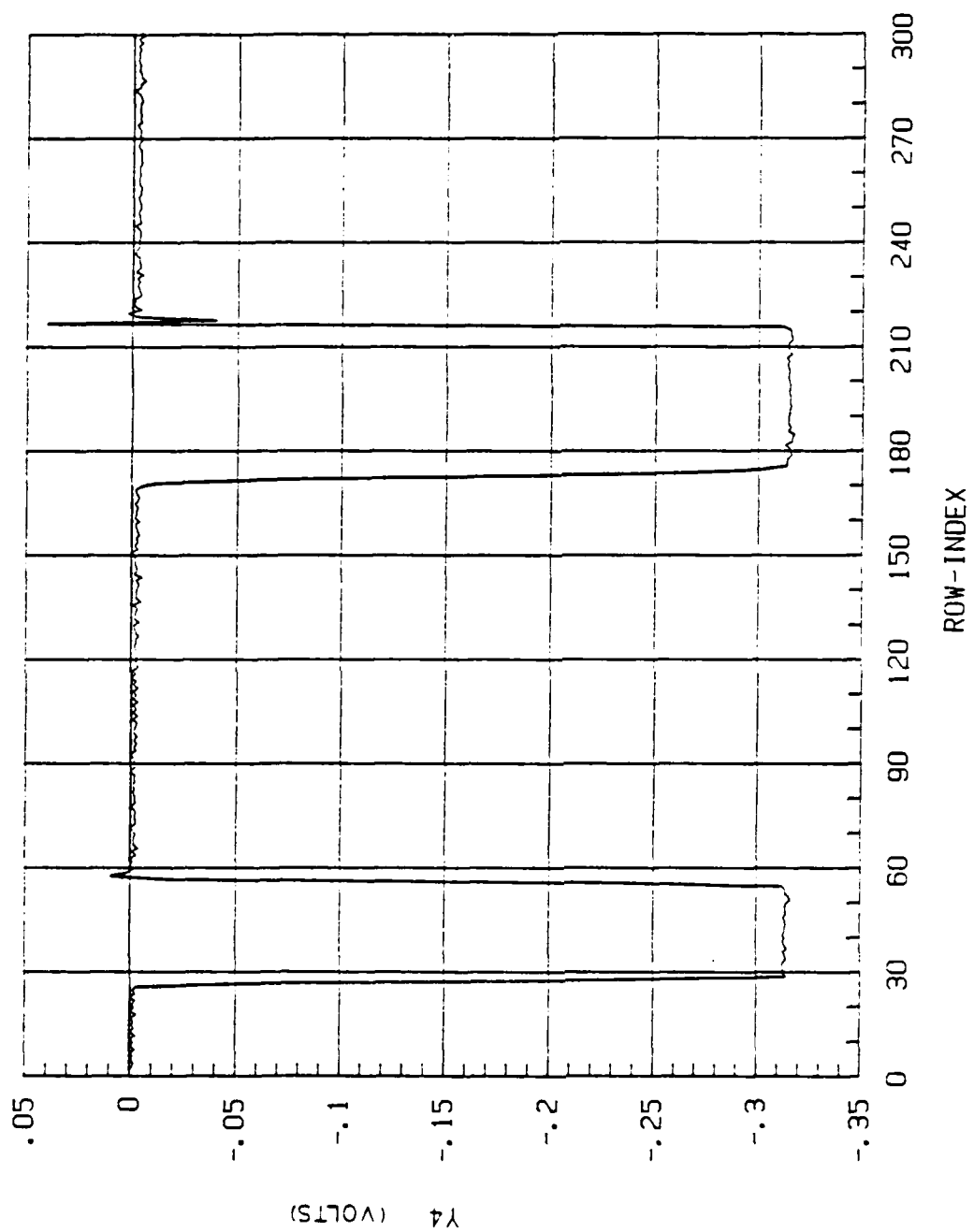
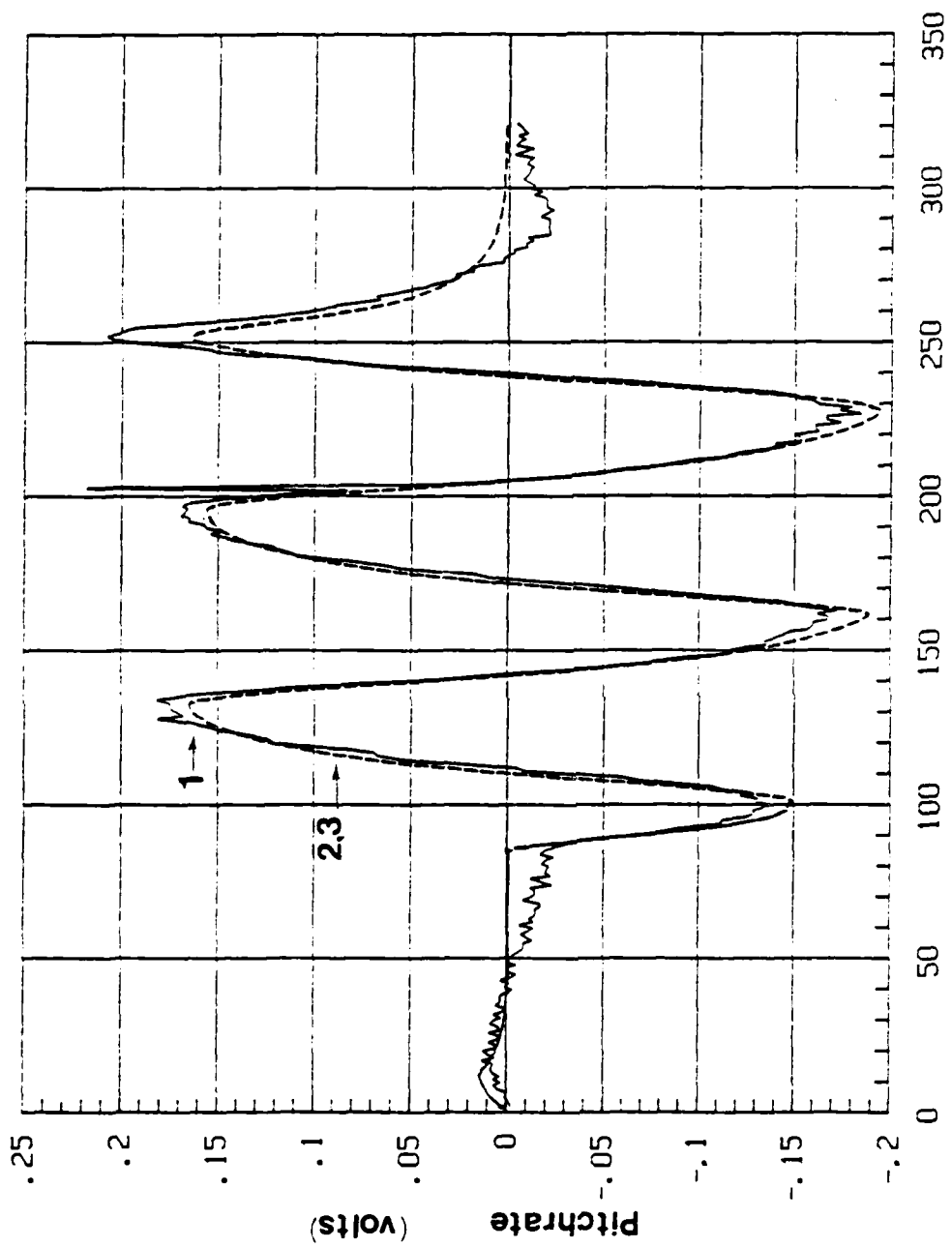


Figure 47 Run 75A





ROW-INDEX  
Figure 49 Run 8/1A

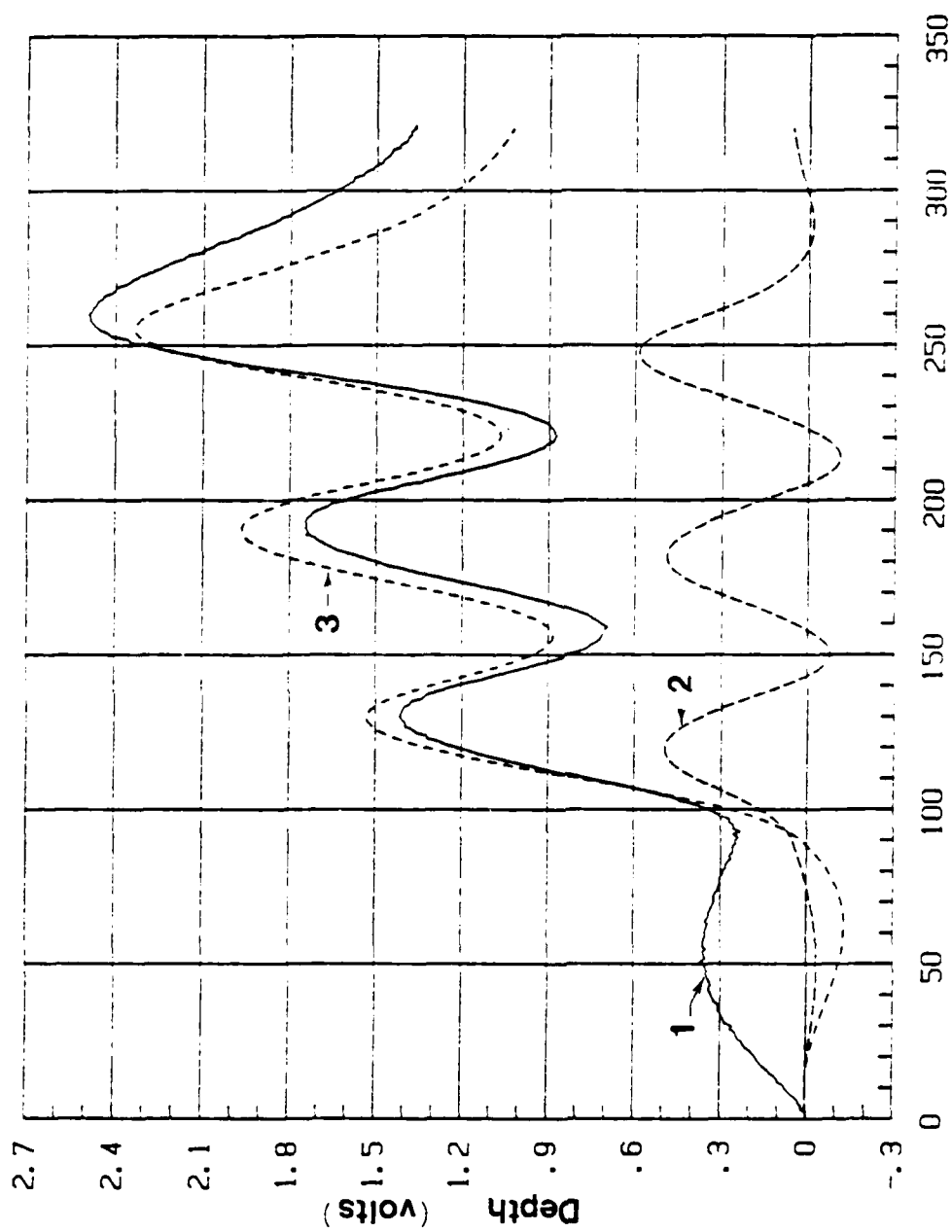


Figure 50 Run 8/1B

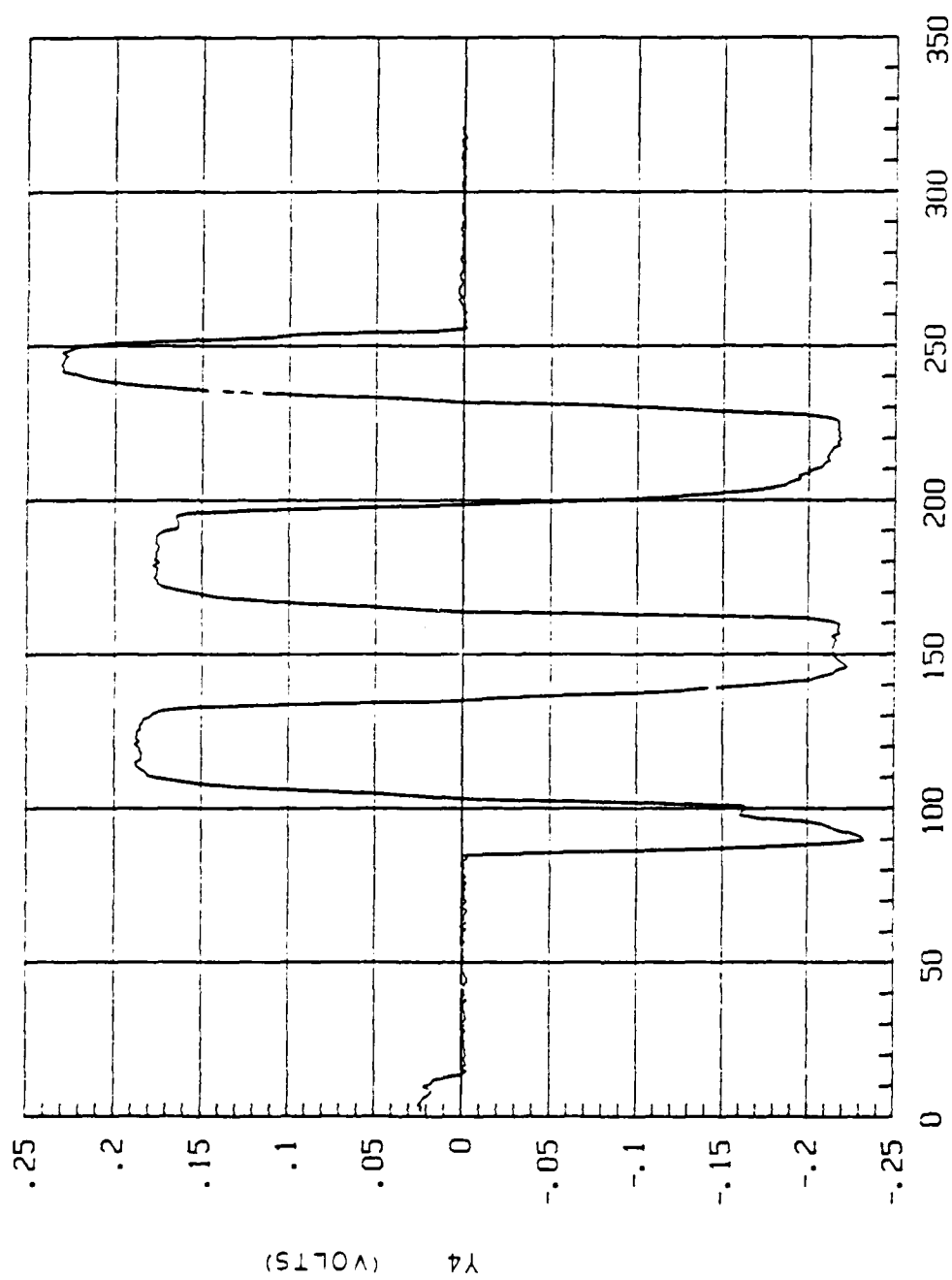


Figure 51 Run 8/1C



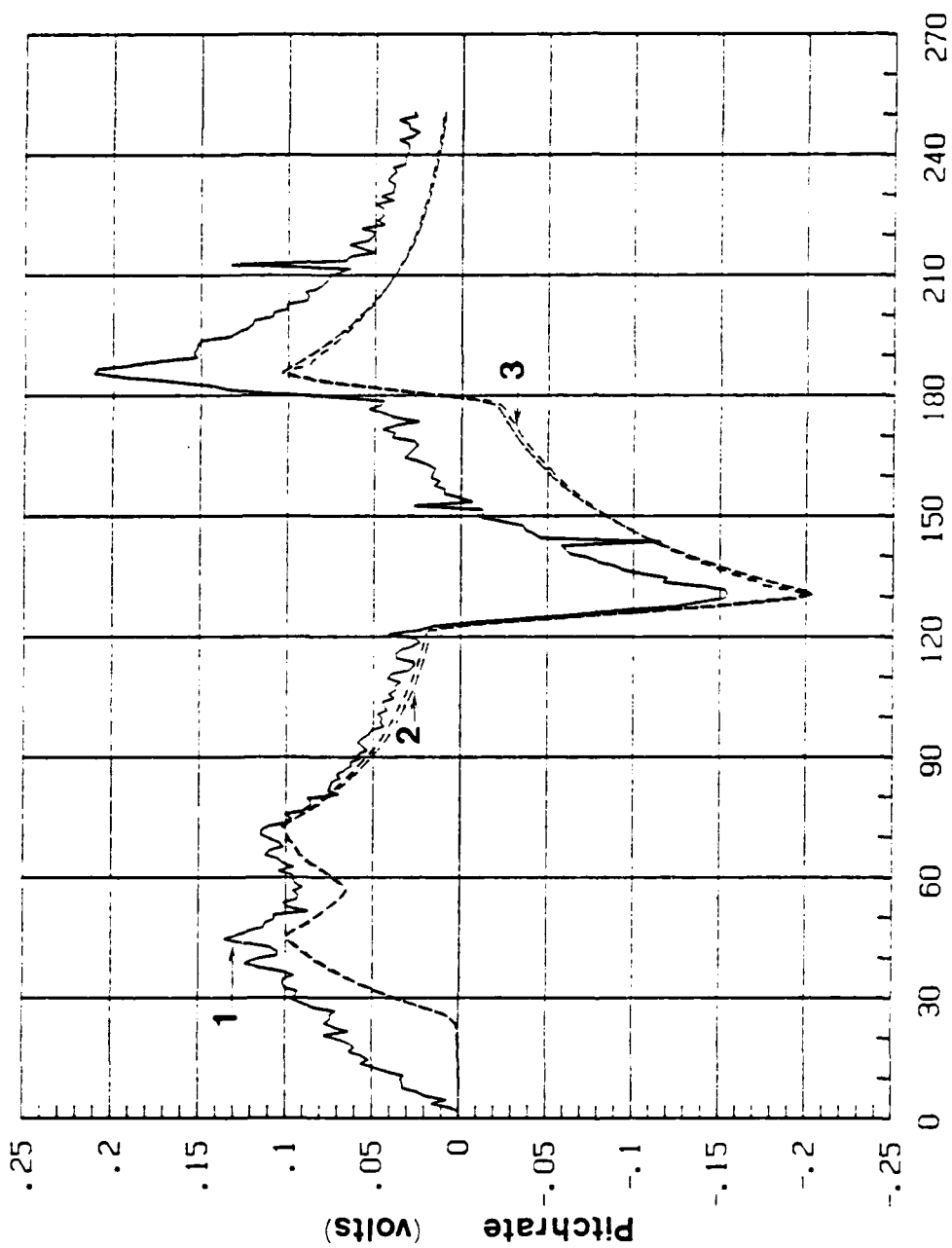


Figure 52 Run 9/1A

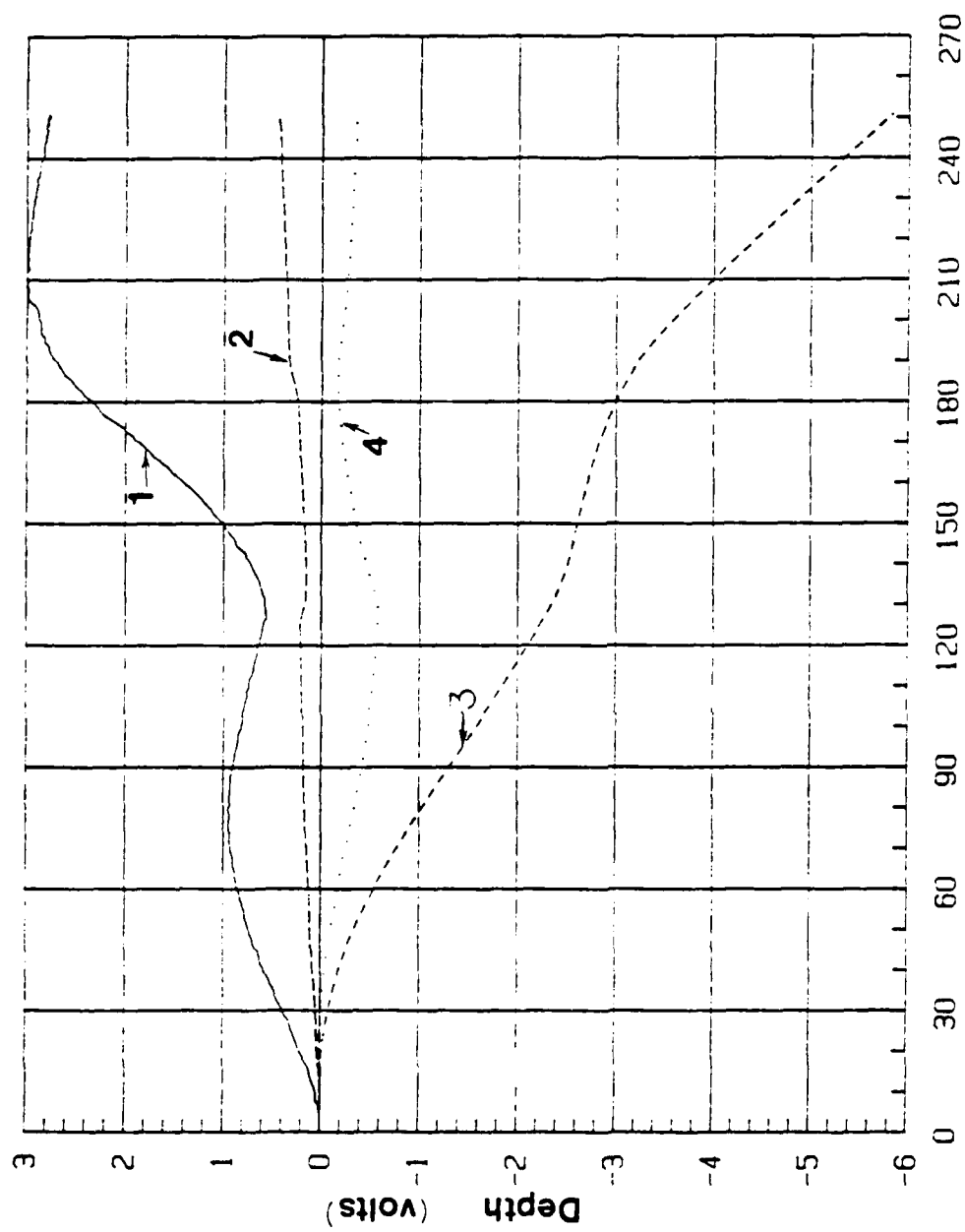


Figure 53 Run 9/1B

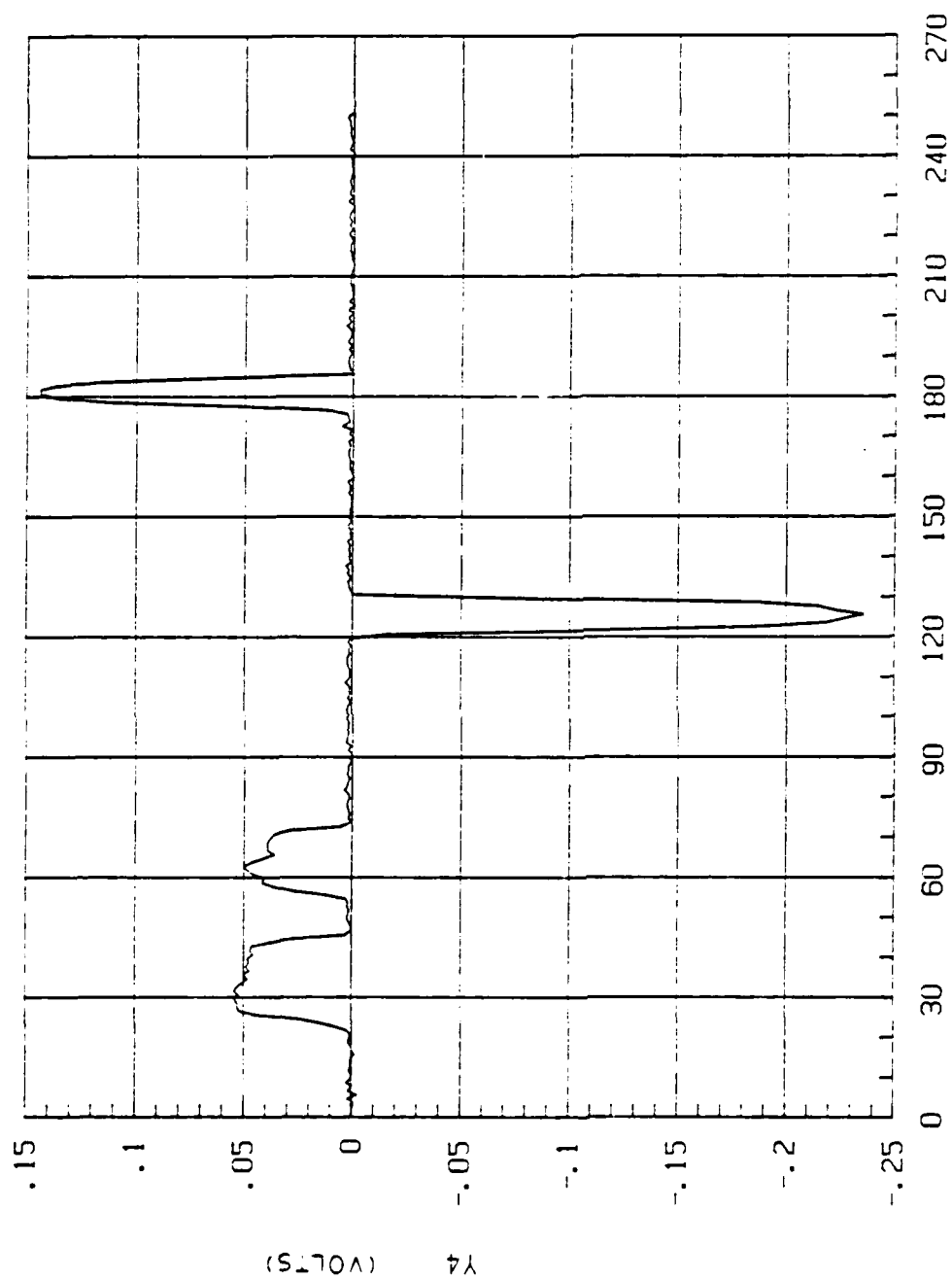


Figure 54 Run 9/1C

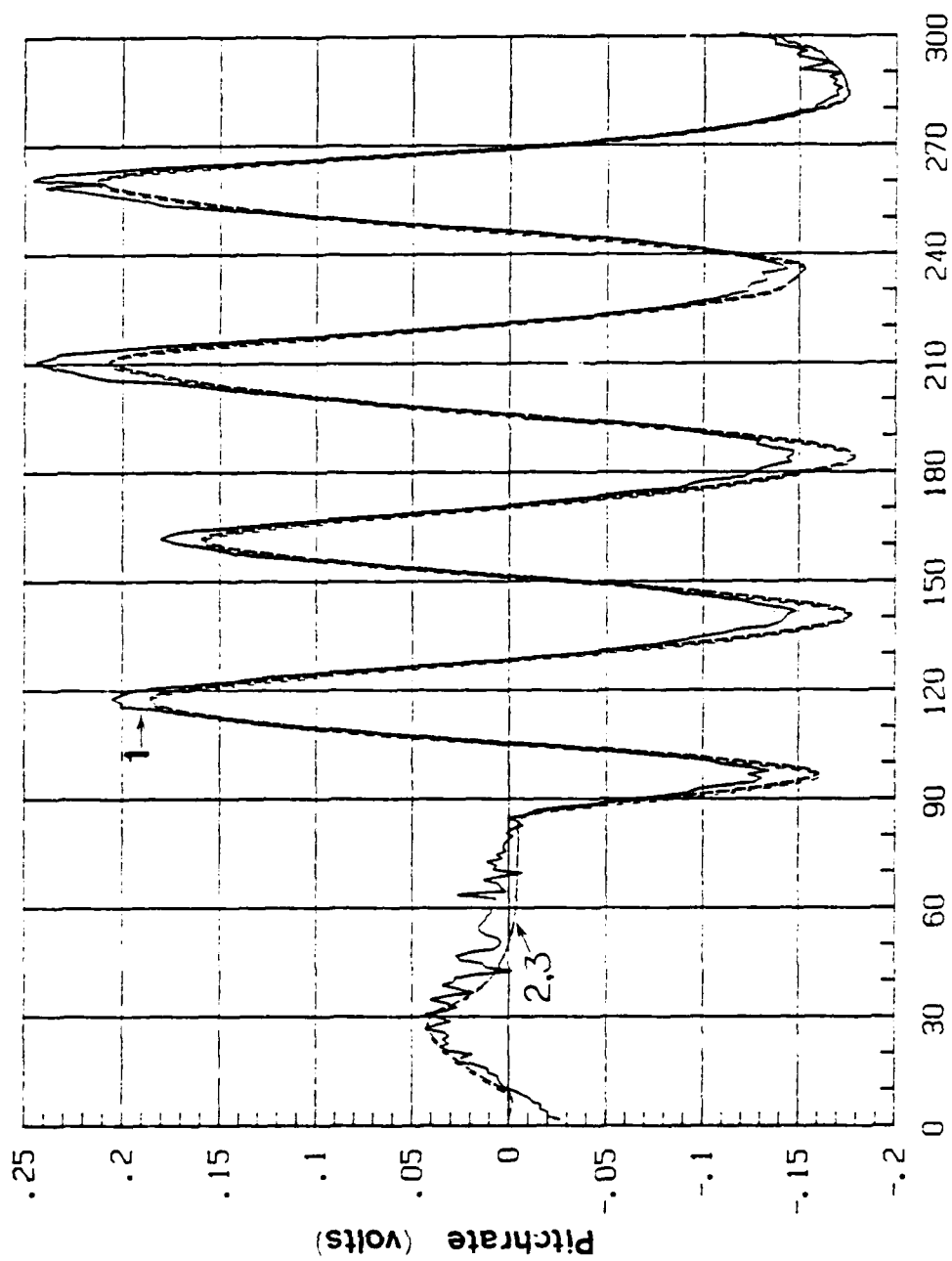
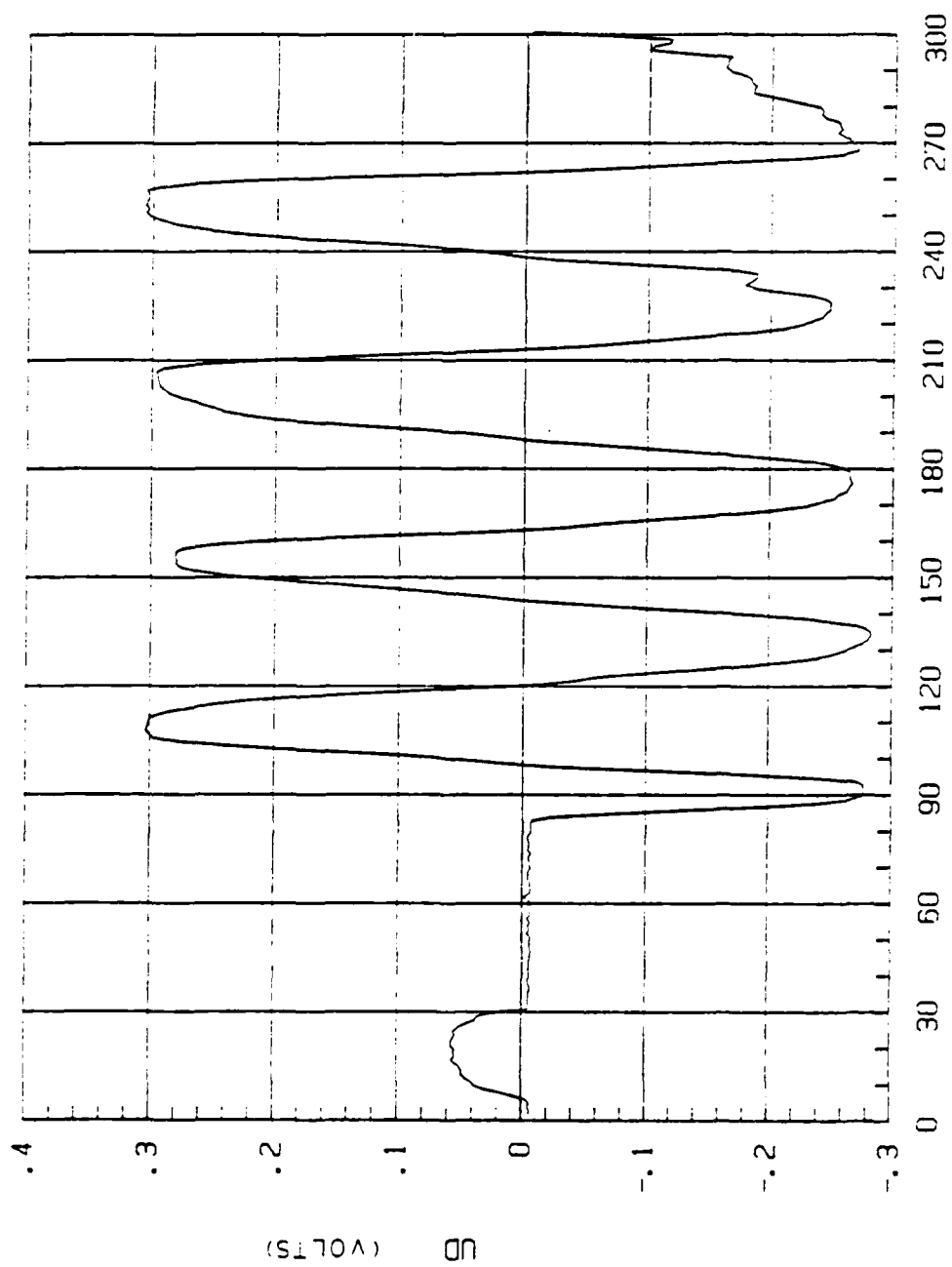


Figure 55 Run 9/2A



ROW-INDEX  
Figure 56 Run 9/2B

## VI. CONCLUSIONS AND RECOMMENDATIONS

### A. CONCLUSIONS

It is evident that excellent results can be achieved by Recursive Least Square Fit of vehicle response data that has been recorded from actual model tests. The development of a controller can proceed with a high probability of excellent results. This is made possible by the availability of accurate transfer function data.

Changes in speed definately alter the vehicle response characteristics as indicated by the changing values of the coefficients for the transfer functions. Adaptive type controllers would most likely be the most efficient means of maintaining an accurate prediction of vehicle response. The strong influence of speed on the values of the system coefficients is evident. In an actual vehicle, speed must be known for purposes of adjusting controller model equations as well as for navigational purposes if accurate vehicle control is necessary. Prediction of pitchrate from dive plane command signals was acceptable when considering open loop conditions were used for test vehicle control. Prediction of depth was much more difficult because of the effects of unmodeled outside disturbances such as the data and power cord, gyro biases and wall effects when operating near the tank bottom or sidewalls. Some data runs were conducted that involved large changes in depth. This resulted in operation near the tank bottom and utilized the full range of the installed depth sensor. Some effect on data output may have taken place which has not been accounted for.

The predominate equation coefficients are those related to inertia and damping. They have the most significant effect on pitchrate as denoted by the fit between actual pitchrate output and both the theoretical and computer predicted output.

The higher order theoretical model equations did not give as good a prediction of depth or pitchrate as hoped, indicating the strong probability that the effective hydrodynamic coefficients and stability derivatives vary.

## B. RECOMMENDATIONS

Further study in identifying actual model hydrodynamic coefficients might provide additional information concerning the importance of various coefficients and their relationship to this particular vehicle shape. System identification with closed loop control should reduce the influence of unmodelled disturbances.

Improvement to the depth sensing system by redesigning the pressure lines could prevent air entrapment, and subsequent errors due to trapped water columns.

Removal of the low range pressure cell associated with the velocity measurement system would allow installation of a sensor for measuring pitch angle directly. This could be achieved by utilizing a higher range differential pressure cell. The high pressure port would be connected to the stagnation tube and the low pressure port would be connected to the sensing line associated with the depth sensor. With proper design, water may be prevented from entering the sensing lines. The columns of air are negligible

to that of the water columns so the cell can be calibrated to read the angle of inclination. Additionally, the following items are suggested:

Redesign of the forward dive plane mechanical linkage assembly is needed. At present, excessive friction exists in the aileron control link collar.

Installation of an additional midsection to the vehicle to accomodate a battery system for vehicle power will reduce the size of the tether, however, the vehicle may then be too large for the present test tank necessitating a larger tank.

The possibility of installing a radiotelemetry device for data transmission should be investigated. This will remove the requirement of a tether altogether.

Establishment of zero initial conditions for all test runs and the minimization of operation in vicinity of tank boundaries will improve usefulness of data.



## LIST OF REFERENCES

1. Baumeister, Theodore, ed., Marks' Mechanical Engineers' Handbook. 6th ed., McGraw-Hill Book Company, 1958.
2. Shigley, Joseph Edward, and Larry D. Mitchell, Mechanical Engineering Design. McGraw-Hill Series in Mechanical Engineering. 4th ed., McGraw-Hill Book Company, 1983.
3. Sarpkaya, T., and M. Isaacson, Mechanics of Wave Forces on Offshore Structures. Van Nostrand Reinhold Company, 1981.
4. Fox, Robert W. and Alan T. McDonald, Introduction to Fluid Mechanics. 2nd ed., John Wiley and Sons, 1978.
5. Hoerner, Sighard F., Aerodynamic Drag. Sighard F. Hoerner, 1951.
6. Streeter, Victor L. and E. Benjamin Wylie, Fluid Mechanics. 8th ed., McGraw-Hill Book Company, 1979.
7. Moffat, Robert J., Pressure Probes for Velocity Measurement, Unpublished, Naval Postgraduate School, 1979.
8. Comstock, John P., ed., Principles of Naval Architecture. New York: The Society of Naval Architects and Marine Engineers, 1967.
9. Delaplane, S., Implementation of a Digital Autopilot For Control of an AUV, M.S.M.E. Thesis, Naval Postgraduate School, Monterey, California, March 1988.

## APPENDIX A

FILE: T2

FORTRAN A

```

TITLE SUBMARINE MOTION SIMULATION
*      K1 = CONTROL DERIV FOR HEAVE
*      K2 = CONTROL DERIV FOR PITCH
*      A1 = LINEAR INERTIA HYD DERIV
*      B1 = LINEAR DAMPING HYD DERIV
*      C1 = COUPLED ROTARY ACCEL HYD DERIV
*      A2 = MOMENT OF INERTIA HYD DERIV
*      B2 = ROTARY DAMPING HYD DERIV
*      C2 = HYDROSTATIC RESTORING MOMENT HYD DERIV
*      D2 = COUPLED LINEAR ACCEL HYD DERIV
PARAM U=1.0, XG=0.0, BG=0.1, L=23.0
*      INITIAL CONDITIONS
CONST W0=0.0, Q0=0.0, T0=0.0, X0=0.0, Z0=0.0
*      HYDRODYNAMIC DERIVATIVE:
CONST K1=0.095, K2=-0.184
CONST A1=1.046, B1=1.295, C1=-0.196
CONST A2=0.072, B2=0.20, C2=1.27, D2=-0.088
      WDOT=(K1*DEL-C1*Q-B1*W)/A1
      W=INTGRL(W0,WDOT)
      QDOT=(K2*DEL-D2*W-C2*THETA-B2*Q)/A2
      Q=INTGRL(Q0,QDOT)
      THETA=INTGRL(T0,Q)
*      DEL=DIVE PLANE ANGLE
      DEL=0.5235987*STEP(0.0) - 0.5235987*STEP(10.0)
*      TRAJECTORY CALCULATION
      ZG=BG/L
      UG=U+ZG*(Q)
      WG=W+XG*(Q)
      ALPHA=6.2831853-THETA
      XDOT=UG*COS(ALPHA) - WG*SIN(ALPHA)
      ZDOT=UG*SIN(ALPHA) + WG*COS(ALPHA)
      X=INTGRL(X0,XDOT)
      Z=INTGRL(Z0,ZDOT)
CONTRL FINTIM=30, DELT=0.001
PRINT 1.0, W,THETA,X,Z
SAVE (S1) 0.005, W,WDOT,DEL
SAVE (S2) 0.005, Q,QDOT,DEL
SAVE (S3) 0.01, X,Z,THETA
GRAPH(G1/S1,DE=TEK618,PO=0,.5) TIME,W,WDOT,DEL
GRAPH(G2/S2,DE=TEK618,PO=0,.5) TIME,Q,QDOT,DEL
GRAPH(G3/S3,DE=TEK618,PO=0,.5) X,Z,THETA
LABEL(G1,DE=TEK618) LINEAR VELOCITIES AND ACCELERATIONS
LABEL(G2,DE=TEK618) ANGULAR VELOCITIES AND ACCELERATIONS
LABEL(G3,DE=TEK618) VERTICAL PLANE MANEUVER
LABEL(ALL,DE=TEK618) FORWARD VELOCITY = 1.0 FT/SEC
END
STOP

```

FILE: T3            FORTRAN A

```
TITLE SUBMARINE MOTION SIMULATION
* K1 = CONTROL DERIV FOR HEAVE
* K2 = CONTROL DERIV FOR PITCH
* A1 = LINEAR INERTIA HYD DERIV
* B1 = LINEAR DAMPING HYD DERIV
* C1 = COUPLED ROTARY ACCEL HYD DERIV
* A2 = MOMENT OF INERTIA HYD DERIV
* B2 = ROTARY DAMPING HYD DERIV
* C2 = HYDROSTATIC RESTORING MOMENT HYD DERIV
* D2 = COUPLED LINEAR ACCEL HYD DERIV
PARAM U=1.0, XG=0.0, BG=0.1, L=23.0
* INITIAL CONDITIONS
CONST W0=0.0, Q0=0.0, T0=0.0, X0=0.0, Z0=0.0
* HYDRODYNAMIC DERIVATIVES
CONST K1=0.095, K2=-0.184
CONST A1=0., B1=0., C1=0., W=0.
CONST A2=0.072, B2=0.20, C2=1.27, D2=0.
* WDOT=(K1*DEL-C1*Q-B1*W)/A1
* W=INTGRL(W0,WDOT)
* QDOT=(K2*DEL-D2*W-C2*THETA-B2*Q)/A2
* Q=INTGRL(Q0,QDOT)
* THETA=INTGRL(T0,Q)
* DEL=DIVE PLANE ANGLE
* DEL=0.5235987*STEP(0.0) - 0.5235987*STEP(10.0)
* TRAJECTORY CALCULATION
ZG=BG/L
UG=U+ZG*(Q)
WG=W+XG*(Q)
ALPHA=6.2831853-THETA
XDOT=UG*COS(ALPHA) - WG*SIN(ALPHA)
ZDOT=UG*SIN(ALPHA) + WG*COS(ALPHA)
X=INTGRL(X0,XDOT)
Z=INTGRL(Z0,ZDOT)
CONTRL FINTIM=30, DELT=0.001
PRINT 1.0, THETA,X,Z
*SAVE (S1) 0.005, W,WDOT,DEL
SAVE (S2) 0.005, Q,QDOT,DEL
SAVE (S3) 0.01, X,Z,THETA
*GRAPH(G1/S1,DE=TEK618,PO=0,.5) TIME,W,WDOT,DEL
GRAPH(G2/S2,DE=TEK618,PO=0,.5) TIME,Q,QDOT,DEL
GRAPH(G3/S3,DE=TEK618,PO=0,.5) X,Z,THETA
*LABEL(G1,DE=TEK618) LINEAR VELOCITIES AND ACCELERATIONS
LABEL(G2,DE=TEK618) ANGULAR VELOCITIES AND ACCELERATIONS
LABEL(G3,DE=TEK618) VERTICAL PLANE MANEUVER
LABEL(ALL,DE=TEK618) FORWARD VELOCITY = 1.0 FT/SEC
END
STOP
```

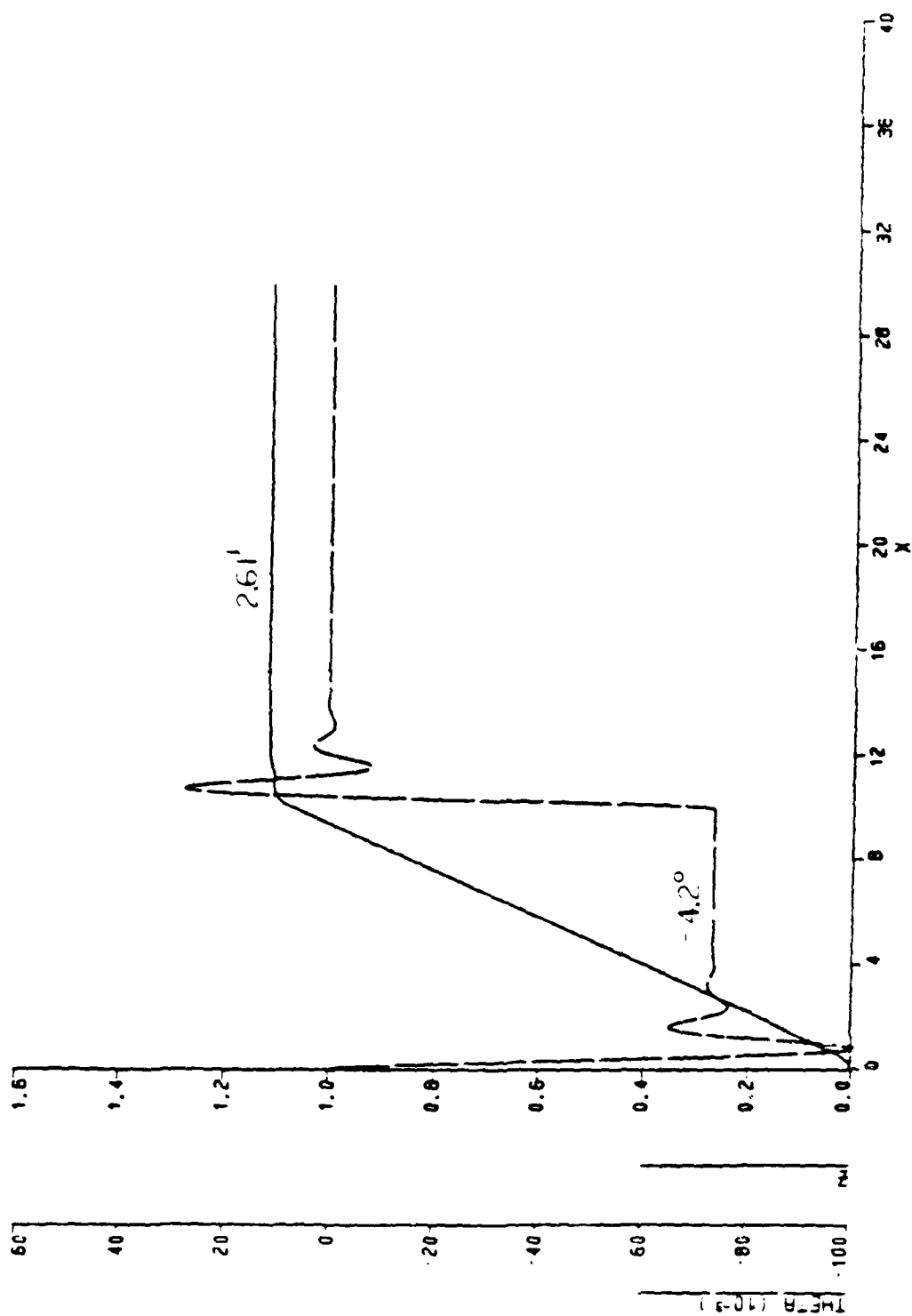
FILE: T4            FORTRAN  A

```
TITLE SUBMARINE MOTION SIMULATION
*      K1 = CONTROL DERIV FOR HEAVE
*      K2 = CONTROL DERIV FOR PITCH
*      A1 = LINEAR INERTIA HYD DERIV
*      B1 = LINEAR DAMPING HYD DERIV
*      C1 = COUPLED ROTARY ACCEL HYD DERIV
*      A2 = MOMENT OF INERTIA HYD DERIV
*      B2 = ROTARY DAMPING HYD DERIV
*      C2 = HYDROSTATIC RESTORING MOMENT HYD DERIV
*      D2 = COUPLED LINEAR ACCEL HYD DERIV
PARAM U=1.0, XG=0.0, BG=0.1, L=28.0
*      INITIAL CONDITIONS
CONST W0=0.0, Q0=0.0, T0=0.0, X0=0.0, Z0=0.0
*      HYDRODYNAMIC DERIVATIVES
CONST K1=0.095, K2=-0.184
CONST A1=0., B1=0., C1=0., W=0.
CONST A2=0.072, B2=0.20, C2=0.00, D2=0.
*      WDOT=(K1*DEL-C1*Q-B1*W)/A1
*      W=INTGRL(W0,WDOT)
*      QDOT=(K2*DEL-D2*W-C2*THETA-B2*Q)/A2
*      Q=INTGRL(Q0,QDOT)
*      THETA=INTGRL(T0,Q)
*      DEL=DIVE PLANE ANGLE
*      DEL=0.5235987*STEP(0.0) - 0.5235987*STEP(1.0)
*      TRAJECTORY CALCULATION
*      ZG=BG/L
*      UG=U+ZG*(Q)
*      WG=W+XG*(Q)
*      ALPHA=6.2831853-THETA
*      XDOT=UG*COS(ALPHA) - WG*SIN(ALPHA)
*      ZDOT=UG*SIN(ALPHA) + WG*COS(ALPHA)
*      X=INTGRL(X0,XDOT)
*      Z=INTGRL(Z0,ZDOT)
CONTRL FINTIM=15, DELT=0.001
PRINT 1.0, THETA,X,Z
*SAVE (S1) 0.005, W,WDOT,DEL
*SAVE (S2) 0.005, Q,QDOT,DEL
*SAVE (S3) 0.01, X,Z,THETA
*GRAPH(G1/S1,DE=TEK618,PO=0,.5) TIME,W,WDOT,DEL
*GRAPH(G2/S2,DE=TEK618,PO=0,.5) TIME,Q,QDOT
*GRAPH(G3/S3,DE=TEK618,PO=0,.5) X,Z,THETA
*LABEL(G1,DE=TEK618) LINEAR VELOCITIES AND ACCELERATIONS
*LABEL(G2,DE=TEK618) ANGULAR VELOCITIES AND ACCELERATIONS
*LABEL(G3,DE=TEK618) VERTICAL PLANE MANEUVER
*LABEL(ALL,DE=TEK618) FORWARD VELOCITY = 1.0 FT/SEC
END
STOP
```

FILE: T5            FORTRAN A

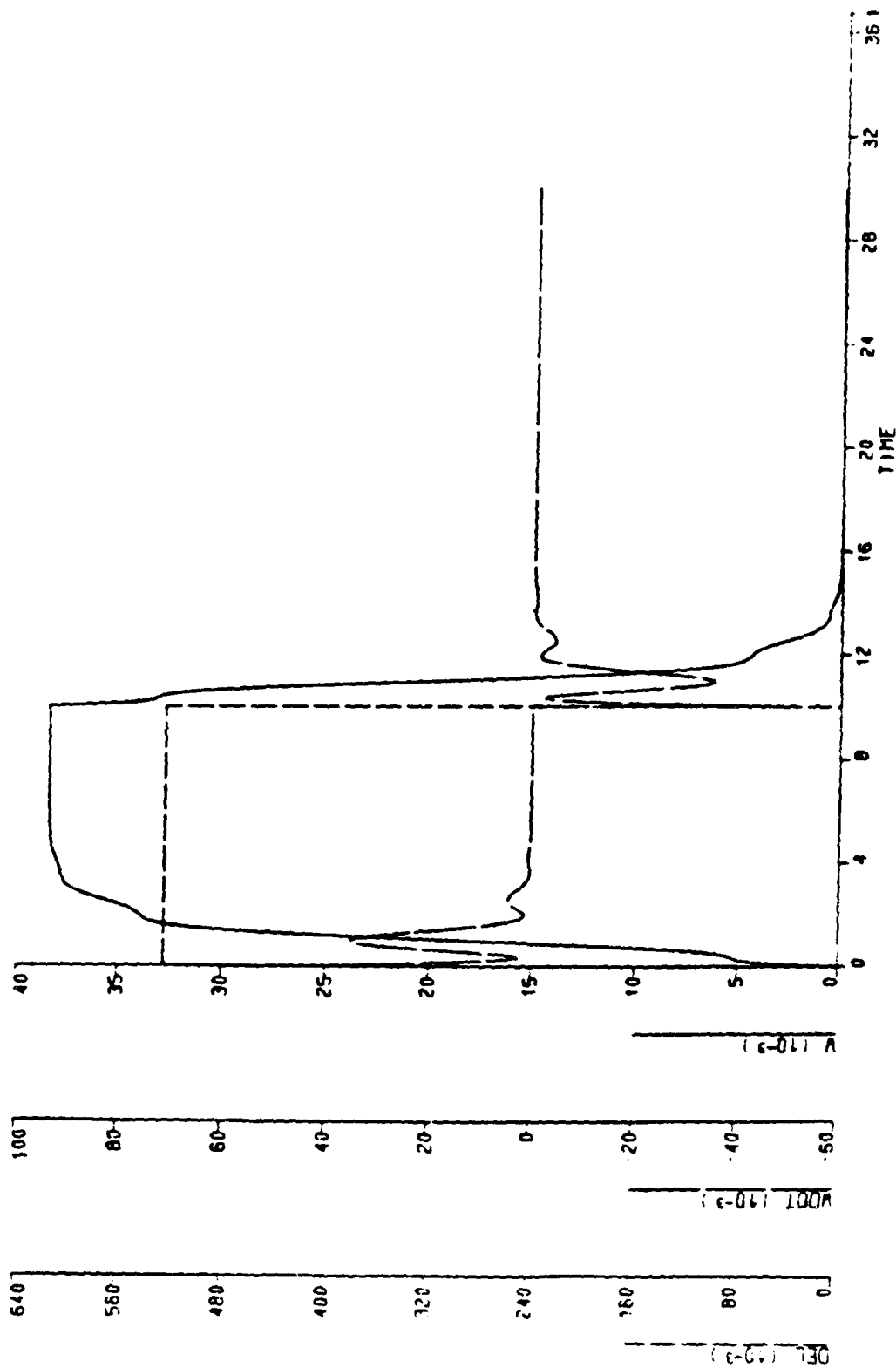
```
TITLE SUBMARINE MOTION SIMULATION
*      K1 = CONTROL DERIV FOR HEAVE
*      K2 = CONTROL DERIV FOR PITCH
*      A1 = LINEAR INERTIA HYD DERIV
*      B1 = LINEAR DAMPING HYD DERIV
*      C1 = COUPLED ROTARY ACCEL HYD DERIV
*      A2 = MOMENT OF INERTIA HYD DERIV
*      B2 = ROTARY DAMPING HYD DERIV
*      C2 = HYDROSTATIC RESTORING MOMENT HYD DERIV
*      D2 = COUPLED LINEAR ACCEL HYD DERIV
PARAM U=1.0, XG=0.0, BG=0.1, L=28.0
*      INITIAL CONDITIONS
CONST W0=0.0, Q0=0.0, T0=0.0, X0=0.0, Z0=0.0
*      HYDRODYNAMIC DERIVATIVES
CONST K1=0.095, K2=-0.184
CONST A1=1.046, B1=1.295, C1=-0.196
CONST A2=0.072, B2=0.02, C2=1.27, D2=-0.088
      WDOT=(K1*DEL-C1*Q-B1*W)/A1
      W=INTGRL(W0,WDOT)
      QDOT=(K2*DEL-D2*W-C2*THETA-B2*Q)/A2
      Q=INTGRL(Q0,QDOT)
      THETA=INTGRL(T0,Q)
*      DEL=DIVE PLANE ANGLE
      DEL=0.5235987*STEP(0.0) - 0.5235987*STEP(10.0)
*      TRAJECTORY CALCULATION
      ZG=BG/L
      UG=U+ZG*(Q)
      WG=W+XG*(Q)
      ALPHA=6.2831853-THETA
      XDOT=UG*COS(ALPHA) - WG*SIN(ALPHA)
      ZDOT=UG*SIN(ALPHA) + WG*COS(ALPHA)
      X=INTGRL(X0,XDOT)
      Z=INTGRL(Z0,ZDOT)
CONTRL FINTIM=30, DELT=0.001
PRINT 1.0, W,THETA,X,Z
SAVE (S1) 0.005, W,WDOT,DEL
SAVE (S2) 0.005, Q,QDOT,DEL
SAVE (S3) 0.01, X,Z,THETA
GRAPH(G1/S1,DE=TEK618,PO=0,.5) TIME,W,WDOT,DEL
GRAPH(G2/S2,DE=TEK618,PO=0,.5) TIME,Q,QDOT,DEL
GRAPH(G3/S3,DE=TEK618,PO=0,.5) X,Z,THETA
LABEL(G1,DE=TEK618) LINEAR VELOCITIES AND ACCELERATIONS
LABEL(G2,DE=TEK618) ANGULAR VELOCITIES AND ACCELERATIONS
LABEL(G3,DE=TEK618) VERTICAL PLANE MANEUVER
LABEL(ALL,DE=TEK618) FORWARD VELOCITY = 1.0 FT/SEC
END
STOP
```

# APPENDIX B



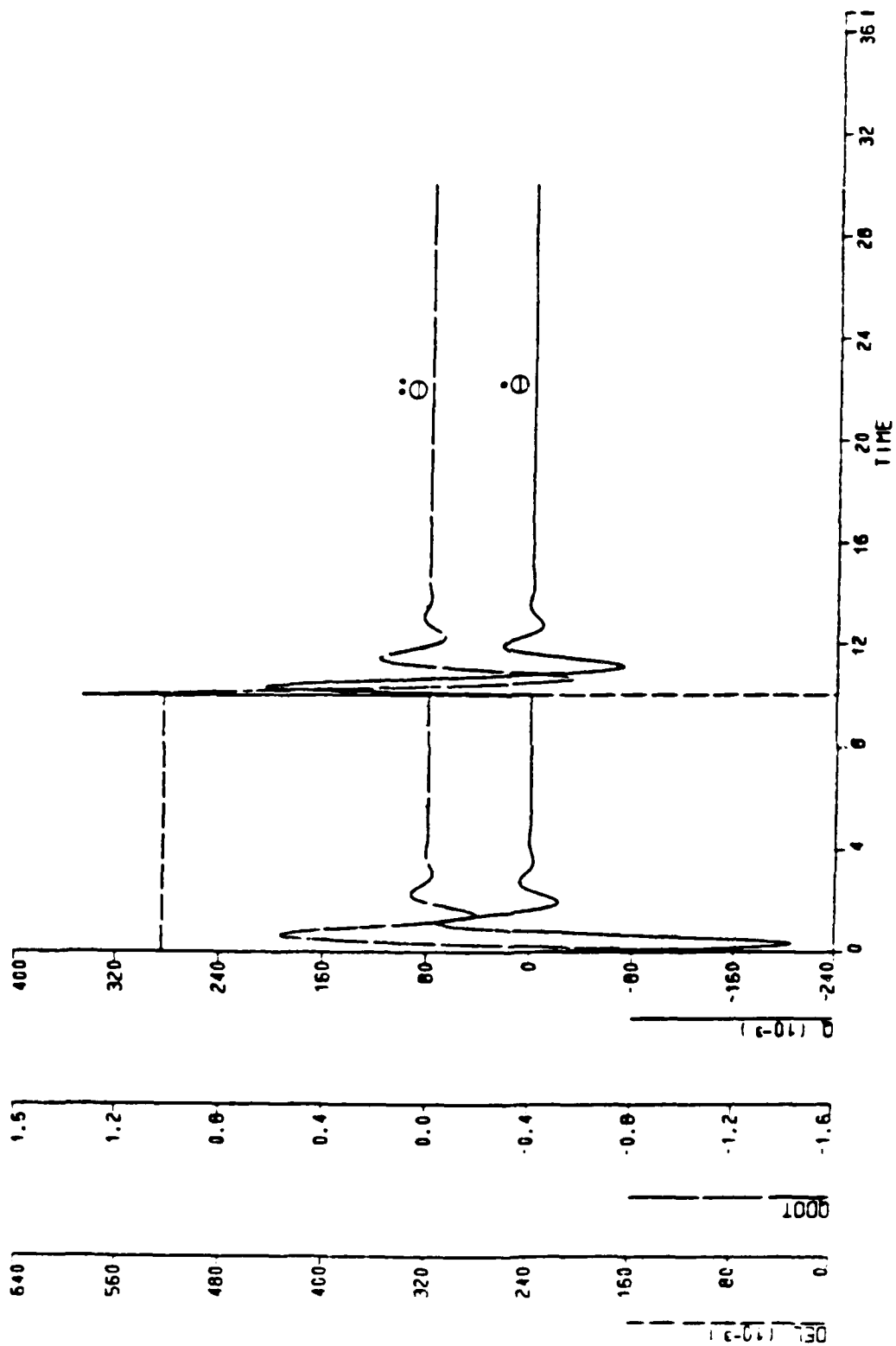
VERTICAL PLANE MANEUVER  
FORWARD VELOCITY - 1.0 FT/SEC

Figure B1 All Derivatives



LINEAR VELOCITIES AND ACCELERATIONS  
FORWARD VELOCITY = 1.0 FT/SEC

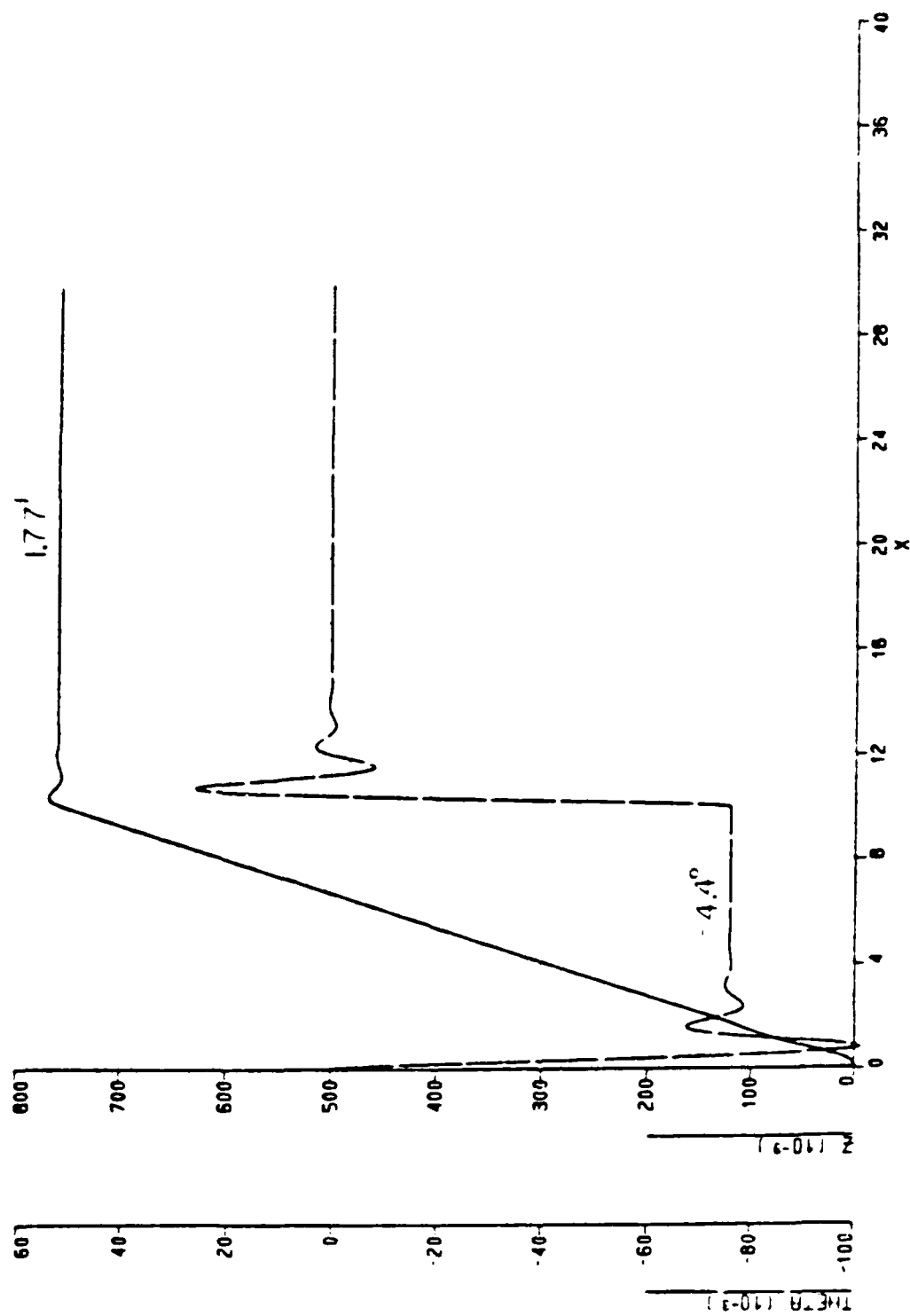
Figure B2 All Derivatives



ANGULAR VELOCITIES AND ACCELERATIONS  
FORWARD VELOCITY - 1.0 FT/SEC

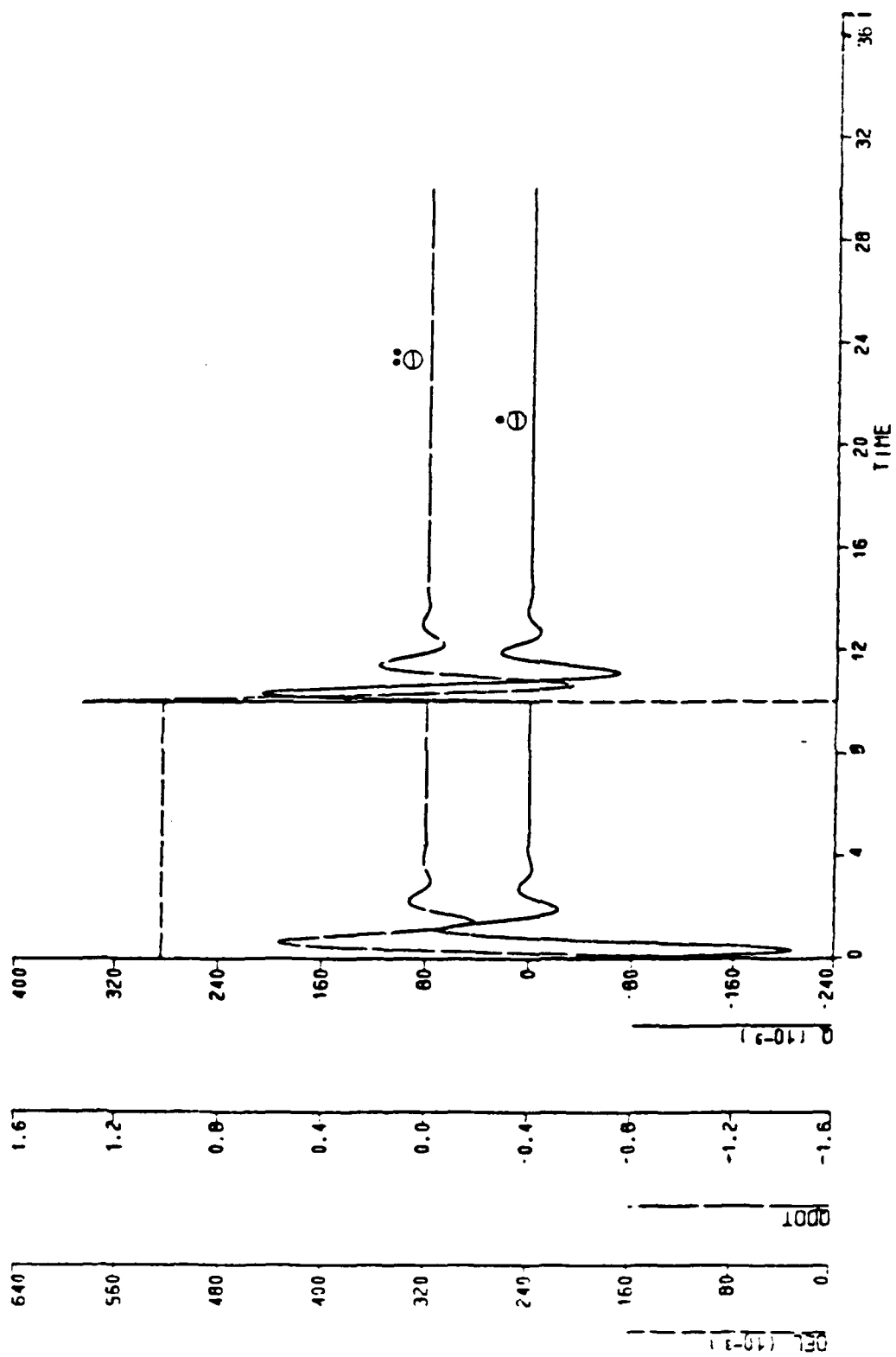
Figure B3 All Derivatives



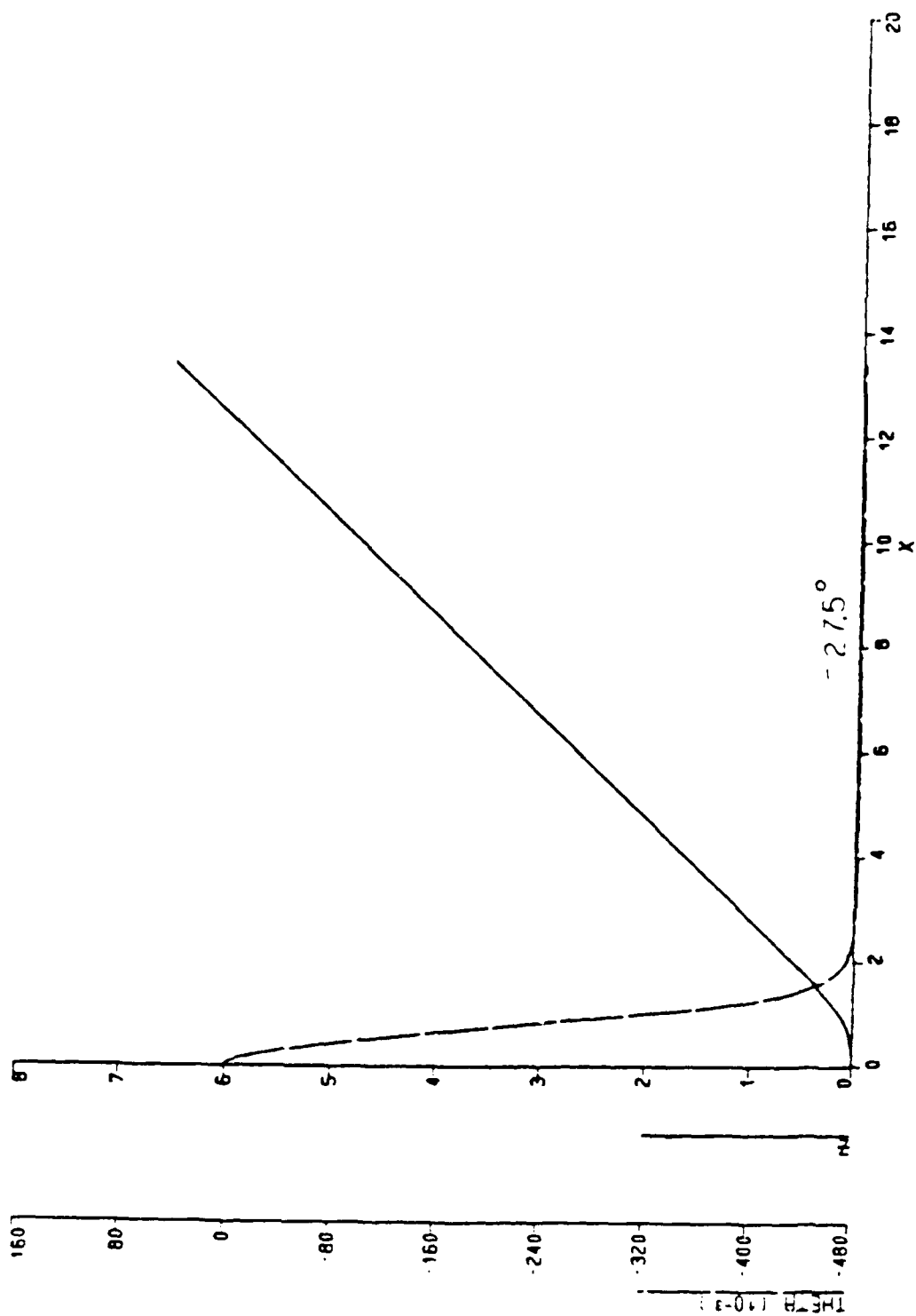


VERTICAL PLANE MANEUVER  
FORWARD VELOCITY = 1.0 FT/SEC

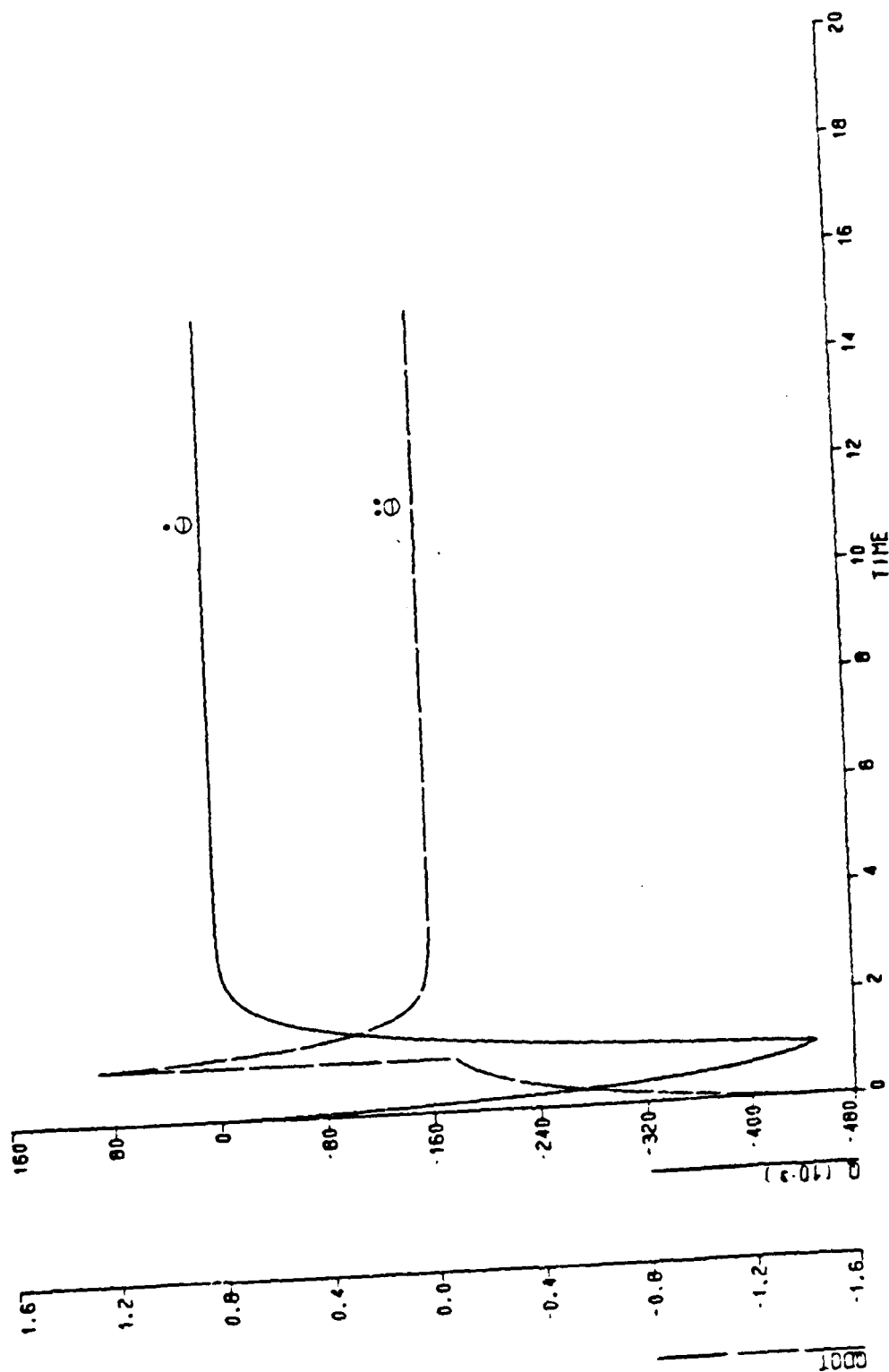
Figure B4 Pitch Equation



ANGULAR VELOCITIES AND ACCELERATIONS  
FORWARD VELOCITY = 1.0 FT/SEC  
Figure B5 Pitch Equation

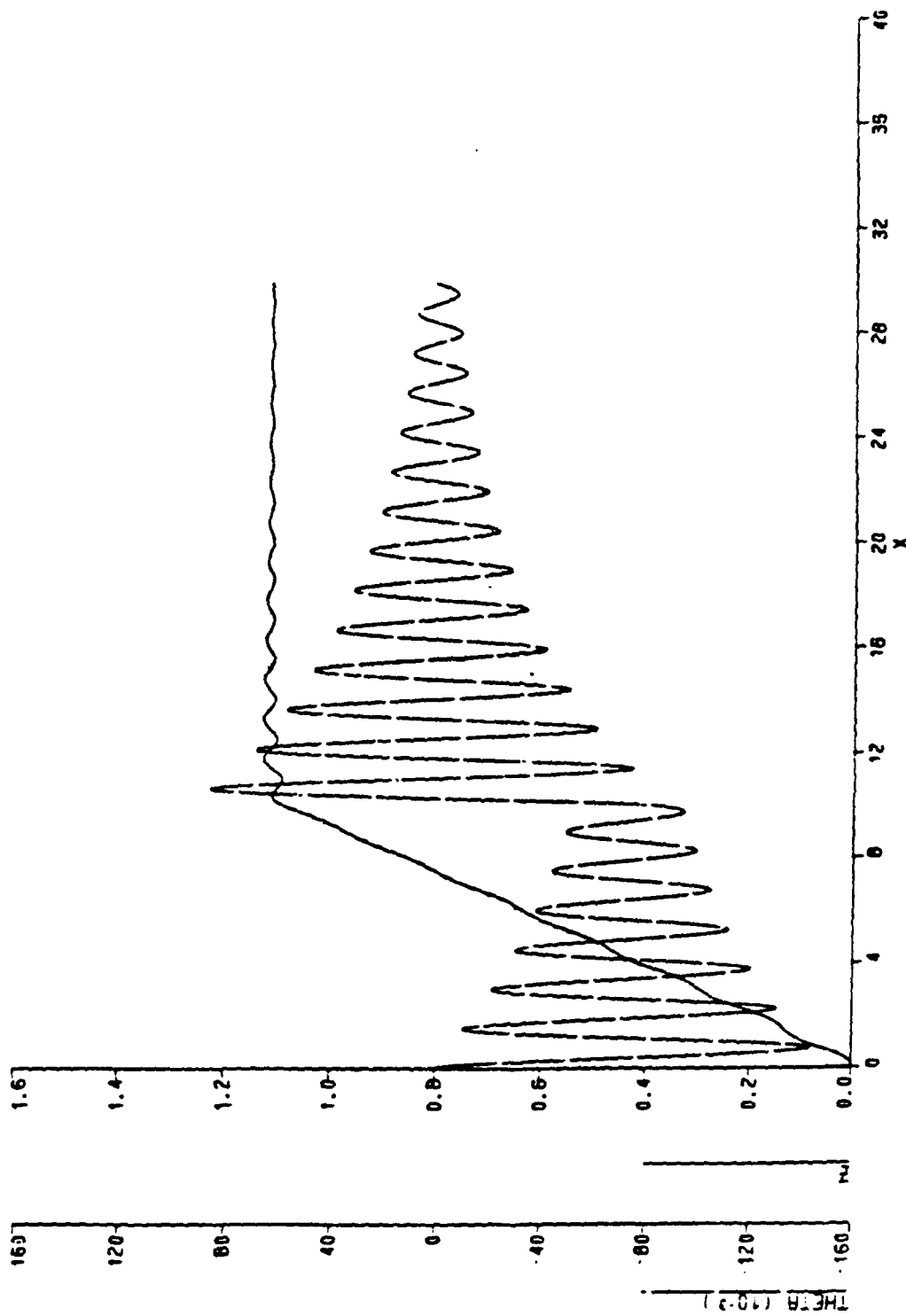


VERTICAL PLANE MANEUVER  
FORWARD VELOCITY - 1.0 FT/SEC  
Figure B6 Zero Restoring Moment

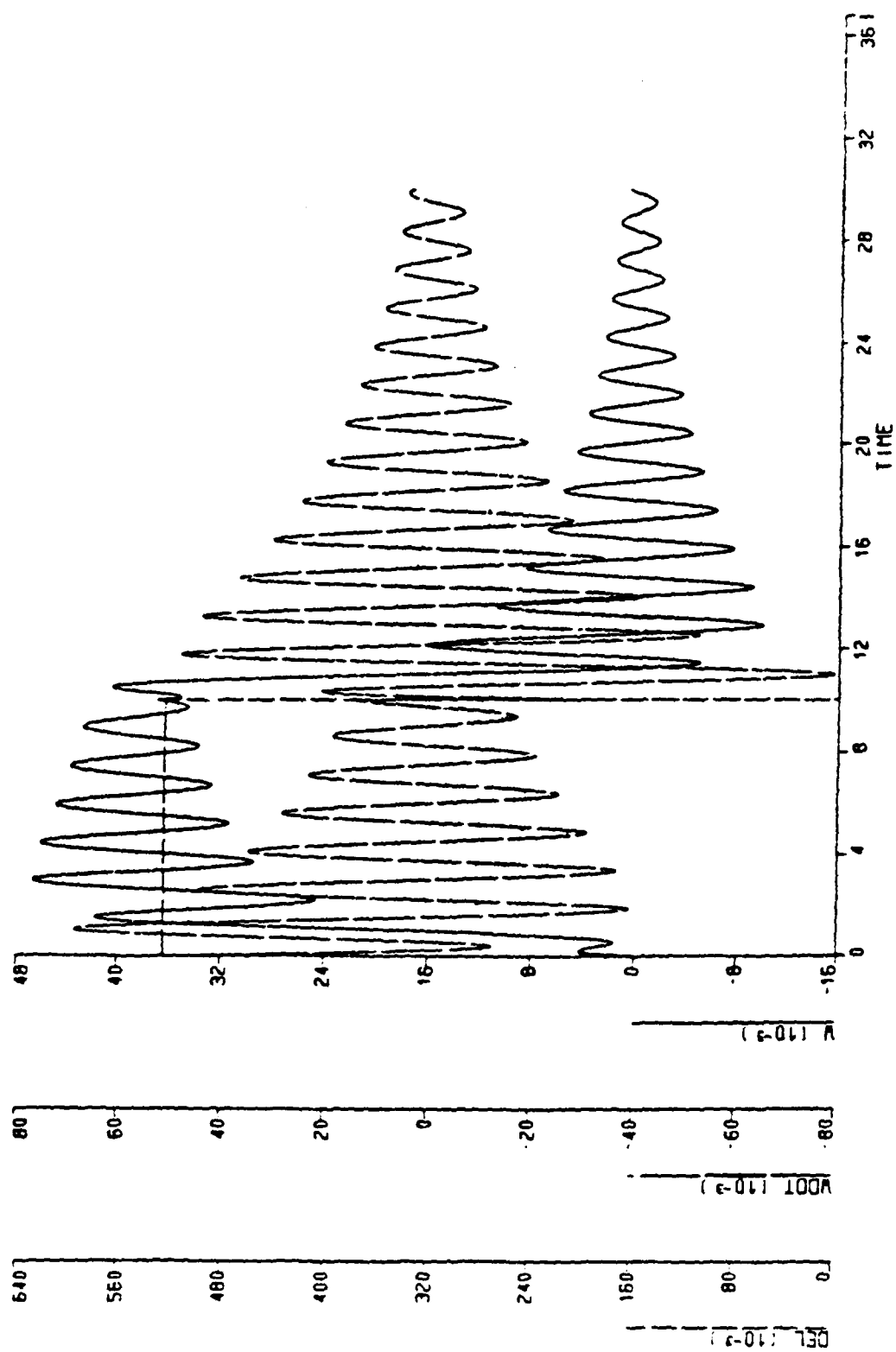


ANGULAR VELOCITIES AND ACCELERATIONS  
FORWARD VELOCITY = 1.0 FT/SEC

Figure B7 Zero Restoring Moment

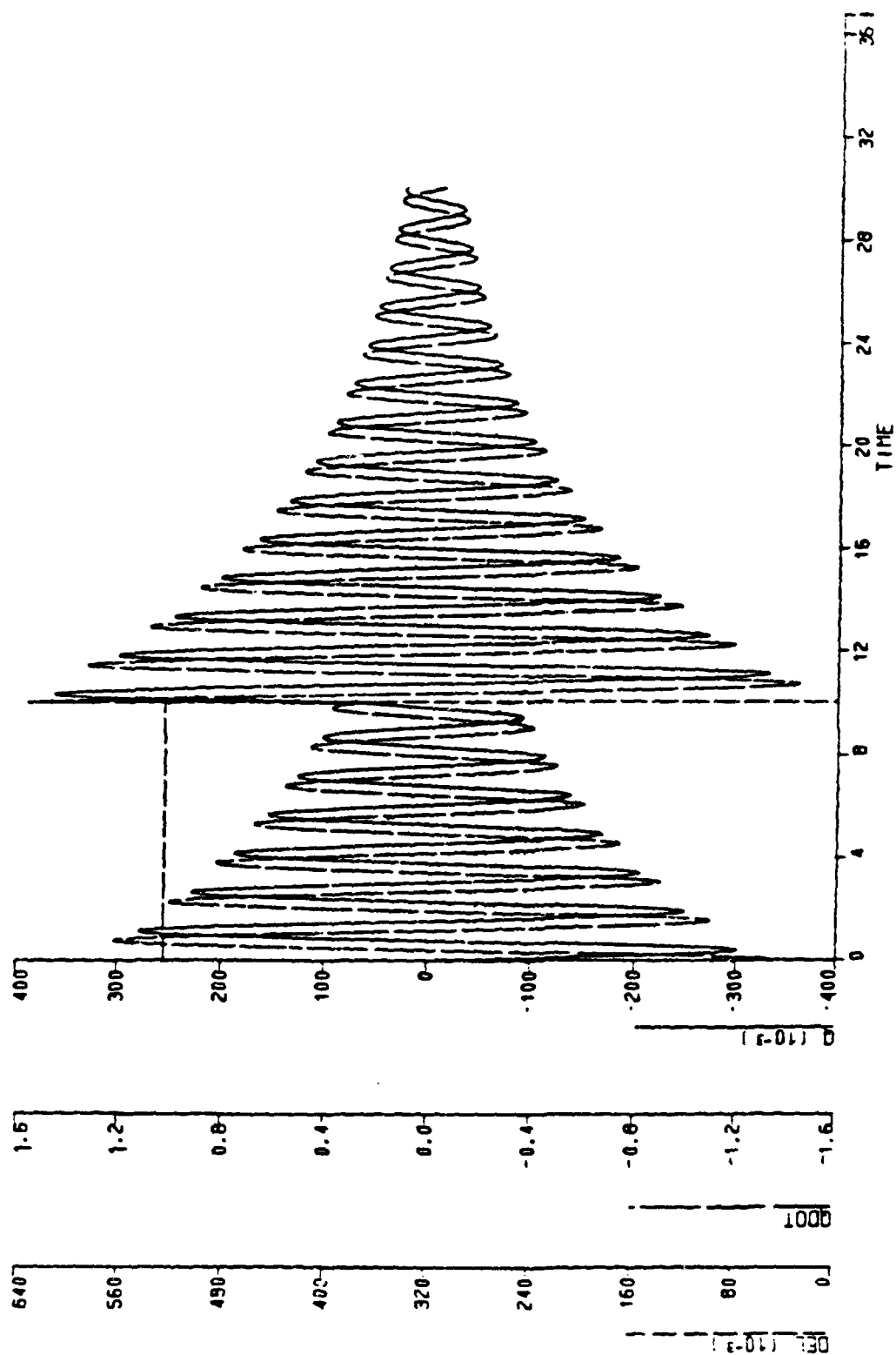


VERTICAL PLANE MANEUVER  
FORWARD VELOCITY = 1.0 FT/SEC  
Figure B8 Reduced Damping



LINEAR VELOCITIES AND ACCELERATIONS  
FORWARD VELOCITY - 1.0 FT/SEC

Figure B9 Reduced Damping



ANGULAR VELOCITIES AND ACCELERATIONS  
FORWARD VELOCITY = 1.0 FT/SEC

Figure B10 Reduced Damping

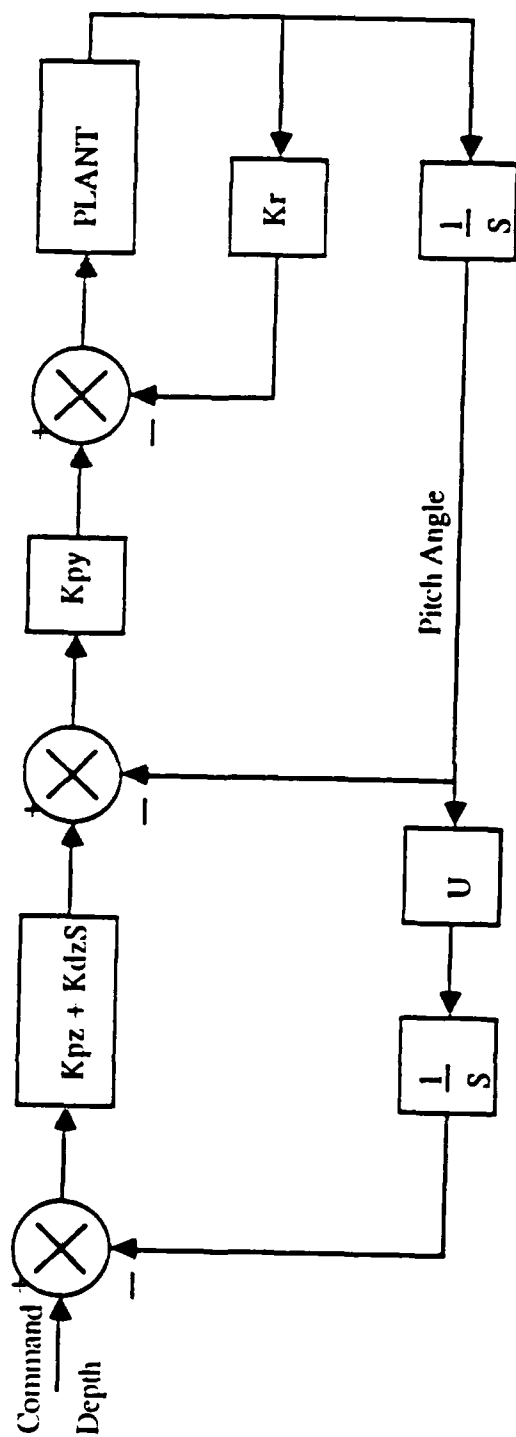
## APPENDIX C

FILE: T6

FORTRAN A

```
TITLE SUBMARINE CONTROLLER SIMULATION
* J = ROTARY MOMENT OF INERTIA WITH ADDED MASS
* B = EFFECTIVE ROTARY DAMPING (BY + KR*KY)
* KPY = PROPORTIONAL GAIN (DIVE ANGLE/PITCH ANGLE ERROR)
* KY = DIVE PLANES CONTROL DERIVATIVE (PITCH)
* KDZ = DERIVATIVE GAIN
* KPZ = PROPORTIONAL GAIN (PITCH ANGLE ERROR/DEPTH ERROR)
* BY = ROTARY DAMPING
* U = FORWARD VELOCITY
CONST J=0.6, BY=0.06, KY=0.14, U=1.0
CONST KPZ=0.25, KDZ=0.60, KPY=0.70, KR=2.0
* INITIAL CONDITIONS
INCON TDOT0=0.0, T0=0.0, Z0=0.0, DEZ0=0.0
      ZC=3.0*STEP(0.0)
      B=BY + KR*KY
      EZ=ZC-Z
      DEZ=DERIV(DEZ0,EZ)
      TC=KPZ*EZ + KDZ*DEZ
      ET=TC-T
      DEL=KPY*ET
      TDDOT=(KY*DEL-B*TDOT)/J
      TDOT=INTGRL(TDOT0,TDDOT)
      T=INTGRL(T0,TDOT)
      ZDOT=U*SIN(T)
      Z=INTGRL(Z0,ZDOT)
CONTRL FINTIM=50, DELT=0.005
PRINT 2.5, DEL,ZC,Z,TC,T
SAVE (S1) 0.005, DEL,ZC,Z
SAVE (S2) 0.005, ZC,TC,T
GRAPH(G1/S1,DE=TEK618,PO=0,.5) TIME,ZC,Z,DEL
GRAPH(G2/S2,DE=TEK618,PO=0,.5) TIME,ZC,T,TC
LABEL(G1,DE=TEK618) DEPTH VARIATION
LABEL(G2,DE=TEK618) PITCH ANGLE VARIATION
LABEL(ALL,DE=TEK618) DEPTH CONTROLLER, U=1.0 FT/SEC
END
STOP
```

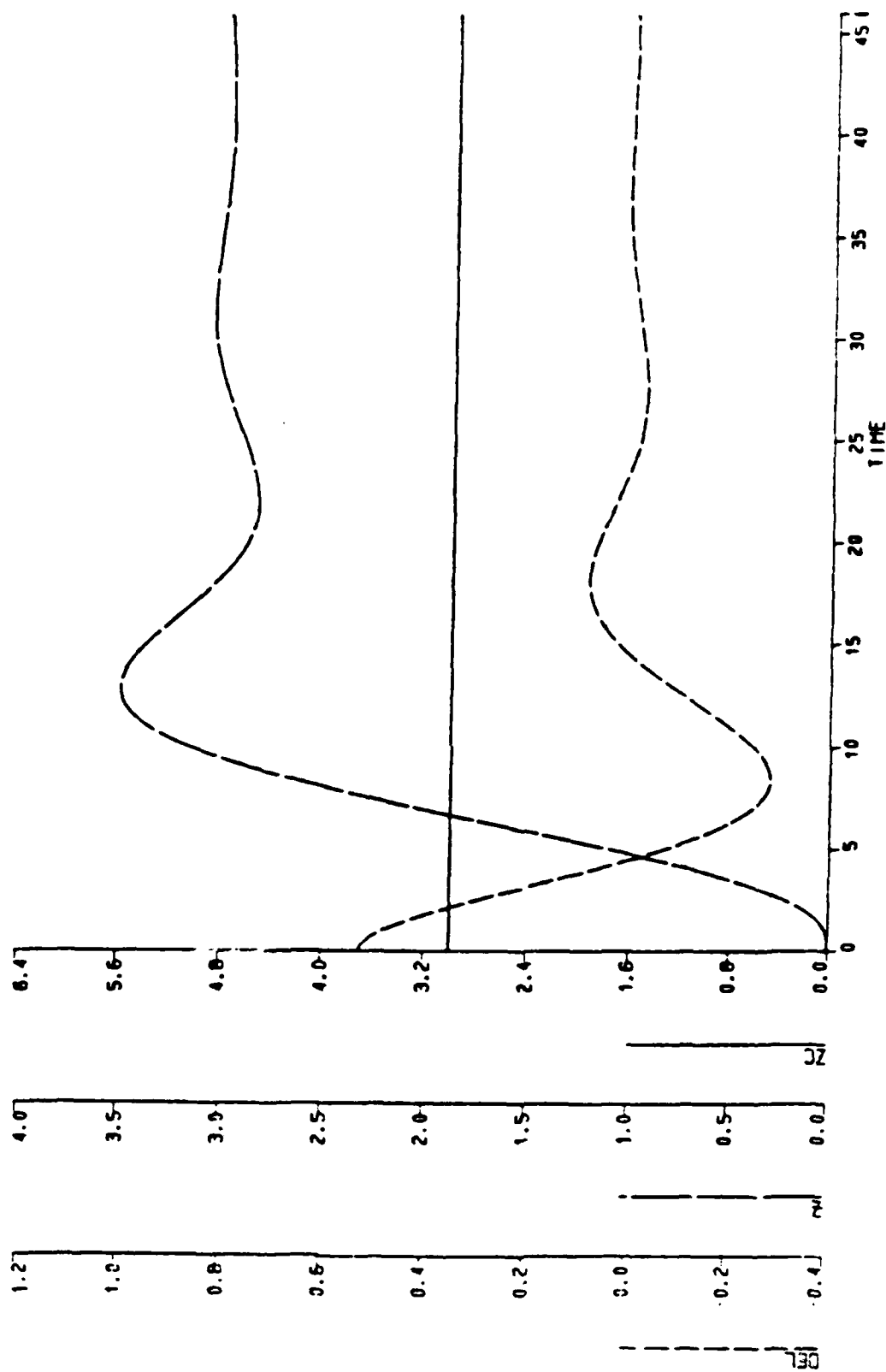




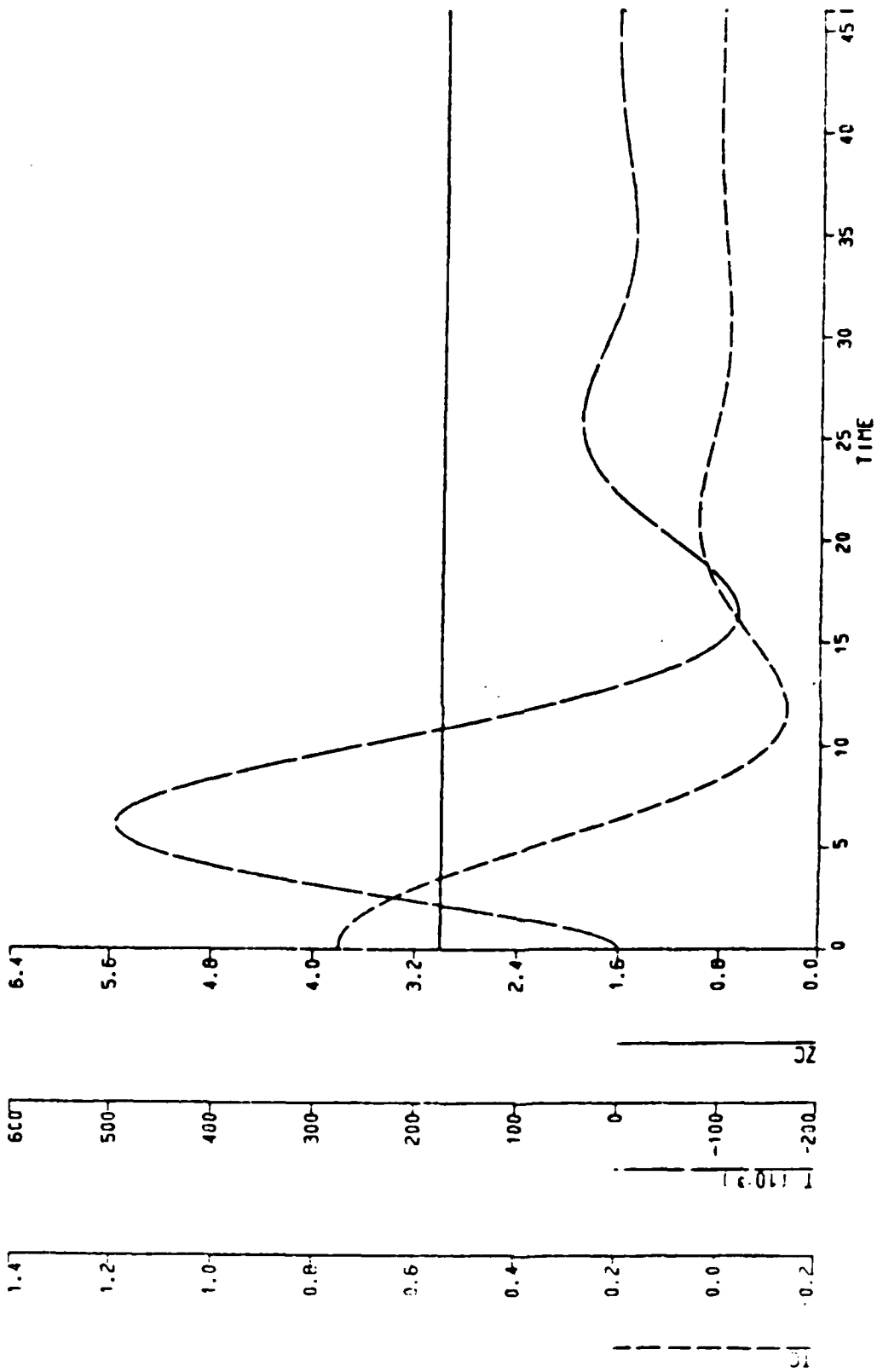
$$G_z = \frac{[K_{pz}K_yK_{py}U + (K_{dz}K_yK_{py}U)S]}{(J_yS^3 + B_{eff}S^2 + [(K_{py}K_y + M_\theta) + K_{dz}K_yK_{py}U]S + K_{pz}K_yK_{py}U)}$$

Effective Damping,  $B_{eff} = B_y + K_r + K_y$

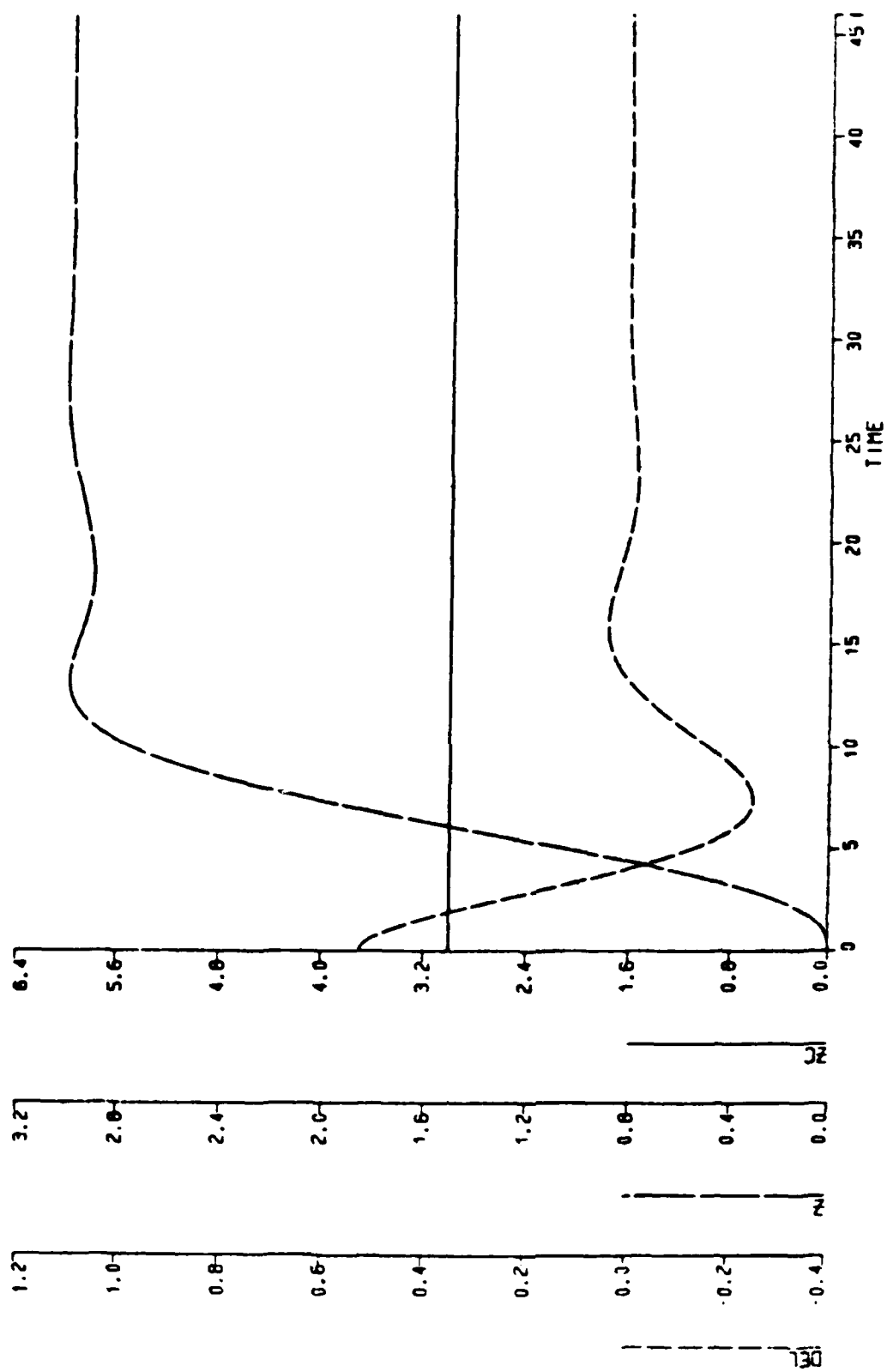
Figure C1 Depth Controller Block Diagram (Heave Not Considered)



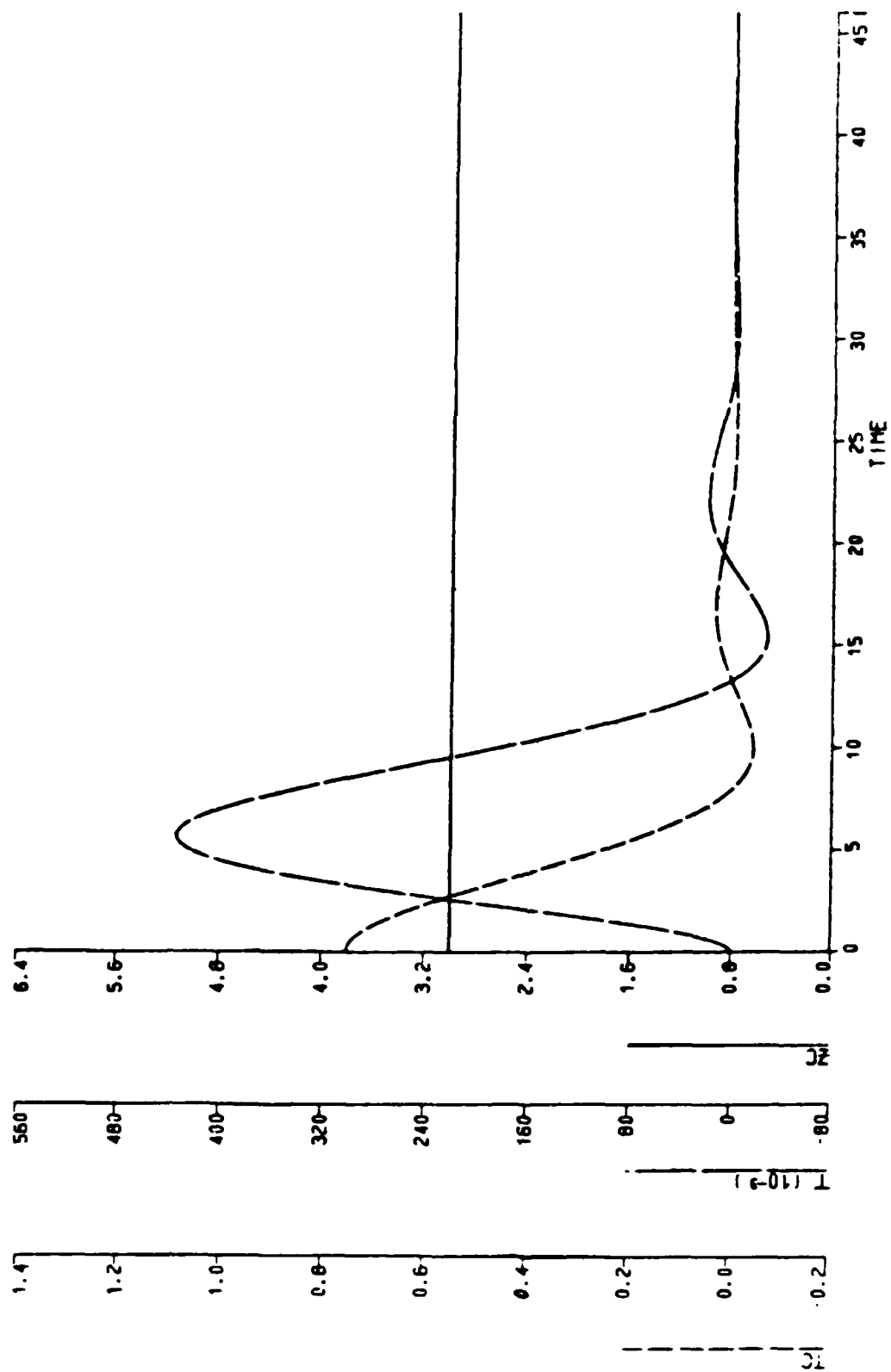
DEPTH VARIATION  
 DEPTH CONTROLLER, U=1.0 FT/SEC  
 Figure C2  $Kdz = 0.25$



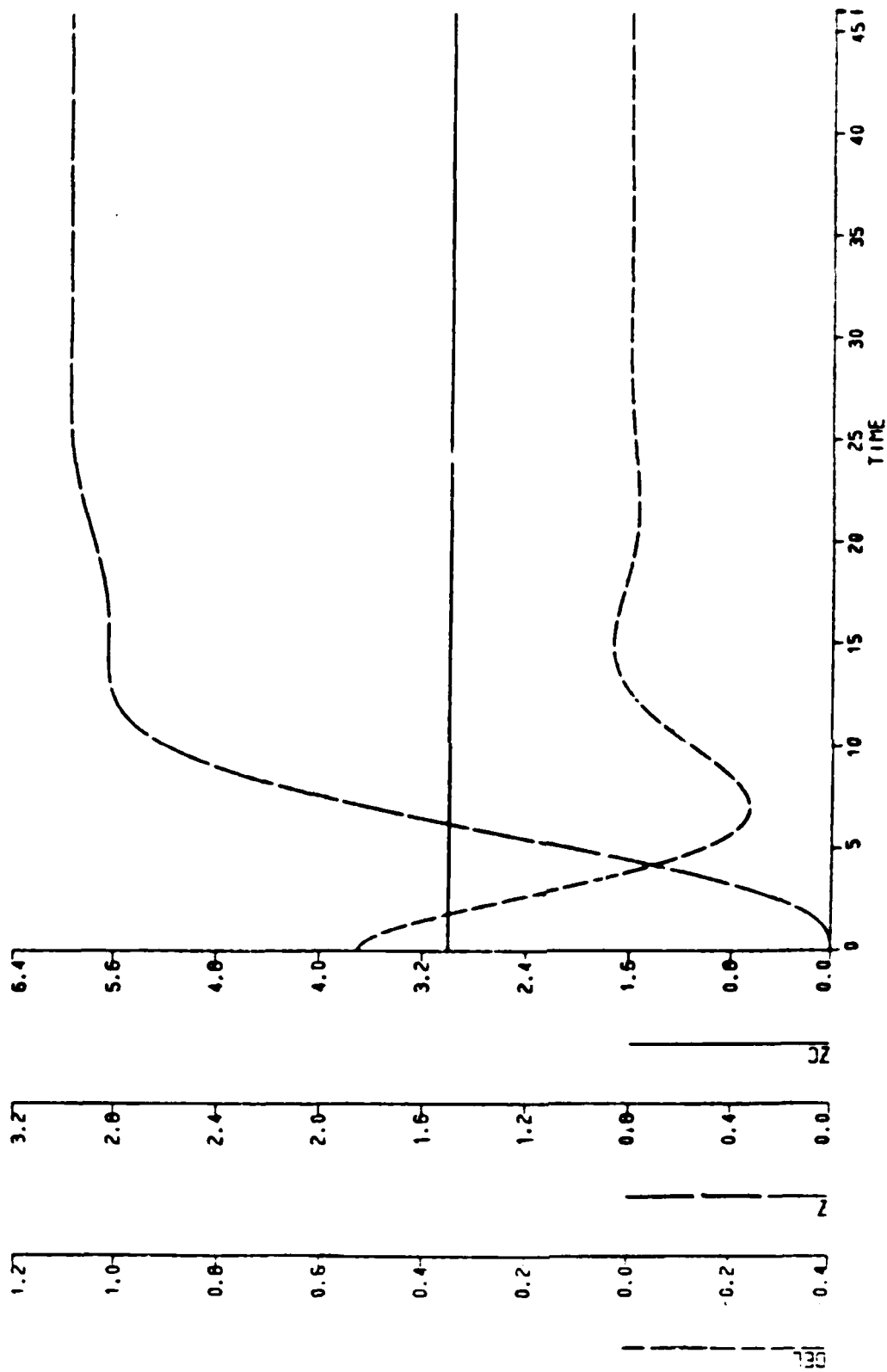
PITCH ANGLE VARIATION  
DEPTH CONTROLLER,  $U=1.0$  FT/SEC  
Figure C3  $Kdz = 0.25$



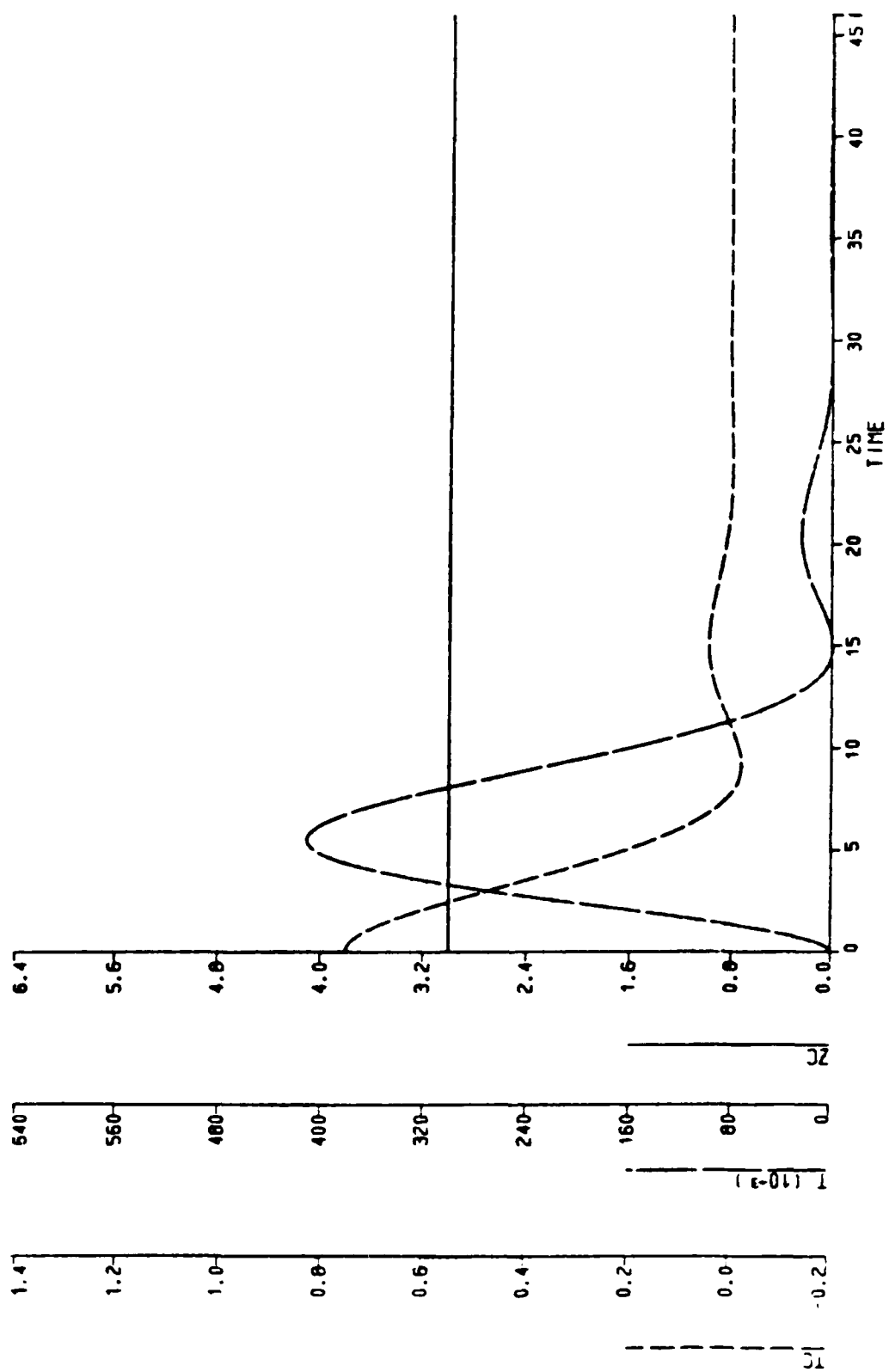
DEPTH VARIATION  
 DEPTH CONTROLLER, U=1.0 FT/SEC  
 Figure C4  $K_d z = 0.60$

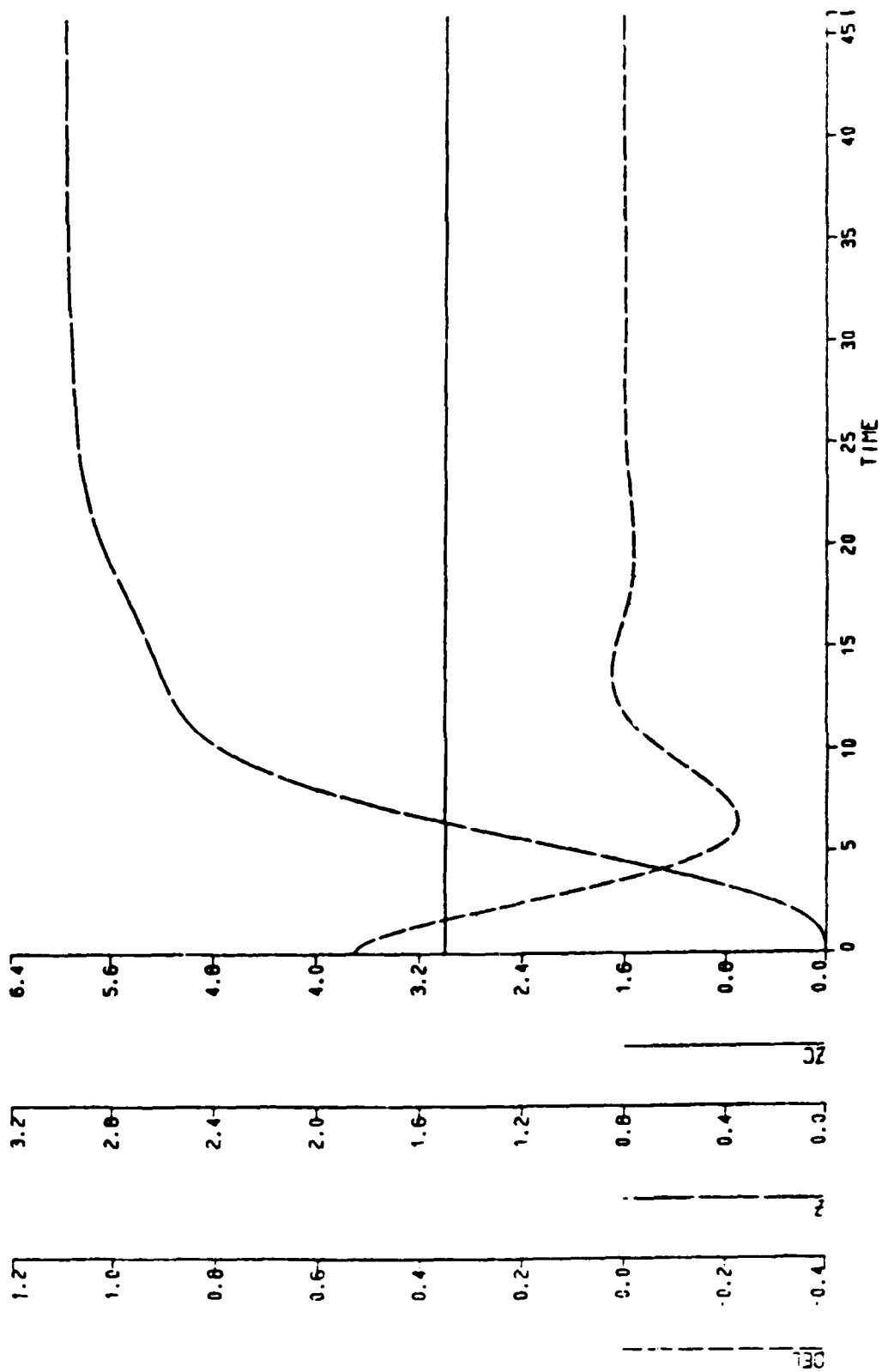


PITCH ANGLE VARIATION  
DEPTH CONTROLLER, U=1.0 FT/SEC  
Figure C5  $K_{dz} = 0.60$



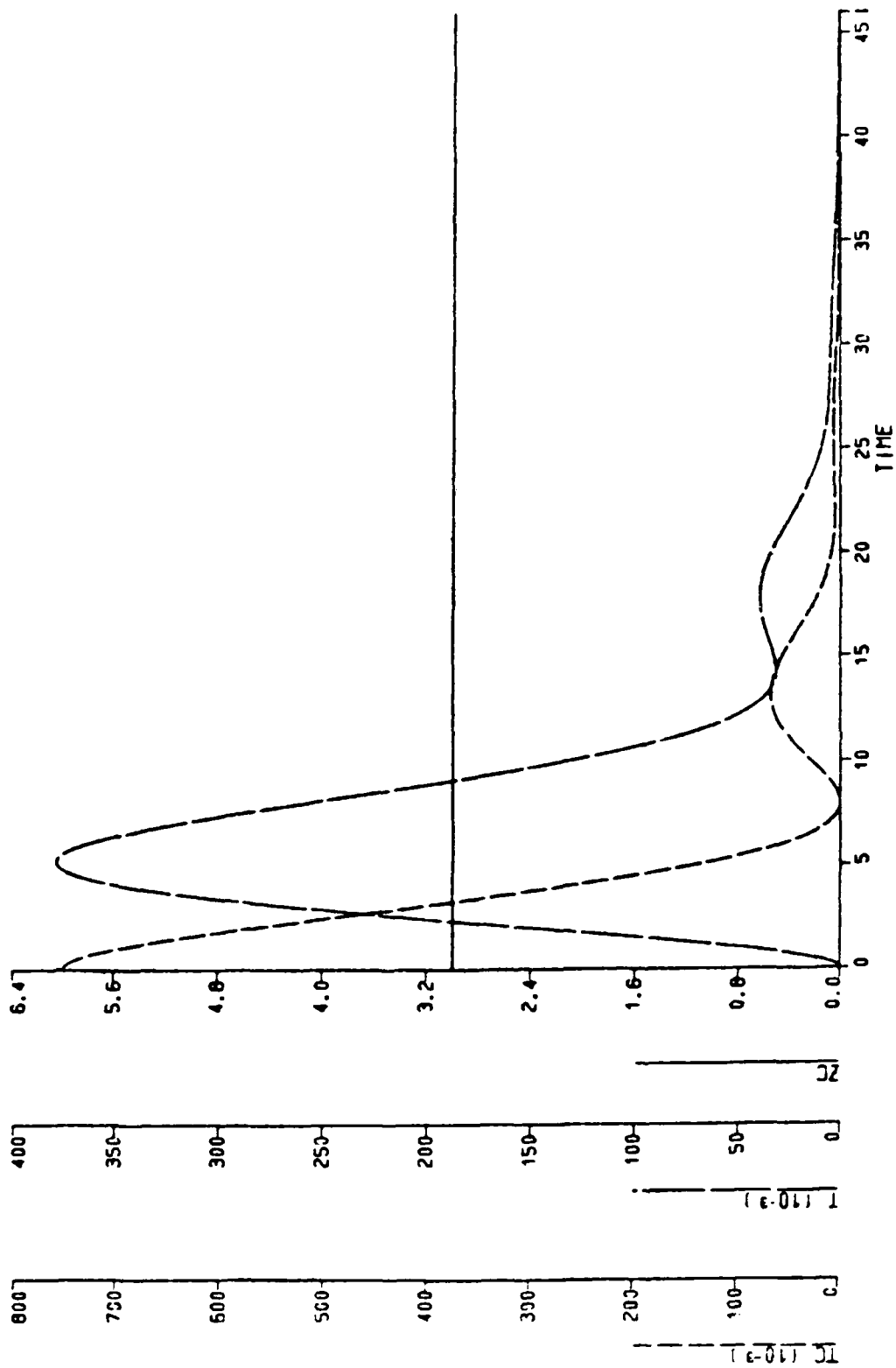
DEPTH VARIATION  
 DEPTH CONTROLLER,  $U=1.0$  FT/SEC  
 Figure C6  $K_d z = 0.75$





DEPTH VARIATION  
DEPTH CONTROLLER,  $U=1.0$  FT/SEC  
Figure C8  $K_{dz} = 1.00$





PITCH ANGLE VARIATION  
DEPTH CONTROLLER,  $U=1.0$  FT/SEC

Figure C9  $Kdz = 1.00$

## INITIAL DISTRIBUTION LIST

	No. Copies
1. Defense Technical Information Center Cameron Station Alexandria, Virginia 22304-6145	2
2. Library, Code 0142 Naval Postgraduate School Monterey, California 93943-5002	2
3. Chairman, Code 69Hy Mechanical Engineering Department Naval Postgraduate School Monterey, California 93943-5004	5
4. Professor D.L. Smith, Code 69Sm Mechanical Engineering Department Naval Postgraduate School Monterey, California 93943-5004	1
5. Professor R. McGhee, Code 52Mz Computer Science Department Naval Postgraduate School Monterey, California 93943-5004	1
6. Professor R. Christi, Code 62Cx Electrical and Computer Engineering Department Naval Postgraduate School Monterey, California 93943-5004	1
7. Dr. G. Dobeck, Code 4210 NCSC Panama City, Florida 32407-5000	1
8. Russ Werneth, Code U25 Naval Surface Weapons Center White Oak, Maryland 20910	1

- |     |   |   |
|-----|---|---|
| 9.  | Paul Heckman, Code 943<br>Head, Undersea AI & Robotics Branch<br>Naval Ocean System Center<br>San Diego, California 92152   | 1 |
| 10. | Dr. D. Milne, Code 1563<br>DTRC, Carderock,<br>Bethesda, Maryland 20084-5000  | 1 |
| 11. | RADM G. Curtis, USN PMS-350<br>Naval Sea Systems Command<br>Washington, D.C. 20362-5101   | 1 |
| 12. | LT Rella L. Lyman, Jr. USN Code 90G<br>Naval Sea Systems Command<br>Washington, D.C. 20362-5101   | 1 |
| 13. | Distinguished Professor G. Thaler, Code 62Tr<br>Electrical and Computer Engineering<br>Department<br>Naval Postgraduate School<br>Monterey, California 93943-5004 | 1 |
| 14. | LT Glenn M. Brunner, USN<br>N116 W21040 Brynwood Lane<br>Germantown, Wisconsin 53022  | 1 |

END

DATE

FILMED

7-88

Dtic